NASA/TM-2020-220567

Effects of Hydrogen Bonding and Molecular Chain Flexibility of Substituted n-Alkyldimethylsilanes On Impact Ice Adhesion Shear Strength

Joseph G. Smith and Christopher J. Whol
Langley Research Center, Hampton, Virginia

Richard E. Kreeger
Glenn Research Center, Cleveland, Ohio

Jose Palacios
The Pennsylvania State University, University Park, Pennsylvania

Maricely Hernandez
Langley Research Center, Hampton, Virginia

February 2020

NASA STI Program . . . in Profile

Since its founding, NASA has been dedicated to the advancement of aeronautics and space science. The NASA scientific and technical information (STI) program plays a key part in helping NASA maintain this important role.

The NASA STI program operates under the auspices of the Agency Chief Information Officer. It collects, organizes, provides for archiving, and disseminates NASA's STI. The NASA STI program provides access to the NTRS Registered and its public interface, the NASA Technical Reports Server, thus providing one of the largest collections of aeronautical and space science STI in the world. Results are published in both non-NASA channels and by NASA in the NASA STI Report Series, which includes the following report types:

- TECHNICAL PUBLICATION. Reports of completed research or a major significant phase of research that present the results of NASA Programs and include extensive data or theoretical analysis. Includes compilations of significant scientific and technical data and information deemed to be of continuing reference value. NASA counter-part of peer-reviewed formal professional papers but has less stringent limitations on manuscript length and extent of graphic presentations.

- TECHNICAL MEMORANDUM. Scientific and technical findings that are preliminary or of specialized interest, e.g., quick release reports, working papers, and bibliographies that contain minimal annotation. Does not contain extensive analysis.

- CONTRACTOR REPORT. Scientific and technical findings by NASA-sponsored contractors and grantees.

- CONFERENCE PUBLICATION. Collected papers from scientific and technical conferences, symposia, seminars, or other meetings sponsored or co-sponsored by NASA.

- SPECIAL PUBLICATION. Scientific, technical, or historical information from NASA programs, projects, and missions, often concerned with subjects having substantial public interest.

- TECHNICAL TRANSLATION. English-language translations of foreign scientific and technical material pertinent to NASA's mission.

Specialized services also include organizing and publishing research results, distributing specialized research announcements and feeds, providing information desk and personal search support, and enabling data exchange services.

For more information about the NASA STI program, see the following:

- Access the NASA STI program home page at http://www.sti.nasa.gov

- E-mail your question to help@sti.nasa.gov

- Phone the NASA STI Information Desk at 757-864-9658

- Write to:
  NASA STI Information Desk
  Mail Stop 148
  NASA Langley Research Center
  Hampton, VA 23681-2199

NASA/TM-2020-220567

Effects of Hydrogen Bonding and Molecular Chain Flexibility of Substituted n-Alkyldimethylsilanes On Impact Ice Adhesion Shear Strength

Joseph G. Smith and Christopher J. Whol
Langley Research Center, Hampton, Virginia

Richard E. Kreeger
Glenn Research Center, Cleveland, Ohio

Jose Palacios
The Pennsylvania State University, University Park, Pennsylvania

Maricely Hernandez
Langley Research Center, Hampton, Virginia

February 2020

Available from:

NASA STI Program / Mail Stop 148
NASA Langley Research Center
Hampton, VA 23681-2199
Fax: 757-864-6500

Effects of Hydrogen Bonding and Molecular Chain Flexibility of Substitute n-Alkyldimethylalkoxylsilanes On Impact Ice Adhesion Shear Strength

Abstract

The effects of hydrogen bonding and molecular flexibility upon ice adhesion shear strength were investigated using aluminum substrates coated with substituted n-alkyldimethylalkoxysilanes. The location of the chemical group substitution was on the opposing end of the linear n-alkyl chain with respect to silicon. Three hydrogen-bonding characteristics were evaluated: 1) non-hydrogen bonding, 2) donor/acceptor, and 3) acceptor. Varying the length of the n-alkyl chain provided an assessment of molecular chain flexibility. Coated and uncoated aluminum surfaces were characterized by receding water contact angle and surface roughness. Ice adhesion shear strength was determined in the Adverse Environment Rotor Test Stand facility from -16 to -8°C that simulated aircraft in-flight icing conditions within the FAR Part 25/29 Appendix C icing envelope. Surface roughness of the coatings was similar allowing for comparison of the test results. An adhesion reduction factor, based on the ice adhesion shear strength data with respect to uncoated aluminum obtained at the same temperature, was calculated to compare the data. The results revealed complex interactions with impacting supercooled water droplets that were interdependent upon ice accretion temperature, surface energy characteristics of water and ice, hydrogen bonding characteristic of the substituent, and length of the n-alkyl chain. To aid in explaining the results, 1) changes in the surface energy component (i.e., non-polar and polar) values that water undergoes during its' phase change from liquid to solid that arise from the freezing of impacting supercooled water droplets on the surface depended upon the temperature during accretion were taken into account and 2) the physical properties (i.e., water solubility and melting point) of small compounds analogous to the substituted n-alkyldimethylalkoxysilanes used in this study were compared.

Abbreviations

AERTS: Adverse Environment Rotor Test Stand facility
AFP: anti-freeze protein
Al: aluminum
AMIL: Anti-Icing Materials International Laboratory
ANOVA: analysis of variance
ARF: adhesion reduction factor
ATR-FTIR: attenuated total reflectance Fourier Transform infrared spectroscopy
Avg: average
CAT: Centrifuge Ice Adhesion Test
C#A: methyl terminated carbon chain length of #, where # = 3, 7, 10, 11, 12
C#H: hydroxy terminated carbon chain length of #, where # = 7, 10, 11
C5MEG: methoxy-2-ethyloxypentyldimethylethoxysilane
DSC: differential scanning calorimetry
FAR: Federal Aviation Regulations
FT-NMR: Fourier Transform nuclear magnetic resonance spectroscopy
HB: hydrogen bonding
HB (Ac): Hydrogen bonding acceptor
HB (D/Ac): Hydrogen bonding donor and acceptor
IASS: ice adhesion shear strength
LWC: liquid water content
MD: molecular dynamics
MVD: median volume diameter
non-HB: non-hydrogen bonding
NP: nanoparticles

OEtOMe: 2-methoxyethoxy
$(OEt)_2OMe$: 2-(2-methoxyethoxy)ethoxy
PSU: Pennsylvania State University
RT: room temperature
R_a: mean roughness
R_q: root mean square roughness
SCW: supercooled water
SCWD: supercooled water droplets
Stndev: standard deviation
TGA: thermogravimetric analysis
Θ_R: receding contact angle
σ: silane grafting density
Σ: tethered density parameter

1. Introduction

Water is ubiquitous upon Earth, existing as a vapor, liquid, and solid (i.e., ice) depending upon location and environmental conditions. In the atmosphere, liquid water can exist as supercooled water droplets (SCWD) at any time throughout the year. SCWD are a metastable form of "pure" water that can be present at temperatures from -35 to 0°C, and even as low as -40°C under laboratory conditions or in cumulonimbus clouds [1-4]. When SCWD impact aircraft surfaces, a nucleation point is provided that allows the impacting SCWD to undergo a phase transition from water to ice. Consequently, it is this phase transition that is a major aviation safety concern with numerous incidents having been documented over the years [5]. Ice formation resulting from SCWD impacting aircraft structures can lead to degradation of aerodynamic performance due to increased weight and drag; potentially leading to loss of lift if left unchecked. These icing events can occur while the aircraft is situated on the ground (i.e., ground icing) or while in-flight (i.e., impact icing).

Ground icing typically occurs at airports that experience cold weather events such as freezing rain/drizzle and results in the grounding of the flight until the vehicle is treated with deicing fluids prior to departure. The deicing fluids are based on ethylene- and propylene-based glycols, and are an environmental concern requiring capture of any overflow at the airport to mitigate environmental exposure.

The work presented herein concerns in-flight icing events, which are entirely different than ground icing. One such difference is the velocity of the water droplet when it impacts the surface - low for ground while high for in-flight icing events. In-flight icing can occur throughout the year under environmental conditions that are conducive to ice accretion when the vehicle traverses through clouds containing freezing precipitation or SCWD [6,7]. Methods to address in-flight icing are based on active technologies utilizing mechanical (e.g., pneumatic boots, electro-impulsive), thermal (i.e., electrothermal, de-icing, bleed air), and chemical (i.e., deicing fluids) approaches [2,8,9]. Active approaches can potentially consume large amounts of energy during use and impart increased vehicle weight, both of which lead to reduced fuel efficiency.

A desirable and attractive approach towards dealing with in-flight icing is one based upon a passive method since it would be functional during the entire flight profile and would not require any power consumption. An example of a passive ice protection configuration is a coating that would exhibit low ice adhesion strength and promote ice shedding upon accretion, or prevent ice formation. However, it must be noted that a coating able to prevent in-flight ice accretion has not been found to date. Although several coating technologies (i.e., superhydrophobic surfaces, Slippery Liquid-Infused Porous Surfaces) have been found to increase the time before water freezes, durability remains an issue [10, 11]. It has been proposed that if a passive coating were to be combined with current mechanical methods, then energy usage (and potentially vehicle weight) could be reduced, thereby increasing fuel efficiency and safety. This is the most probable usage scenario if a durable coating can be developed as one can not test the material under all icing encounters. Additionally, lengthy certification can be envisioned and is best addressed by gradual implementation to gain flight heritage.

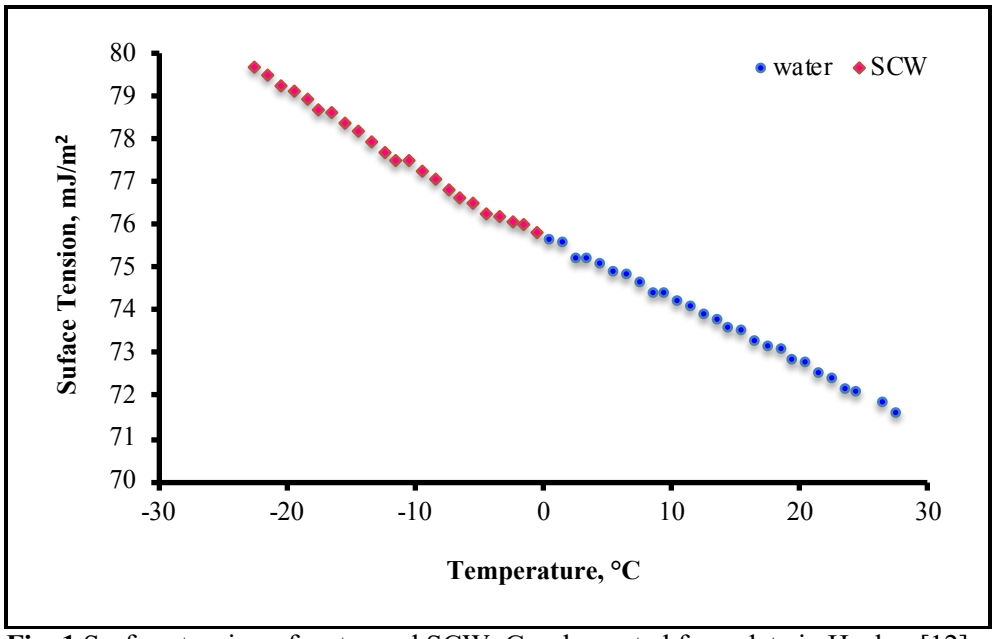

Fig. 1 Surface tension of water and SCW. Graph created from data in Hacker [12].

To attain a better understanding of in-flight icing resulting from impacting SCWD, one has to examine the surface tension properties of supercooled water (SCW) and ice. Water surface tension is of interest especially for runback that is typically observed under glaze ice conditions, or when the aircraft surface is heated and the resultant melted ice flows back along the surface and refreezes on a cold unheated area in an aft location. A plot of the surface tension of water and SCW with respect to temperature (Fig. 1) reveals that as temperature decreases the surface tension increases linearly ($R^2 = 0.996$) from 71.6 to 79.7 mJ/m^2 at 27.5 and -22.5°C, respectively [12]. Surface tension consists of both polar and nonpolar (i.e., van der Waals forces) components and for water at 20°C these are 51.0 and 21.8 mJ/m^2, respectively, and at 0°C are 52.3 and 23.3 mJ/m^2, respectively [13].

As discussed, SCW is a metastable form of water that undergoes a rapid phase change from liquid (i.e., SCWD) to solid (i.e., ice) upon impacting an aircraft surface releasing heat (i.e., heat of fusion) to the surrounding environment (i.e., atmosphere and airframe) [14]. Along with this phase change, the surface tension and its associated components (i.e., polar and nonpolar) change simultaneously. (The surface tension of a solid is known as surface energy and for water it is known that the surface tension and surface energy are identical.) This is important, especially regarding ice formed from SCWD impacting the aircraft surface. As shown in Fig. 2, the total surface energy of water at 0°C is approximately 71% that of ice at 0°C. The values for the polar and nonpolar components of ice and water as calculated from a water-ice system at 0°C are also indicated. Even though ice has a total surface energy greater than that of water, the polar and nonpolar components of ice and water at 0°C undergo a dramatic reversal suggesting that ice has an enhanced nonpolar characteristic. These dramatic changes in SCW and ice properties at 0°C (i.e., phase change and surface energy components) may have profound implications regarding the various ice types generated during in-flight icing events. In addition, this variation in surface energy contributions may complicate analysis of materials regarding ice adhesion minimization and prevention as determined from liquid water contact angles.

In-flight SCWD impact events resulting in ice accretion on aircraft surfaces generally occur at temperatures between -20 and 0°C as a consequence of the vehicle traversing through a cloud containing SCWD or freezing precipitation [6,7]. SCWD present in clouds generally have median volume diameters (MVD) $\leq$ 20 μm, but can approach diameters as high as 50 μm [3]. When SCWD impact an aircraft surface the resultant ice accretion can be in the form of clear/glaze, rime, or mixed ice (Fig. 3) depending on the air temperature (-20 to 0°C), liquid water content (LWC, 0.3-0.6 g/m^3), and SCWD size (MVD of 15-40 μm) present at the time of the impact event [15,16]. LWC represents the mass of water present in a specified area of dry air. As any of these variables increase in amount (i.e., LWC, droplet size, impact velocity, or

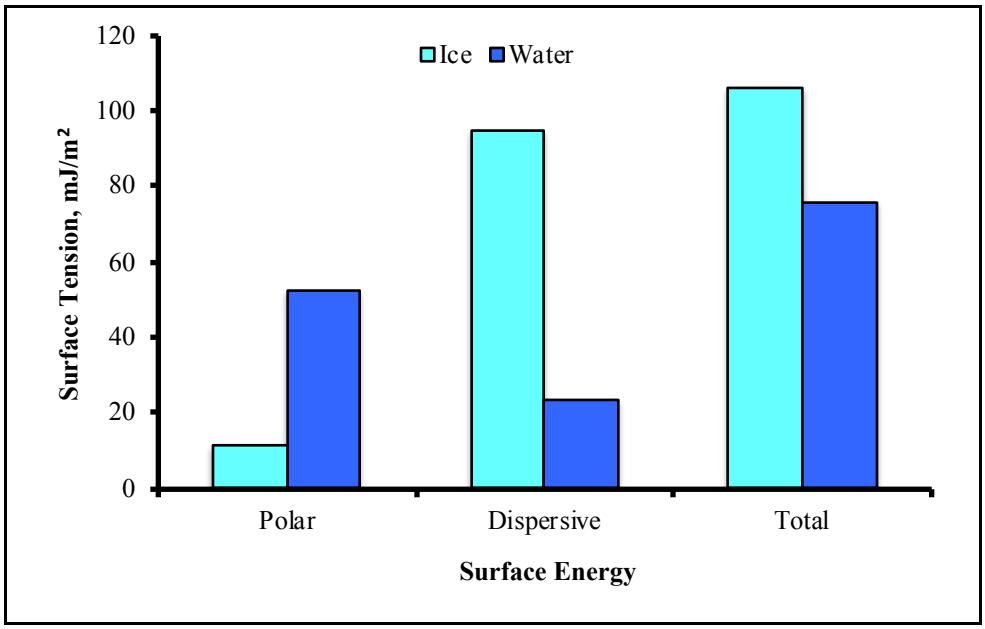

Fig. 2 Surface energy of water and ice at 0°C. Created from data in Kloubek [13].

temperature), rime ice transitions into glaze ice. How fast impacting SCWD freeze on the surface is governed by heat transfer from the aircraft surface that depends on a complicated balance of mechanisms (i.e., kinetic heating, convective cooling, latent heat, sensible heat, and evaporative cooling)[14].

Images of the types of accreted ice are shown in Fig. 3. Clear/glaze ice results from large SCWD impacting the surface where some of the water does not immediately freeze. Instead it flows along the surface and slowly freezes upon the surface as the liquid traverses it, which is a phenomenon known as runback. It is at this time that surface tension (of water on the aircraft surface) comes into play. Since the freezing event occurs slowly, not much air is entrapped in the accreted ice. As a result, ice accretes as a clear to nearly transparent sheet. Depending on the environmental conditions present during the SCWD impact event, the water present can freeze into horns and fishtail shapes protruding into the airstream from the ice surface.

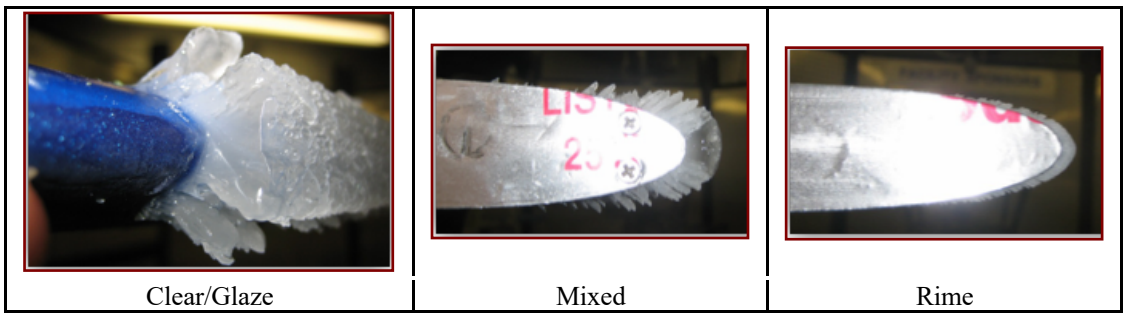

Fig. 3 Accreted impact ice types.

Rime ice is the result of small SCWD impacting a surface that either immediately or rapidly freeze upon, contact entrapping air in the accreted ice, thus affording a milky/opaque appearance. Due to differences in the conditions under which clear/glaze and rime ices are accreted, the former is typically denser, harder, and is translucent or clear [8]. Interestingly, rime ice typically has a greater ice adhesion strength than that observed for glaze ice even though rime ice has a lower density that is associated with the manner in which it is accreted and the temperature [17,18]. During the duration of an in-flight icing event, the aircraft can experience environmental conditions that favor the accretion of clear/glaze ice or rime ice at different times resulting in what is referred to as mixed ice.

To determine whether clear/glaze or rime ice will be accreted upon the vehicle surface, a parameter known as the freezing fraction is used. It refers to the quantity of impinging water that freezes upon impact with the surface [18] as defined by Messinger [14] and based on the energy balance of the system where the equilibrium temperature is 0°C. When the freezing fraction approaches unity, rime ice is formed. Clear/glaze ice is associated with values <1. Liquid water has a value of 0. For static surfaces (e.g., wing leading edge), clear/glaze ice accretion is a concern due to its non-aerodynamic shape and the effect of aerodynamic forces upon it [18]. On rotating surfaces (e.g., turbofans, propellers), however, rime ice formation is an issue [18]. Regardless of the type accreted, ice adhesion strength to aircraft surfaces generally increases as temperature decreases.

As discussed, a passive approach based on coatings that mitigate the formation of ice or reduce ice adhesion strength is desirable. Consequently, a majority of the coatings work with respect to icing has focused on hydrophobic and superhydrophobic materials [19-21]. These characteristics, while advantageous for removal of water from the surface, have been observed to not necessarily translate into the coating being icephobic. Superhydrophobic surfaces have been reported to delay icing, but durability over repeated icing-deicing cycles and icing events occurring in humid environments are potential issues [11,19,22]. An increase in ice adhesion strength on superhydrophobic surfaces, after a number of these icing-deicing episodes, is thought to be affiliated with an increase in the contact area of the ice and solid surface [23]. Studies into improving the durability of superhydrophobic surfaces have been covered in a recent review [11]. One thing to keep in mind with regards to hydrophobic/superhydrophobic surfaces as aircraft coatings besides durability is how these surfaces will affect the wettability characteristics of deicing fluids.

Research has demonstrated that surface roughness considerably increases ice adhesion strength [24,25]. The mechanism for this increase is explained as mechanical clamping of water droplets to the surface morphology [24]. Thus, it is highly desirable to have a smooth surface (i.e., small roughness) to reduce ice adhesion strength

Textured surfaces infused with a liquid such as Slippery Liquid-Infused Porous Surfaces have also been reported to considerably decrease the ice adhesion strength of impact ice, but retention of the infused liquid is a concern [20, 26-29]. Hydrogen bonding (i.e., polar) surfaces have also been evaluated but to a lesser degree. A novel coating approach based on the incorporation of anti-freeze proteins (AFPs) into a coating has provided promising results [30]. The AFP containing coating relies upon ice growth inhibition and formation prevention via an absorption mechanism (i.e., hydrogen bonding) as found in certain fish (i.e., winter flounder) and insects [31]. However, as seen with other coatings, durability was an issue presumably due to denaturation of the AFP. Another hydrogen bonding material, poly(vinyl alcohol) (PVA), has been observed to bind to ice via the pendant hydroxy groups and inhibit additional growth [32-36]. However, PVA is water-soluble and hence would not be useful as a coating.

The surface energies of the coatings just described range from superhydrophobic to hydrophilic. This makes it difficult to determine which attributes would be the most effective with regards to in-flight icing. A possible explanation may lie with the nature of the surface energy values of SCW and ice and the phase change that occurs during ice accretion in-flight. Based on the change from liquid water, having predominantly polar surface energy properties, to ice, with predominantly nonpolar surface energy properties as discussed earlier; the objective of the study reported herein was to evaluate the effect that hydrogen bonding (HB) had upon ice adhesion shear strength (IASS) under simulated in-flight icing conditions [37,38]. This study evaluated aluminum (Al) substrates that were coated with substituted n-alkyldimethylalkoxysilanes of varying n-alkyl chain length and HB characteristics and testing of these samples in a simulated icing environment generated in the Adverse Environment Rotor Test Stand (AERTS) facility located at The Pennsylvania State University (PSU) [25]. This simulated icing environment was within that described in the FAR Part 25/29 Appendix C icing envelope [39, 40]. The substituent on the n-alkyldimethylalkoxysilane, located on the terminus of the n-alkyl chain, was varied to evaluate different coating HB characteristics with respect to water and its effect upon IASS: non-hydrogen bonding (non-HB), HB (donor/acceptor) [HB (D/Ac)], and HB acceptor [HB (Ac)]. As a qualitative means to determine functionalized n-alkyldimethylsiloxane surface density on the Al substrates, silica nanoparticles (NP) were functionalized with several of the compounds to assess the phase behavior of these systems over the temperature range investigated in AERTS.

Two important considerations with regards to the work presented herein are as follows: 1) The results reported were obtained from SCWD impacting coated surfaces under a specific set of conditions and thus may not be representative of how the coating would perform under all icing conditions. 2) Testing under conditions that generate what is known as freezer ice (i.e., where water slowly freezes upon the surface) may afford results that differ from those obtained in this study due to the manner in which the ice is formed/accreted.

Comparison of results described herein with other test facilities is challenging due to testing methodology and conditions [i.e., strain rates, how ice is accreted on the surface (freezer vs. impacting SCWD) etc. Facilities that have been used to determine ice adhesion strength include the Icing Research Tunnel (IRT) at NASA Glenn Research Center, AERTS at PSU, and the Centrifuge Ice Adhesion Test (CAT) at Anti-Icing Materials International Laboratory (AMIL). Consequently, to compare IASS results between facilities, an adhesion reduction factor (ARF) was calculated from average IASS values of the coating and uncoated reference samples (i.e., typically an Al substrate) according to the following equation [41-43].

$$\text{ARF} = \frac{\text{(average IASS of uncoated substrate surface at temperature)}}{\text{(average IASS of coated substrate surface at temperature)}}$$

ARF is a measure of the relative performance of a coated substrate surface compared to the uncoated substrate surface with regard to IASS determined at a particular temperature, test method, and set of conditions. The ARF of the uncoated substrate (i.e., control) is defined as 1 at each test temperature. An ARF > 1 implies that the coating performed better (i.e., lower ice adhesion) than the uncoated substrate whereas ARF values < 1 indicates greater ice adhesion on the coated surface.

Tests conducted by AMIL using the CAT on numerous coatings have reported ARF values ranging from 0.5 to 1000 with respect to Al 6061-T6, the uncoated reference surface [43]. The test conditions though differ from those in this study in that ice was accreted statically at -8°C with water droplets having a MVD of 320 μm to simulate freezing drizzle conditions. The ice accreted samples were then allowed to stand for 1 h at -10°C after thermal equilibrium was reached. The samples are subsequently tested in the centrifuge that is accelerated at 300 rpm/s for 30 s with the end of the test occurring when ice sheds from the sample. It should be noted that the AMIL CAT is representative of ground icing events. Consequently, ARF values obtained at AMIL would not be readily comparable to those obtained in AERTS which simulates in-flight icing events using an order of magnitude smaller MVD (20 μm) SCWD and active accretion conditions.

Regardless of the test method, the ideal ARF value should be as high as possible (i.e., lowest IASS) as dictated by the anticipated end use environment that the coating will be exposed to and that laboratory testing mimics. An ice adhesion strength of ~20 kPa has been suggested as a benchmark for passive ice removal by wind or vibration [21]. The temperature for this benchmark though was not provided and may be assumed to be temperature independent. Depending on the material performance relative to the uncoated control at various test temperatures, ARF values could either vary or be the same over the range of test temperatures. Therefore, one should strive to obtain the highest overall ARF over the entire anticipated performance regime that the coating will experience.

Since the substituted n-alkyldimethylalkoxysilanes were anticipated to lack long term durability towards impact icing events, the knowledge gained under this study would be applied to develop potential low ice adhesion coatings based on durable polymeric formulations in continuing work. Durability with respect to resistance to aircraft fluids, impact (tension and compression), abrasion, UV weathering, rain erosion, etc. would need to be determined for a successful coating. Of these, rain erosion is the toughest test to pass and to date no coating for a wing leading edge application has passed.

2. Experimental

2.1 Materials

Propyldimethylmethoxysilane (C3A), n-decyldimethylchlorosilane (C10A), n-dodecyldimethyl chlorosilane (C12A), dimethylethoxysilane were purchased from Gelest Inc. and used as-received. Heptyl-

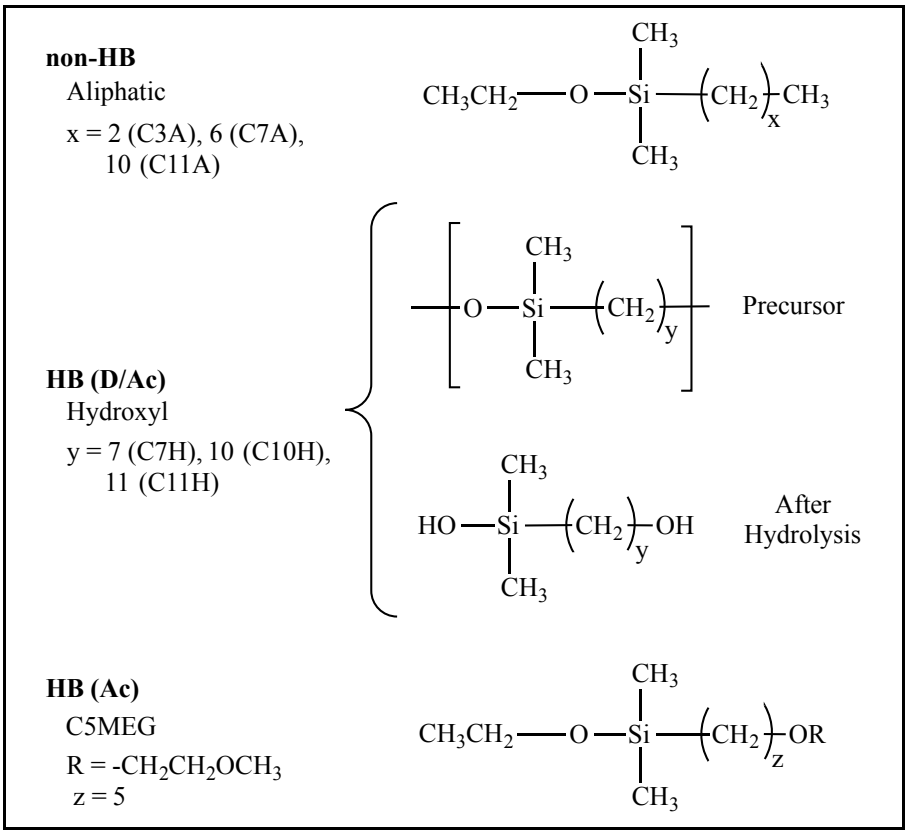

Fig. 4 Structures and hydrogen bonding type of materials used for coating Al.

(C7A) and undecenyl- (C11A) dimethylethoxysilanes were prepared as previously reported [38]. Chlorodimethylsilane, anhydrous tetrahydrofuran, triethylamine, hexanes, 6-hepten-1-ol, 9-decen-1-ol, 10-undecen-1-ol, 2-methoxyethanol, 5-bromopent-1-ene, potassium hydroxide, pentane, and 10% platinum on carbon (Pt/C) were purchased from commercial sources and used as-received. Silica NP (average diameter of 100 nm) were purchased from Polysciences Inc. All other chemicals were purchased from commercial sources and used as-received. The general structure and HB characteristic of each material is shown in Fig. 4. C#A (non-HB) and C#H [HB (D/Ac)] denoted the methyl (A) and hydroxy (H) terminated species, respectively, where # signifies the number of carbon atoms in the n-alkyl chain. Al 3003 alloy sheets (30.5 cm x 30.5 cm x 0.0406 cm) were purchased from McMaster Carr.

2.2 HB (D/Ac) compounds (C7H, C10H, C11H)

The HB (D/Ac) compounds in Fig. 4 were prepared as described in Sections 2.2.1 and 2.2.2. Proton (^{1}H), carbon (^{13}C), and silicon (^{29}Si) Fourier transform nuclear magnetic resonance (FT-NMR) spectroscopies were performed on deuterated chloroform solutions using a Bruker 300 MHz multinuclear FT-NMR to validate material structure. Attenuated total reflectance Fourier transform infrared (ATR-FTIR) spectroscopy was performed on a Nicolet iS5 FTIR spectrometer using the ID7 ATR accessory to confirm functionality [38].

2.2.1 n-Alken-1-oxydimethylsilanes

Into a flame dried three-necked 250 mL round-bottom flask fitted with a magnetic stir bar, nitrogen inlet, pressure equalizing dropping funnel, and drying tube containing Drierite™ was charged the appropriate vinyl alcohol (6-hepten-1-ol, 9-decen-1-ol, or 10-undecen-1-ol), tetrahydrofuran, and triethylamine (20% molar excess with respect to the vinyl alcohol). The flask was then immersed in an ice-water bath for approximately 0.5 h prior to the dropwise addition of chlorodimethylsilane (equimolar quantity with respect to triethylamine) to the stirred solution under a nitrogen atmosphere. Upon addition of chlorodimethylsilane, a white precipitate and fog immediately formed. Once the addition was complete,

the stirred mixture was allowed warm to RT. After stirring for approximately 18 h, the reaction mixture was vacuum filtered to remove the white precipitate. The precipitate was washed with hexanes and the washings combined with the prior filtrate. The solvent was removed via rotoevaporation to afford a cloudy yellow oil. Additional hexanes were added and the flask placed in a refrigerator to precipitate residual salts. The salts were then removed via vacuum filtration and the solvent by rotoevaporation to afford the crude n-alken-1-oxydimethylsilanes in 85 to 95% yield. The as-isolated products were vacuum distilled to afford the pure compounds as clear liquids.

6-hepten-1-oxydimethylsilane: 61% yield. ^{1}H NMR (ppm): 5.67 – 5.5 [m, 1H, H_2C=**C**$\mathbf{H}$-CH_2-CH_2-$(CH_2)_5$-CH_2-O-Si$(CH_3)_2$-H], 4.8 – 4.7 [m, 2H, $\mathbf{H_2C}$=CH-CH_2-CH_2-$(CH_2)_5$-CH_2-O-Si$(CH_3)_2$-H], 4.43 – 4.4 [septuplet, 1H, H_2C=CH-CH_2-CH_2-$(CH_2)_5$-CH_2-O-Si$(CH_3)_2$-**H**], 3.49 – 3.4 (q, 2H, H_2C=CH-CH_2-CH_2-$(CH_2)_5$-$\mathbf{CH_2}$-O-Si$(CH_3)_2$-H], 1.88 – 1.8 (q, 2H, H_2C=CH-$\mathbf{CH_2}$-CH_2-$(CH_2)_5$-CH_2-O-Si$(CH_3)_2$-H], 1.37 – 1.3 [t, 2H, H_2C=CH-CH_2-$\mathbf{CH_2}$-$(CH_2)_5$-CH_2-O-Si$(CH_3)_2$-H], 1.2 – 1.1 [broad s, 10H, H_2C=CH-CH_2-CH_2-$\mathbf{(CH_2)_5}$-CH_2-O-Si$(CH_3)_2$-H], 0.0 [s, 6H, H_2C=CH-CH_2-CH_2-$(CH_2)_5$-CH_2-O-Si$\mathbf{(CH_3)_2}$-H]. ^{13}C NMR (ppm): 60.31, 35.57, 33.93, 31.17, 25.33, 24.83, 20.69, 18.48, 16.19, 0.02. ^{29}Si (ppm): 17.35. ATR-FTIR (cm^{-1}): 3078 (-CH=CH_2 stretch), 2112 (-SiH stretch), 1095 (Si-O-CH_2 stretch)

9-decen-1-oxydimethylsilane: 67% yield. ^{1}H NMR (ppm): 5.67 – 5.5 [m, 1H, H_2C=**C**$\mathbf{H}$-CH_2-CH_2-$(CH_2)_5$-CH_2-O-Si$(CH_3)_2$-H], 4.8 – 4.7 [m, 2H, $\mathbf{H_2C}$=CH-CH_2-CH_2-$(CH_2)_5$-CH_2-O-Si$(CH_3)_2$-H], 4.43 – 4.4 [septuplet, 1H, H_2C=CH-CH_2-CH_2-$(CH_2)_5$-CH_2-O-Si$(CH_3)_2$-**H**], 3.49 – 3.4 (q, 2H, H_2C=CH-CH_2-CH_2-$(CH_2)_5$-$\mathbf{CH_2}$-O-Si$(CH_3)_2$-H], 1.88 – 1.8 (q, 2H, H_2C=CH-$\mathbf{CH_2}$-CH_2-$(CH_2)_5$-CH_2-O-Si$(CH_3)_2$-H], 1.37 – 1.3 [t, 2H, H_2C=CH-CH_2-$\mathbf{CH_2}$-$(CH_2)_5$-CH_2-O-Si$(CH_3)_2$-H], 1.2 – 1.1 [broad s, 10H, H_2C=CH-CH_2-CH_2-$\mathbf{(CH_2)_5}$-CH_2-O-Si$(CH_3)_2$-H], 0.0 [s, 6H, H_2C=CH-CH_2-CH_2-$(CH_2)_5$-CH_2-O-Si$\mathbf{(CH_3)_2}$-H]. ^{13}C NMR (ppm): 140.86, 115.77, 65.9, 64.1, 35.4, 34.1, 31.0, 30.8, 30.5, 27.3, 0. ^{29}Si (ppm): 4.9. ATR-FTIR (cm^{-1}): 3078 (-CH=CH_2 stretch), 2109 (-SiH stretch), 1093 (Si-O-CH_2 stretch)

10-undecen-1-oxydimethylsilane: 69% yield. ^{1}H NMR (ppm): 5.67 – 5.54 [m, 1H, H_2C=**C**$\mathbf{H}$-CH_2-$(CH_2)_7$-CH_2-O-Si$(CH_3)_2$-H], 4.8 – 4.7 [m, 2H, $\mathbf{H_2C}$=CH-CH_2-$(CH_2)_7$-CH_2-O-Si$(CH_3)_2$-H], 4.44 – 4.38 [septuplet, 1H, H_2C=CH-CH_2- $(CH_2)_7$-CH_2-O-Si$(CH_3)_2$-**H**], 3.43 – 3.39 [t, 2H, H_2C=CH-CH_2-$(CH_2)_7$-$\mathbf{CH_2}$-O-Si$(CH_3)_2$-H], 1.87 – 1.8 [t, 2H, H_2C=CH-$\mathbf{CH_2}$-$(CH_2)_7$-CH_2-O-Si$(CH_3)_2$-H], 1.4 – 1.1 [broad s, 14, H_2C=CH-CH_2-$\mathbf{(CH_2)_7}$-CH_2-O-Si$(CH_3)_2$-H], 0.0 [s, 6H, H_2C=CH-CH_2-$(CH_2)_7$-CH_2-O-Si$\mathbf{(CH_3)_2}$-H]. ^{13}C NMR (ppm): 140.75, 115.77, 65.9, 64.6, 35.4, 34.4, 34.1, 31.1, 31.0, 31.0, 30.9, 30.7, 30.5, 27.4, 0. ^{29}Si (ppm): 5.1. ATR-FTIR (cm^{-1}): 3077 (-CH=CH_2 stretch), 2109 (-SiH stretch), 1093 (Si-O-CH_2 stretch)

2.2.2 Poly(n-Alkyldimethylsiloxane)s

Into a 50 mL single-necked round-bottom flask fitted with a magnetic stir bar was charged the appropriate n-alken-1-oxydimethylsilanes from Section 2.2.1 and hexanes [(approximate 20% (w/v)]. The flask was then immersed in an ice-water bath for approximately 0.5 h prior to the addition of 10% Pt/C. The mixture was then allowed to warm to RT with stirring. After stirring for approximately 18 h, the reaction mixture was vacuum filtered through Celite 545 to remove the catalyst. The solvent was removed by rotoevaporation to afford the polymer as a clear to light yellow liquid. The as-isolated polymers were used to coat Al substrates as described in Section 2.4

poly(n-heptyldimethylsiloxane): 85% yield. ^{1}H NMR (ppm): 3.5 [t, 2H, -CH_2-$(CH_2)_4$-CH_2-$\mathbf{CH_2}$-O-Si$(CH_3)_2$-], 1.4 [t, 2H, -CH_2-$(CH_2)_4$-$\mathbf{CH_2}$-CH_2-O-Si$(CH_3)_2$-], 1.2 [s, 8H, -CH_2-$\mathbf{(CH_2)_4}$-CH_2-CH_2-O-Si$(CH_3)_2$-], 0.5 [t, 2H, -$\mathbf{CH_2}$-$(CH_2)_4$-CH_2-CH_2-O-Si$(CH_3)_2$-], 0.0 [s, 6H, -CH_2-$(CH_2)_4$-CH_2-CH_2-O-Si$\mathbf{(CH_3)_2}$-]. ^{13}C NMR (ppm): 64.9, 64.4, 35.6, 35.2, 34.9, 34.7, 33.7, 31.4, 27.9, 25.3, 25, 18.5, 0. ^{29}Si (ppm): 17.1. ATR-FTIR (cm^{-1}): 1097 (-Si-O-CH_2 stretch).

poly(n-decyldimethylsiloxane): 88% yield. ^{1}H NMR (ppm): 3.5 – 3.46 [t, 2H, -CH_2-$(CH_2)_7$-CH_2-$\mathbf{CH_2}$-O-Si$(CH_3)_2$-], 1.45 – 1.41 [t, 2H, -CH_2-$(CH_2)_7$-$\mathbf{CH_2}$-CH_2-O-Si$(CH_3)_2$-], 1.19 [s, 14H, -CH_2-$\mathbf{(CH_2)_7}$-CH_2-CH_2-O-Si$(CH_3)_2$-], 0.5 – 0.4 [t, 2H, -$\mathbf{CH_2}$-$(CH_2)_7$-CH_2-CH_2-O-Si$(CH_3)_2$-], 0.0 [s, 6H, -CH_2-$(CH_2)_7$-CH_2-CH_2-O-

Si**(CH₃)₂**-]. ^{13}C NMR (ppm): 64.9, 35.6, 34.9, 31.8, 31,7, 31.6, 31.5, 28, 27.9, 25.3, 18.5, 0. ^{29}Si (ppm): 17.0. ATR-FTIR (cm^{-1}): 1094 (-Si-O-CH_2 stretch).

poly(undecyldimethylsiloxane): 84% yield. ^{1}H NMR (ppm): 3.51 – 3.46 [t, 2H, -$(CH_2)_{10}$-**CH_2**-O-Si$(CH_3)_2$-], 1.43 – 1.2 [broad, 20H, -**$(CH_2)_{10}$**-CH_2-O-Si$(CH_3)_2$-], 0.0 [s, 6H, -$(CH_2)_{10}$-CH_2-O-Si**$(CH_3)_2$**-].^{13}C NMR (ppm): 62.5, 33.2, 32.5, 29.4, 29.3, 29.2, 29, 25.5, 22.9, 16.0, -2.4. ^{29}Si (ppm): 17.2. ATR-FTIR (cm^{-1}): 1093 (-Si-O-CH_2 stretch).

2.3 HB (Ac) compound (C5MEG)

The HB (Ac) compound in Fig. 4 was prepared as described in Sections 2.3.1 and 2.3.2.

2.3.1 5-(1-Methoxyethoxy)-pent-1-ene

The title compound was prepared in 34% yield after vacuum distillation as described in the literature [44]. ^{1}H NMR (ppm): 5.82 – 5.68 (m, 1H, H_2C=**CH**-CH_2-CH_2-CH_2-O-CH_2-CH_2-O-CH_3), 4.99 – 4.86 (m, 2H, **H_2C**=CH-CH_2-CH_2-CH_2-O-CH_2-CH_2-O-CH_3), 3.53 – 3.45 (m, 4H, H_2C=CH-CH_2-CH_2-CH_2-O-**CH_2-CH_2**-O-CH_3), 3.43 – 3.39 (t, 2H, H_2C=CH-CH_2-CH_2-**CH_2**-O-CH_2-CH_2-O-CH_3), 3.32 (s, 3H, H_2C=CH-CH_2-CH_2-CH_2-O-CH_2-CH_2-O-**CH_3**), 2.09 – 2.02 (q, 2, H_2C=CH-**CH_2**-CH_2-CH_2-O-CH_2-CH_2-O-CH_3), 1.68 – 1.58 (q, 2H, H_2C=CH-CH_2-**CH_2**-CH_2-O-CH_2-CH_2-O-CH_3). ^{13}C NMR (ppm): 138.26, 114.69, 72.03, 70.84, 70.51, 59.10, 30.3, 28.72. ATR-FTIR (cm^{-1}): 3076 (-CH=CH_2 stretch), 1639 (C=C stretch) 1107 (CH_2-O-CH_2 stretch).

2.3.2 Methoxy-2-ethyloxypentyldimethylethoxysilane

Into a 50 mL single-necked round-bottom flask fitted with a magnetic stir bar was charged 5-(1-methoxyethoxy)-pent-1-ene (7.82 g, 0.0542 mol) and dimethylethoxysilane (7.19 g, 0.0690 mol). The flask was then immersed in an ice-water bath for approximately 0.5 h prior to the addition of 10% Pt/C (0.134 g). The stirred mixture was then allowed to warm to RT. After stirring for approximately 18 h, pentane was added and the reaction mixture vacuum filtered through Celite 545 to remove the catalyst. The solvent was removed by rotoevaporation to afford the title compound in 82% yield as a light brown liquid. It was then vacuum distilled to afford 5.69 g (42 % yield) of a clear liquid. ^{1}H NMR (ppm): 3.7 – 3.52 (m, 2H, CH_3-**CH_2**-O-Si$(CH_3)_2$-CH_2-CH_2-CH_2-CH_2-CH_2-O-CH_2-CH_2-O-CH_3), 3.52 – 3.43 (m, 4H, CH_3-CH_2-O-Si$(CH_3)_2$-CH_2-CH_2-CH_2-CH_2-CH_2-O-**CH_2-CH_2**-O-CH_3), 3.41 – 3.34 (t, 2H, CH_3-CH_2-O-Si$(CH_3)_2$-CH_2-CH_2-CH_2-CH_2-**CH_2**-O-CH_2-CH_2-O-CH_3), 3.3 (s, 3H, CH_3-CH_2-O-Si$(CH_3)_2$-CH_2-CH_2-CH_2-CH_2-CH_2-O-CH_2-CH_2-O-**CH_3**), 1.58 – 1.46 (t, 2H, CH_3-CH_2-O-Si$(CH_3)_2$-CH_2-CH_2-CH_2-**CH_2**-CH_2-O-CH_2-CH_2-O-CH_3), 1.33 – 1.2 (m, 4H, CH_3-CH_2-O-Si$(CH_3)_2$-CH_2-**CH_2-CH_2**-CH_2-CH_2-O-CH_2-CH_2-O-CH_3), 1.17 – 1.05 (m, 3H, **CH_3**-CH_2-O-Si$(CH_3)_2$-CH_2-CH_2-CH_2-CH_2-CH_2-O-CH_2-CH_2-O-CH_3), 0.84 – 0.77 (t, 1H, CH_3-CH_2-O-Si$(CH_3)_2$-**CH_2**-CH_2-CH_2-CH_2-CH_2-O-CH_2-CH_2-O-CH_3), 0.57 – 0.43 (b, 1H, CH_3-CH_2-O-Si$(CH_3)_2$-**CH_2**-CH_2-CH_2-CH_2-CH_2-O-CH_2-CH_2-O-CH_3), 0.08 -m -0.08 (m, 6H, CH_3-CH_2-O-Si**$(CH_3)_2$**-CH_2-CH_2-CH_2-CH_2-CH_2-O-CH_2-CH_2-O-CH_3).^{13}C NMR (ppm): 62.5, 33.2, 32.5, 29.4, 29.3, 29.2, 29, 25.5, 22.9, 16.0, -2.4. ^{29}Si (ppm): 7.25. ATR-FTIR (cm^{-1}): 1110 (CH_2-O-CH_2 stretch), 1075 (-Si-O-CH_2 stretch).

2.4 Coatings

Prior to application of coating solutions, Al panels were treated with Chemetall Pace B-82 (diluted by a factor of seven with deionized water) to remove surface contaminants present from manufacture followed by a water rinse and allowed to dry under ambient conditions. Approximate 2% (w/v) coating solutions were prepared by adding a mixture of ethanol:water:methylene chloride (82:6:12) to a vial containing approximately 0.3 g of the appropriate substituted n-alkyldimethyalkoxysilane material(s). Several drops of glacial acetic acid were then added to the RT mixture to adjust the pH to approximately 5 to generate the corresponding silanol. The vial was placed on a mechanical shaker for 10 to 15 min at RT to allow for the cleavage reaction to occur. The solution was subsequently applied to the Al panel via a Badger 250-2 basic spray gun and allowed to stand at RT for approximately 1 h prior to an ethanol rinse to remove residual solvent, unreacted material, and self-condensation products. The coated panel was air dried overnight under

ambient conditions and subsequently placed in an air oven at approximately 110°C for approximately 0.25 h.

2.5 Silica NP functionalization

Silica NP (average diameter: 100 nm) were functionalized with select substituted n-alkyldimethylsilyl moieties by immersion in a solution of the hydrolyzed precursor alkoxysilane. The hydrolysis solution consisted of a 95% ethanol-5% water mixture adjusted to a pH of approximately 5 with glacial acetic acid. To this solution a substituted n-alkyldimethylalkoxysilane was added to afford a 10% (w/w) mixture that was agitated on a mechanical shaker at RT. This solution was then added to a petri dish containing the silica nanoparticles to a volume sufficient to cover the nanoparticles that was then covered to allow for mild agitation ensuring complete wetting of the nanoparticles. This mixture was allowed to stand for approximately 5 min at RT to allow for particle functionalization followed by evaporation of the solvent. Methylene chloride (5 mL) was subsequently added to the residue and the mixture transferred to a centrifuge tube. The mixture was centrifuged at approximately 2000 RPM for 5 min to separate the reaction by-product that was subsequently removed using a Pasteur pipet. This process was repeated followed by air drying of the functionalized nanoparticles for 2 h at RT.

2.6 Characterization

2.6.1 Functionalized silica NP

Differential scanning calorimetry (DSC) was performed on a Setaram DSC-131 at a heating rate of 5°C/min, which has been demonstrated to enable crystal growth to occur during cooling. [45-47] To erase any thermal history, each sample was held at 30°C for 20 min followed by an isothermal hold at 200°C for 15 min. The sample was then cooled to -50°C and held for 40 min followed by heating to 200°C during which time data was collected. The sample was held at 200°C for 20 min then cooled to RT. Thermogravimetric analysis (TGA) was performed on a Seiko Instruments TG/DTA 220 in air at 5°C/min. Samples were heated to 100°C and held for 30 min to remove bound water followed by heating to 550°C. To confirm silane functionalization on the silica NP, transmission FTIR of the sample suspended in a potassium bromide matrix was performed using a Thermo Nicolet NEXUS 670 FTIR spectrometer.

2.6.2 Coatings

A First Ten Angstroms FTA 1000B goniometer was used to acquire contact angle data at RT using an 8 μL droplet of water deposited on the sample surface. Tilting axis measurement was utilized to determine receding contact angle (θ_R). Interfacial tension measurements were made on a suspended droplet prior to testing to verify liquid purity and precision of the focused image. Contact angles were determined by droplet shape analysis.

Surface roughness of uncoated and coated Al panels was determined using a Bruker Dektak XT Stylus Profilometer. Measurements were conducted using a 12.5 μm tip at a vertical range of 65.5 μm with an applied force of 10 mg. Data were collected over a 0.5 mm length with a 50 s duration at a resolution of 0.033 μm/point. Five single line scans at different locations were collected and processed using a two-point leveling subtraction. The resultant mean roughness (R_a) and root mean square roughness (R_q) values were then determined.

2.7 Simulated in-flight icing testing

A simulated in-flight icing environment was provided by the AERTS facility (Fig. 5) located at PSU. A specialized set of rotor blades designed to measure impact IASS were attached to an 89.5 KW motor affording a rotor diameter of 2.74 m. For IASS determination, test specimens were cut from coated Al sheets (10.16 cm x 15.24 cm) and mounted on a beam located at the rotor tip that bends under centrifugal loads. Voltage measured across strain gauges at the beam root was used to measure ice load. When the accreted ice sheds under the centrifugal loads, the beam springs back and the voltage increases. Gauges were calibrated using the 0 Hz voltage and operation voltage for the known tip mass. The ice load was determined from the sharp voltage increase measured at the time of natural ice shedding.

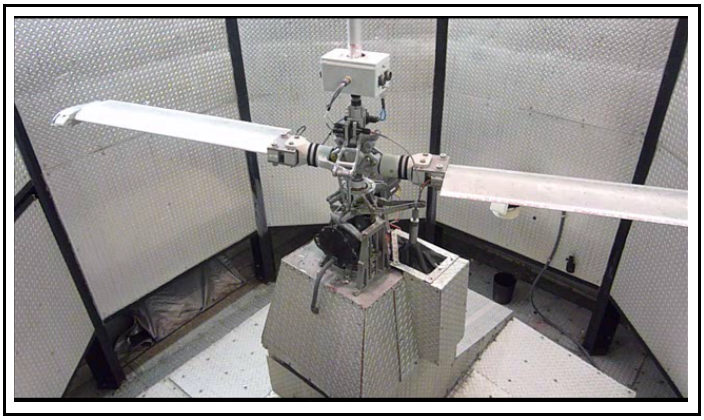

Fig. 5 AERTS at PSU.

The ice-shed area was measured by sketching the free-of-ice area onto graph paper and IASS calculated by dividing the ice load by the measured area. For a detailed description of the ice adhesion measurement procedure refer to [25] and [48]. Testing in this study was conducted with AERTS operating at 6.67 Hz (tip speed of 229 km/h) at temperatures of -8, -12, and -16°C within the FAR Part 25/29 Appendix C icing envelope [26]. The icing cloud density (i.e., LWC) was 1.9 g/m^3 and consisted of water droplets with a MVD of 20 μm. Based on the rotor configuration, two specimens were examined during each test run. Tests were conducted in triplicate at all three test temperatures commencing at -16°C and ending at -8°C using the same two specimens throughout.

2.8 Statistical data treatment

Statistical comparison of all IASS test results discussed in Section 3 was performed using an analysis of variance (ANOVA) single factor test to evaluate more than two means with an α of 0.05. The null hypothesis was that the populations were all equal and occurred when $F < F_{critical}$ and $p > \alpha$. The null hypothesis can be rejected if $F > F_{critical}$ or $p < \alpha$ since statistically significant differences exist between some of the population means. If the null hypothesis was rejected, then student t-tests assuming unequal variances were performed at an α of 0.05 to determine statistical differences as suggested by ANOVA test results. The standard accepted value for two means differing statistically is a p value < 0.05.

3. Results and Discussion

3.1 Why substituted n-alkyldimethylalkoxysilanes?

Water can interact with a surface through non-HB (i.e., non-polar) and HB (i.e., polar) effects. The HB effect can be further broken down as donor and acceptor interactions. To evaluate the effect each of the various HB type had upon the IASS of impact ice, substituted n-alkyldimethylalkoxysilanes containing an appropriate terminal functionality were utilized to coat Al substrates. Substituted alkoxysilanes are generally applied to a substrate (e.g., metal, plastic, fiber) surface to modify properties such as wettability, surface energy, and adhesion between materials [49-52]. Similar to carbon in the number of substituents that can bond to it, the silicon atom of an alkoxysilane can possess one, two, or three alkoxy groups in addition to bonding to a substituted carbon atom. The choice of the number of alkoxy substituents determines whether a monolayer, or potentially a multilayer (approaching a thin polymer) coating would be generated on the substrate surface. Hydrolysis of a trialkoxysilane generates the corresponding trisilanol that can react with an appropriate functionality (typically hydroxy groups) present on the substrate surface to form a single (i.e., oxane) bond between the substrate and the compound. The two remaining silanols can either react with a neighboring silanol, with another surface functionality present on the substrate surface, or remain unreacted on the surface. Additional trisilanols can subsequently react with these residual groups to generate a surface that is typically polymeric in nature and can be several layers thick. For this work, the presence of unreacted silanols would complicate the evaluation of how the different types of HB

influence IASS. Dialkoxysilanes would form surfaces comparable to those obtained with the trialkoxysilanes. However, the presence of a single alkoxy group, as present in a monoalkoxysilane, forms a monosilanol upon hydrolysis that, when deposited onto the substrate surface, leads to the formation of a monolayer. The importance of this monolayer formation is that the effect of the appropriate functionality on the terminus of the parent monoalkoxysilane has upon IASS would not be clouded by HB (D/Ac) contributions due to hydroxy groups of the remaining silanols present as described for the other two cases. Therefore, substituted n-alkyldimethylalkoxysilanes were chosen for this study where the terminal group on the n-alkyl chain with respect to the silicon atom on the opposing end was varied from a non-HB (i.e., methyl, A), HB (D/Ac) (i.e., hydroxy, H), and HB (Ac) (i.e., methoxy) characteristics.

3.2 Synthesis of poly(n-alkyldimethylsiloxane)s as precursors to n-hydroxyalkyl-1-dimethylsilanols

With the exception of C3A, which was commercially available, the substituted monoalkoxysilanes [i.e., non-HB and HB (Ac)] shown in Fig. 4 were prepared by known chemical reactions with the structures confirmed by FT-NMR and ATR-FTIR spectroscopies [39]. The preparation of hydroxy terminated alkoxysilanes required that the terminal hydroxy group of the vinylic alcohol be masked. If left unmasked, the hydroxy group could react with the hydrogen functionality present on the silane under hydrosilation conditions. Therefore, the vinylic alcohols were reacted with chlorodimethylsilane to afford 1-n-alkyldimethylsilanes (Fig. 6) to form an A-B monomer [39]. An A-B monomer is difunctional and for n-alkenyldimethylsilane, the two reactive functionalities are the vinyl and Si-H groups [53]. These A-B monomers were then reacted under hydrosilation conditions to afford the corresponding polymers –

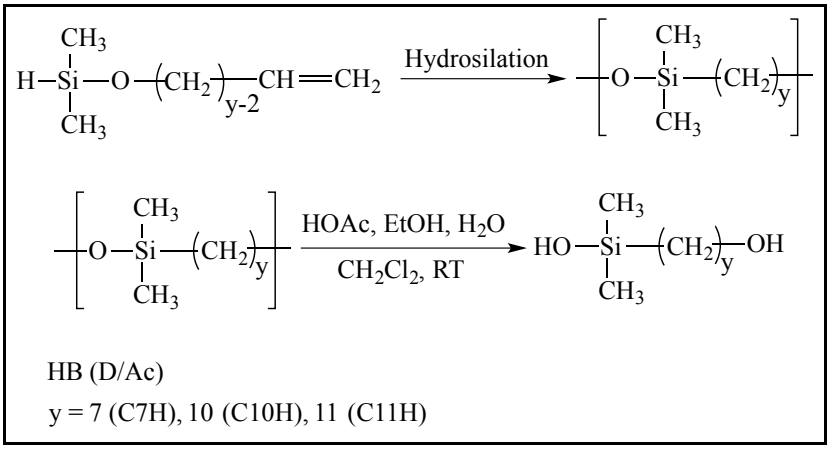

Fig. 6 Hydrosilation product and subsequent hydrolytic cleavage to form HB (D/Ac) monosilanol deposition material.

poly(n-alkyldimethylsiloxane)s [54]. Under the acidic hydrolysis conditions used to prepare the solution for spray coating the Al substrate, the hydroxy and silanol groups were generated simultaneously due to the hydrolysable nature of the siloxane linkage in the polymer backbone. Regeneration of the polymer by reaction of the hydroxy group on the terminus of the n-alkyl chain and silanol would be anticipated to be minimal under the reaction conditions employed since the resultant alkoxysilane bond would be unstable. There is a potential for the formation of self-condensation products between two monosilanols; however, this has been reported to be slow - taking up to several hours [52].

3.3 Formation of substituted n-alkyldimethylsilyl surfaces on Al

As depicted in Fig. 7 for the non-HB materials, the resultant monosilanols generated from the hydrolytic cleavage of the substituted monoalkoxysilanes condense with hydroxy groups present on the Al substrate that was precleaned with a solution to remove the oxide surface present and oils, etc. from manufacture, forming a covalent (i.e., oxane) bond. The HB (Ac) coating was prepared in a similar fashion. HB (D/Ac) coatings were obtained from the hydrolytic cleavage product shown in Fig. 6 that would condense with the

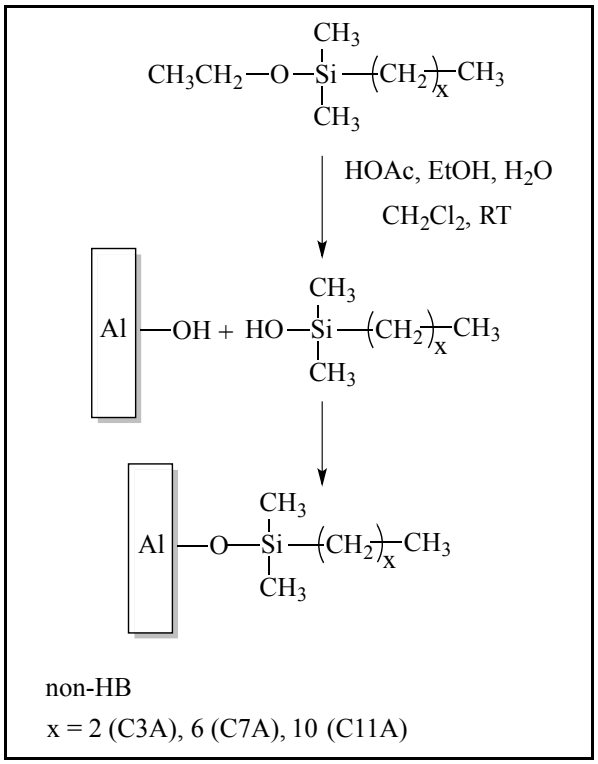

Fig. 7 Reaction scheme for deposition of substituted 1-n-alkyldimethylethoxysilane on Al surface.

Al substrate as depicted in Fig. 7. After standing for approximately 1 h after spray deposition, the coated surface was rinsed with ethanol to remove unreacted material which is a typical method to remove excess material [49].

Structures of the resultant coatings on the Al substrate are illustrated in Fig. 8 along with the corresponding HB characteristics with respect to water. The terminal methyl group of the non-HB moiety does not interact with water whereas the terminal hydroxy and methoxy functionalities exhibit HB (D/Ac) and HB (Ac) interactions, respectively. Due to the variance of the n-alkyl chain length present in the non-HB and HB (D/Ac) series and between series, the effect of molecular chain flexibility upon IASS was also examined in this study. Flexibility in a material can provide local stresses that encourage crack growth thereby reducing ice adhesion strength [55]. The compounds in Fig. 8 are depicted as being normal to the substrate surface. However, it has been reported that alkyl groups connected to a silicon surface via a carbon-silicon bond lie at an angle [56]. The tilt angle of the materials used in this work to the Al surface was not determined.

3.4 Substituted n-alkyldimethylsiloxane surface density

Molecular layers comprised of aliphatic chains with polar functionalities at one or both ends, such as surfactants, phospholipids, fatty acids, etc., often undergo self-assembly into a variety of configurations: micelles, lamellar layers, vesicles, etc. [57]. For the purpose of the work described here, the use of silanes with a single reactive functionality prevented the formation of multilayered surfaces, which reduced the potential complexity of the surfaces generated for ice adhesion testing. These surfaces though could still undergo oriented interactions resulting in the presence of phase-like behavior. Such interactions are well documented in phospholipid bilayer systems where the phases are described as gel and liquid phases with the degree of order and diffusion rates being the greatest disparities between states [58]. Even within the liquid phase, often ordered and disordered states exist, each of which exhibits different properties as a result of the strength of interaction between neighboring molecules. Thus, with the similarity of the systems investigated in this work, and those known to exhibit this type of phase behavior, the thermal behavior of these materials was evaluated. Although the ice adhesion experiments were performed on surfaces

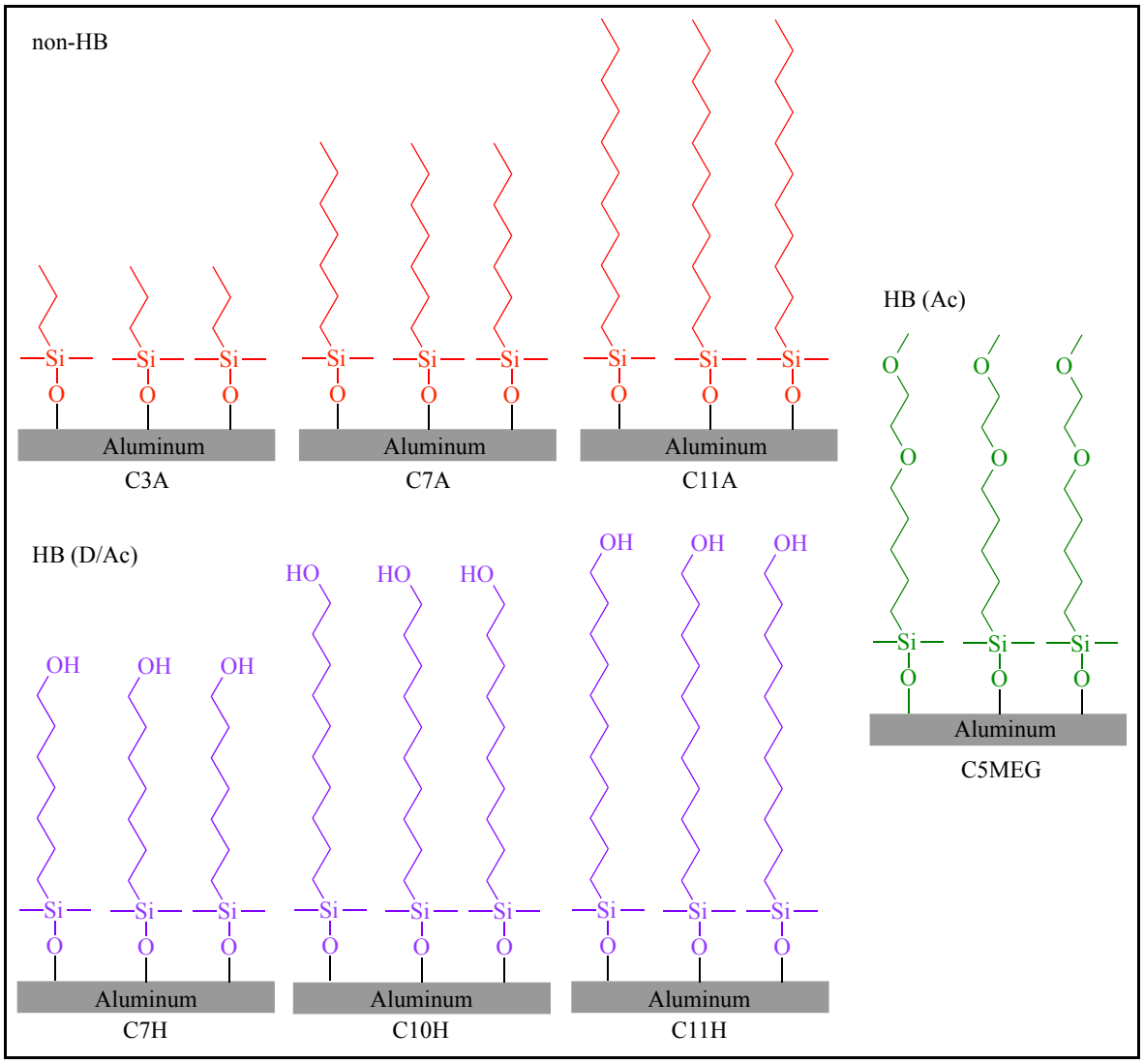

Fig. 8 Illustration of substituted n-alkyldimethylsiloxanes on Al substrate.

functionalized with the substituted silanes described herein, the silane density on a flat surface was not sufficient to investigate its thermal behavior using traditional techniques. Therefore, 100 nm silica NP were functionalized with the same substituted n-alkyldimethylalkoxysilanes. At this size, the relative curvature experienced by a silane molecule was nearly equivalent to that of a flat surface. The silica NP were functionalized by immersion in an ethanolic solution of the hydrolyzed alkoxysilane. Functionalization of the silica NP was verified using transmission FTIR (Fig. 9).

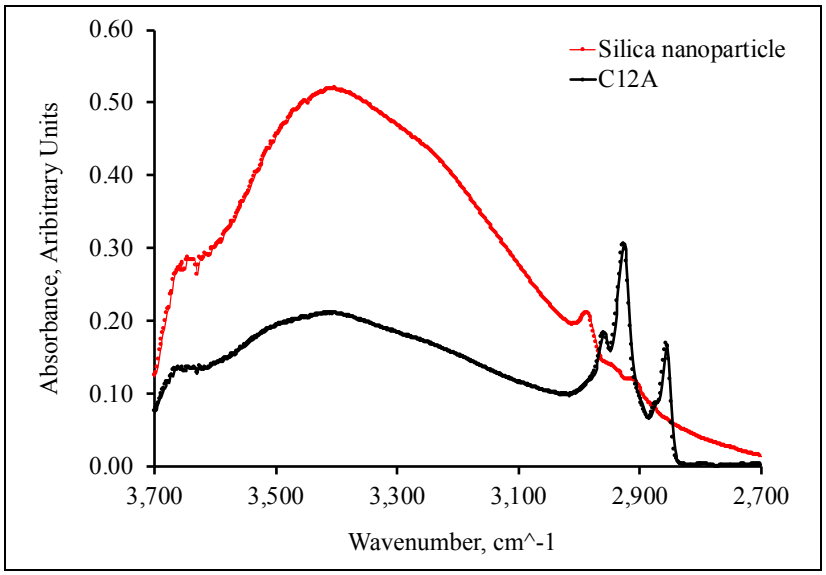

Fig. 9 Transmission FTIR spectra for hydrolyzed silica NP (red line) and n-dodecyldimethylsilyl (C12A) functionalized silica NP (black line) from 3700-2700 cm^{-1}.

Silica NP exposed to the same conditions but without the presence of a silane were used as a control. The intensity of the broad –OH stretch (3500-3300 cm^{-1}) present in the blank spectrum (Fig. 9) diminished upon functionalization concomitant with new peaks appearing around 2900 cm^{-1} that were indicative of aliphatic C-H stretching bands. These bands were associated with the n-alkyldimethyl functionalities suggesting that functionalization had occurred between the substituted n-alkyldimethylsilanols and the NP surface hydroxy groups. A graph of relative absorbance values as a function of chain length at 2900 cm^{-1} for C#A samples relative to that of the treated silica NP is shown in Fig. 10. The data followed an exponential relationship with relative absorbance increasing with increasing aliphatic chain length. Data for the C#H functionalized series (not shown here) did not exhibit a defined dependence as evident by R^2 = 0.49.

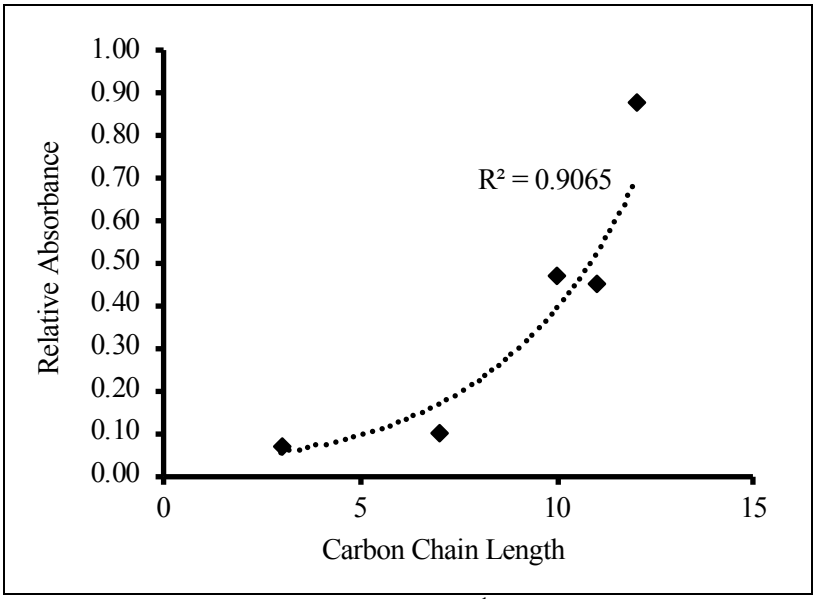

Fig. 10 Relative absorbance at 2900 cm^{-1} normalized to treated silica NP.

The first derivative of the DSC thermogram was used to determine the phase behavior of the functionalized silica NP. Although literature suggested that the phase transition temperature should increase as the chain length increased for the aliphatic silane series this relationship was not observed over the range of aliphatic chain lengths investigated here (Table 1). The orientation of these functionalities as well as the loading level on the silica NP has been reported to influence the respective thermal properties [59]. Although silica NP functionalized with C10A exhibited a lower transition temperature than C12A and C11A, the transition temperature measured for C7A was much higher. As will be discussed, this may be explained by the different functionalization density for the C7A surface relative to the other materials. No phase transition was observed for C3A functionalized silica NP. A decrease in phase transition temperature was observed between the C10H and C11H functionalized silica NP while the difference was negligible between the C7H and C10H samples. Comparing aliphatic and hydroxy-terminated species of the same length was also of interest to ascertain the orientational impact that the HB(D/Ac) interactions had for the hydroxy-terminated materials. Due to the HB (D/Ac) interactions present for the hydroxy-terminated systems, the transition temperatures were higher than the non-HB compounds of the same carbon chain length, except for the C7 series. For comparison, melting temperatures for analogous straight-chain alkanes and terminal carbon-substituted alcohols are included in Table 1.

Table 1. Phase Transitions of Functionalized Silica NP
Compared to Analogous Small Compounds

n-alkyl carbon chain length	Phase Transition, °C			
	non-HB	Alkyl Equivalent	HB (D/Ac)	Alcohol Equivalent
7	3	-91[60]	-13	-34[64]
10	-22	-30[61]	-14	7[65]
11	-14	-26[62]	-6	11[66]
12	-15	-10[63]	not prepared	24[67]

Literature suggests that the way these functionalities are oriented and the silane loadings on the particles influences their thermal properties. [13] Therefore, TGA was performed on the silane-functionalized silica NP to determine the population density of silanes on the NP surface. Pristine silica NP and NP immersed in the ethanolic solution, without the presence of a silane, were analyzed. The similarity of temperature-dependent weight loss for these two samples suggested that there was no significant silica NP modification occurring during the hydrolysis process in the absence of a silane. An approximate mass loss of 4% was observed in the RT to 100°C region for all samples corresponding to water loss (Fig. 11). For silane-functionalized silica NP, a significant weight loss event observed above 200°C suggested silane degradation/detachment from the surface.

Therefore, TGA data from 150 to 500°C was used to determine silane grafting density, σ, and % functionalization. Once the percent weight loss was determined for each sample, the silane grafting density was calculated (see Appendix). According to literature, the average density of hydroxy groups on a silicon dioxide surface is approximately five (5) -OH groups/nm^2 and is independent of how the particle was prepared or the structural characteristics of the oxide [16]. This provided an upper limit of the number of molecules that can bond to the silica surface assuming the attachment was restricted to a 2-D plane. The functionalized NP had an average diameter of 100 nm and were large enough that this assumption should hold as a reference value when calculating percent silane functionalization on the silica NP (see Appendix).

Estimates for silane loadings from literature suggest that the minimum amount of monolayer coverage loading by silanes for particles < 1 μm in size is 1.5%. [2] Calculated silane grafting densities for the silica NP described above are shown in Table 2. The data suggested an interesting point regardless of silane end groups: silanes with longer chains (C10, C11, C12) appeared to be more densely packed than shorter, bulkier molecules (C3) on the silica surface with the exception of C7A and C7H where C7H was of

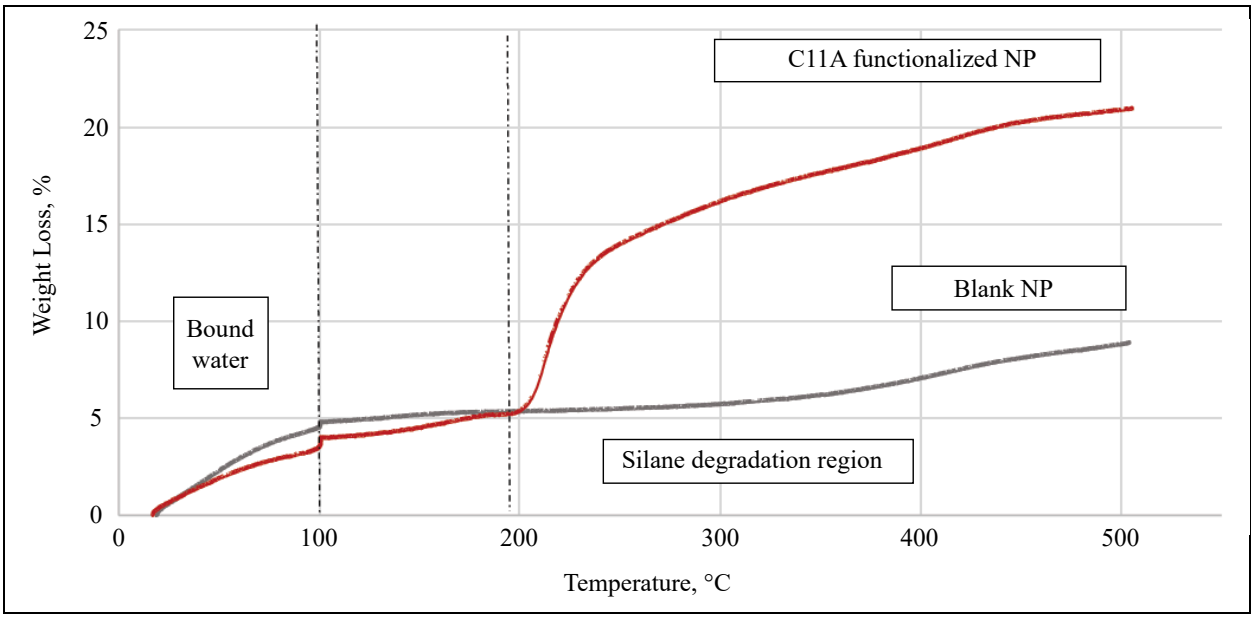

Fig. 11 Dynamic TGA thermogram of blank and C11A functionalized NP.

comparable magnitude to the longer species. Other phenomena that may be occurring is that the surface may have "seeding" sites that establish chain orientation and allow for closer packing of molecules on the surface [3,4].

The radius of gyration, R_g, for each molecule was calculated using Flory theory to further explore how the silane molecules were oriented on the silica NP surfaces according to: [17,18]

$$R_g \sim N^{v}b \qquad (1)$$

where N is the number of monomers, v is the Flory exponent, and b is the length of the oligomer in which case is calculating the radius for just one monomer. Since silanes are readily soluble in alcohol solutions, the value used for v is that of a good solvent, 3/5. Each silane was drawn in Hyperchem Lite [68] and geometrically optimized to determine b. These values were utilized to determine a molecular areal occupancy for comparison against grafting density of the molecules on the silica surface (Table 2).

Table 2. Silane NP Surface Functionalization Properties Determined from TGA Data

Silane	σ, molecules/nm^2	Functionalization, %	Radius of Gyration (R_g), nm	tethered density parameter, Σ
C3A	0.08	2	0.7	0.13
C7A	0.05	1.3	1.2	0.24
C10A	0.34	7	1.6	2.75
C11A	0.21	4	1.7	2.04
C12A	0.44	9	1.9	4.87
C7H	0.29	16	1.3	1.65
C10H	0.68	14	1.7	6.35
C11H	0.48	10	1.9	5.12

A wealth of literature on computational studies investigating the dynamics of brush formations on flat surfaces [14,19] as well as spherical surfaces exists, but very little experimental data on polymer brush behavior on spherical silica surfaces is available. Therefore, in order to characterize the conformation of the silane oligomers studied here, the silica NP were estimated as planar surfaces. For flat surfaces, there are three generally accepted conformations of tethered polymer brushes that are related to a reduced tethered density parameter, Σ :

$$\Sigma = \sigma\pi R_g^2 \qquad (2)$$

When $\Sigma < 1$, the polymer brush is considered to be in a mushroom conformation characterized by weak interactions between polymer chains. When $\Sigma \geq 5$, the polymer is considered to be in a highly stretched conformation characterized by strong interactions. For $1 < \Sigma < 5$, the system is considered to be in a cross-over regime between these two extreme cases. Interestingly, the Σ values determined for the aliphatic systems appear to exhibit a transition from the mushroom conformation to an extended conformation (Fig. 12). The transition appears to occur between carbon chain lengths of eight and ten atoms and the data correlated well with a sigmoidal function. Considering the differences between terminal group chemical functionality, the data indicated that species with hydrophilic groups in their terminus were consistently more closely packed than their hydrophobic counterparts. This suggested there was stretching of chains to minimize segment to segment interactions. The hydroxy groups at the end of the chains were likely undergoing HB interactions enabling greater functionalization densities and limiting chain movements.

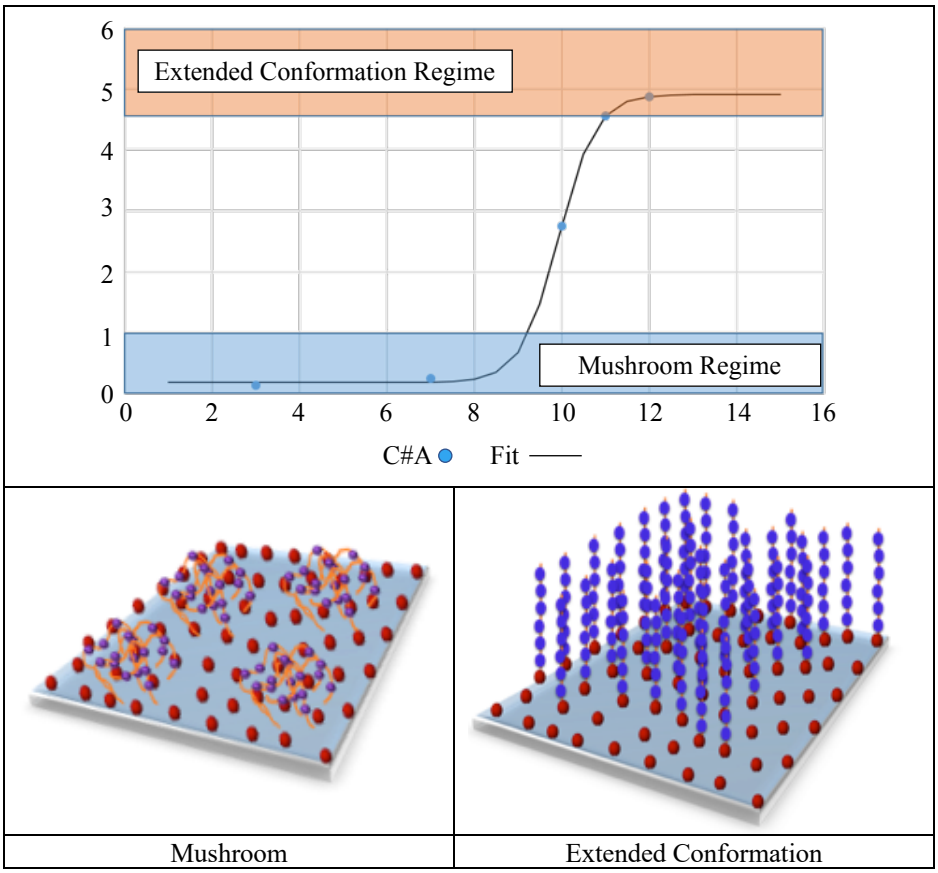

Fig. 12 Calculated Σ values determined for the aliphatic silane (C#A) functionalized silica NP.

3.5 Neat substituted n-alkyldimethylsiloxane coated surfaces

Deposition of a single substituted n-alkyldimethylalkoxysilane component onto the Al surface as depicted in Fig. 7 allowed for the evaluation of neat (i.e., homogeneous) coatings (Fig. 8) regarding IASS. Surface roughness of the coated Al panels was determined with the data reported in Table 3 with respect to HB type. The similar values of the coated substrates ensured that the individual coated surfaces were of comparable roughness to enable data comparison. According to ASTM A480 (Finish #7), the surface roughness data for the Al control and the coated surfaces in Table 3 suggested a smooth surface [69].

The θ_R with respect to water was determined on the coated Al panels with the data reported in Table 3 according to HB type. Contact angle goniometry allowed for the determination of surface functionality effects from the monolayer generated on the Al from the respective substituted monosilanols with water. Comparing the θ_R for water, the general trend was non-HB ≥ HB (Ac) > HB (D/Ac). Within the non-HB series (i.e., C3A, C7A, and C11A), the C11A surface had a lower value compared to the shorter chain members of the series and may be a result of packing density as described above. The lower θ_R for water for C11A compared to C3A and C&A may be associated with Σ (Table 2) that suggested C11A may exist in a cross-over regime between mushroom and extended conformation while C3A and C7A were in a mushroom conformation. The θ_Rs of water on the C10H and C11H surfaces followed the expected trend for HB (D/Ac) compared to C11A of the non-HB surfaces. The larger θ_R for water for C11H compared to C10H is presumably due to an odd-even carbon chain length effect. Molecular dynamics (MD) simulations investigating the effect of alcohol-terminated monolayers of uniform length upon ice growth found that an odd number of carbon atoms in the alkyl chain of the material making up the monolayer provided a smooth surface whereas an even number was found to have a higher surface roughness due to tilting of the hydroxy functionality [70]. This higher molecular roughness may allow for water to spread more upon the C10H surface. The θ_R for water of the C7H surface was significantly larger than the longer chain members of the HB (D/Ac) series and appeared to be more in-line with the non-HB series. From Table 2, Σ suggests C7H exists in a cross-over area between the mushroom and extended conformation regimes while C10H and C11H exist in an extended conformation regime. Comparing the θ_R for water of the C7H and C7A coatings found that the expected trend for the θ_R for water with respect to the hydroxy [HB (D/Ac)] and methyl (non-HB) terminated species,

Table 3. Surface Characterization of Neat Coatings

Al Surface	Receding Water Contact Angle (θ_r), °		Mean Roughness (Ra), μm		Root Mean Square Roughness (Rq), μm	
	Avg[1]	Stndev[2]	Avg	Stndev	Avg	Stndev
Control (Uncoated)	58	14	0.326	0.048	0.388	0.060
non-HB						
C3A	87	2	0.324	0.078	0.406	0.103
C7A	88	2	0.282	0.105	0.354	0.130
C11A	78	5	0.702	0.298	0.800	0.323
HB (D/Ac)						
C7H	73	3	0.512	0.013	0.634	0.021
C10H	24	2	0.708	0.100	0.854	0.108
C11H	31	2	0.320	0.040	0.392	0.044
HB (Ac)						
C5MEG	79	1	0.390	0.199	0.466	0.217

1. Average
2. Standard deviation

respectively, was followed. Here Σ (Table 2) suggests that C7H exists in the cross-over regime (mushroom and extended conformations) while C7A exists in the mushroom regime. C11A (non-HB), C10H and C11H [HB (D/Ac)], and C5MEG [HB (Ac)] were of comparable n-alkyl chain length thus allowing for comparison of the end group functionality. The trend for the Θ_R for water with respect to these surfaces was non-HB ~ HB (Ac) > HB (D/Ac). The similar θ_R for water of the C5MEG and C11A surfaces were not expected since the former can participate with water through HB (Ac) interactions. The Σ (Table 2) for C10H suggests a highly stretched conformation while C11A would exist in the cross-over regime between the mushroom and extended conformations. The Σ for C5MEG was not determined but given the similar θ_R for water with C11A it would be anticipated to exist in the cross-over regime as well.

IASS results for uncoated Al and Al substrates coated with a single (i.e., neat) substituted n-alkyl-dimethylsiloxane compound on the Al surface are shown in Fig. 13. Since two specimens of each material were used during the entire test regime and test runs at each temperature were conducted in triplicate, large deviations in the six measurements at the same temperature suggested possible degradation or removal of the coating from the substrate. In addition, an increase in IASS as the test temperature increased using these same specimens likewise suggested that the coating may have undergone some degradation or partial removal.

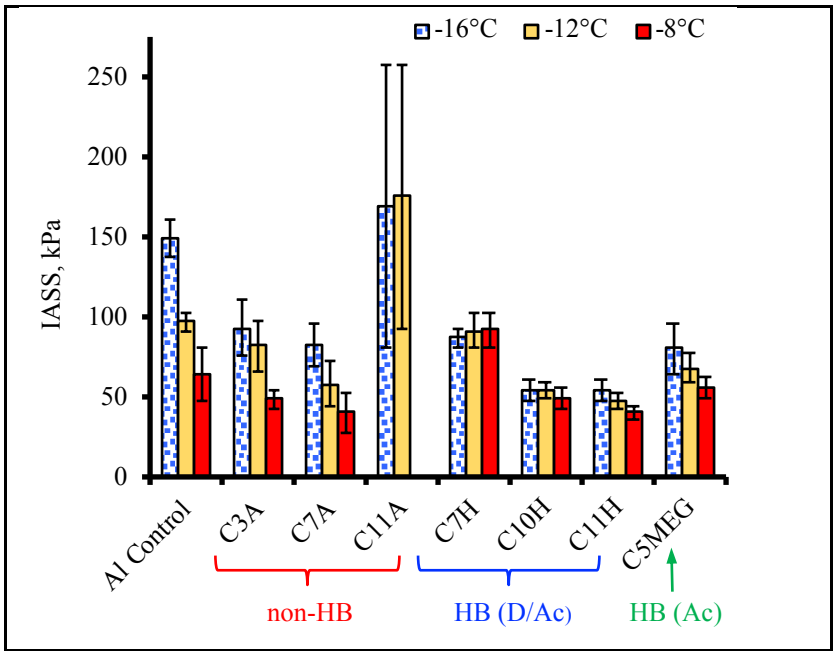

Fig. 13 IASS of neat substituted n-alkyldimethylsiloxane coating compositions compared to uncoated Al.

The accepted standard deviation in the AERTS is 20% due to the nature of the test. To determine if the IASS results obtained for the coatings (Fig. 13) differed statistically from the uncoated Al control at each temperature a single factor ANOVA was performed. The p-value was < 0.001 suggesting that some of the coatings differed statistically from the control and one another and was also supported by F being greater than $F_{critical}$. The data however suggested that some of the coatings did not differ therefore a student t-test was performed. In general, $p \leq 0.003$ suggested that the IASS for the coatings differed from the control at the various test temperatures. Exceptions were 1) C3A at -8 and -12°C ($p = 0.07$ and 0.147, respectively), 2) C11A at -12 and -16°C ($p = 0.123$ and 0.308, respectively), 3) C7H at -12°C ($p = 0.161$), 4) C10H at -8°C ($p = 0.074$), and 5) C5MEG at -8°C ($p = 0.194$).

Generally, the average IASS shown in Fig. 13 was observed to decrease with increasing temperature as expected. A single factor ANOVA comparing the IASS results of a coating at each test temperature determined that the values differed statistically ($p \leq 0.008$) with the exception of 1) C7H ($p = 0.645$) and 2)

C10H ($p = 0.260$). A student t-test performed on the various temperature comparisons for these two compositions found that the values did not differ statistically. Since C11A was tested only at -16 and -12°C, a student t-test was performed that resulted in a p-value of 0.458 suggesting that the results did not differ statistically. The average IASS for C11A and C7H was observed to increase as temperature increased suggesting coating degradation or removal from the substrate. A further indication that the C11A coating may have experienced degradation or removal from the surface is provided by the large standard deviation at the two test temperatures and will be discussed in Section 3.5.1. The standard deviation for C7H however was comparable to that of other tested materials implying that coating degradation or removal may not have occurred. In addition, experimental results obtained for mixed coatings, and discussed later, questions whether degradation or removal are the only reasons that could explain the reversal of the expected IASS temperature dependence for these two coatings.

The goal of this study was to evaluate the effect that HB characteristic and molecular flexibility had upon IASS. Accepting the statistical results that some of the coatings did not differ statistically, a comparison of the average values was performed to determine trends. As discussed earlier, ARF is a better comparison of the data and was determined for each of the neat coating compositions with the results shown graphically in Figs. 14 -18. ARF was determined on average IASS values from the coated and uncoated Al surfaces. Dashed and/or dotted lines connecting ARF values at the various test temperatures are for illustrative purposes only.

3.5.1 Non-hydrogen bonding coatings

Statistical comparison of the IASS results for the non-HB in Fig. 13 was conducted for the three coatings. A single factor ANOVA performed on the -12 and -16°C values resulted in the data at -12°C to differ statistically ($p = 0.006$) while at -16°C no statistical difference was observed ($p = 0.078$). Since the IASS results for C11A had a large standard deviation, a student t-test was performed comparing the C3A and C7A IASS data at the three test temperatures. For the -12 and -16°C data, the coatings were determined to differ statistically ($p = 0.006$ and 0.027, respectively). However, the data at -8°C for these two coatings were determined to not differ statistically where $p = 0.123$. The data at each of the three test temperatures were then compared for each individual coating, C3A and C7A, using a single factor ANOVA resulting in $p \leq 0.003$ suggesting that the data differed statistically. However, statistical evaluation of the C11A IASS data using the student t-test found that the results obtained at the two test temperatures did not differ statistically ($p = 0.458$).

To further examine the data and identify trends, the average IASS results were used to determine ARF values for each of the coatings at each temperature with the results presented in Fig. 14. The observed trend was C7A > C3A > C11A and suggested that a change of ± four (4) methylene groups with respect to C7A influenced non-HB coating performance. A decrease in n-alkyl chain length (i.e., C3A) relative to C7A presumably allowed for more interaction of impacting SCWD with the underlying Al substrate and higher IASS. The θ_R for water for C3A and C7A though were comparable as reported in Table 3.

The average IASS data for C11A (Fig. 13) showed that IASS increased with increasing temperature in opposition to the expected IASS trend with respect to temperature. Since testing commenced at -16°C, the C11A coating may have experienced degradation or removal from the surface resulting in an increase in IASS at -12°C as implied by the large standard deviation at both test temperatures. To determine if the coating was indeed undergoing degradation, samples were examined for surface roughness initially then after two and six runs at -16°C. It was found that the surface roughness increased approximately 40% after the first two tests with a further 3% increase after six tests. If removal of the coating from the surface was indeed taking place one would anticipate that the IASS and ARF values at -12°C would approach that of the control surface which is not the case. To recall, data on silica NP suggested that Σ for C11A (Table 2) existed in a cross-over regime between the mushroom and extended chain conformations whereas C3A and C7A were in the mushroom regime. The extended conformation of C11A implied by Σ suggests that the alkyl chain could serve as mechanical clamping sites for accreting ice leading to coating degradation as seen with the large standard deviation (Fig. 13). The Σ value is based on the packing density for alkyl chains that have equilibrated to the lowest energy state. Outside influences such as ice accretion would not be expected to alter this state, but this was not studied here.

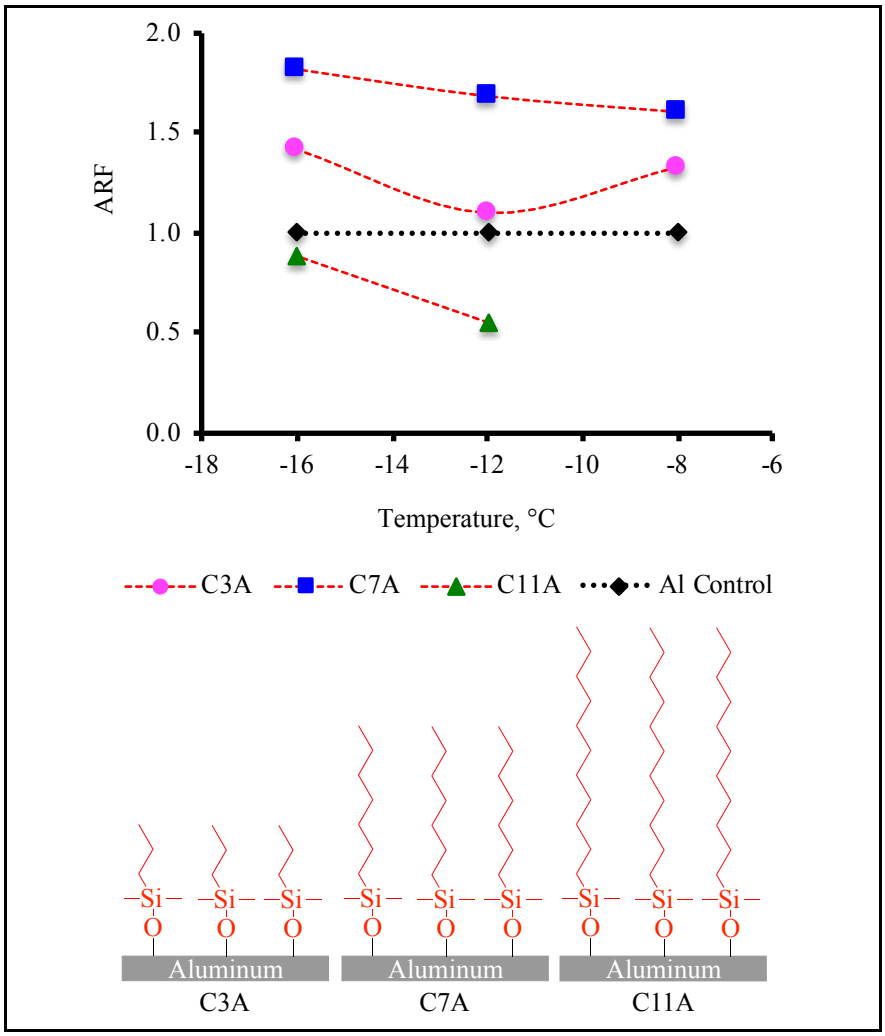

Fig. 14 ARF of neat non-HB coating compositions compared to uncoated Al.

3.5.1.1 Comparison to small non-hydrogen bonding compound analogs

To aid in explaining the results, the water solubility and melting point of analogous aliphatic hydrocarbons, with respect to the non-HB coatings, were compared and are shown in Table 4. The greater water solubility of propane suggests that SCWD may interact more effectively with C3A than C7A. In addition, the melting points of propane and heptane suggest that the C3A and C7A coatings may be in a "fluid-like" state under the simulated impact icing conditions. This may be a possibility given that the precursor n-substituted alkyldimethylalkoxysilanes used to prepare these coatings were liquids. It should be noted that the water solubility and thermal properties of the coatings examined in this study were not determined and are thus inferred. Based on the data in Table 4, it would have been anticipated that the IASS/ARF results for C11A, with an increase of four methylene groups relative to C7A, would have been the best for this series. The water solubility of undecane (analogous hydrocarbon to C11A) in Table 4 is two orders of magnitude lower than heptane suggesting that this may be the case. [62] The melting point of undecane shown in Table 4 though was significantly higher than the other two hydrocarbons in Table 4, but still lower than that of the SCWD impact icing temperatures investigated. Since the precursor alkyldimethylalkoxysilane used in the preparation of the C11A coating was a liquid as the other materials, it would be anticipated that C11A may be in a "fluid-like" state as well. However, the expected improved performance relative to the other two coatings in this series was not the case, with C11A being the worst performer. As shown in Table 3, the θ_R of water for C11A was slightly lower compared to the other two coatings in this series even though the water solubility of the analogous hydrocarbon was significantly lower (Table 4). Due to the larger size of C11A compared to the other non-HB coatings, the packing density

Table 4. non-HB Coating Comparison to Analogous Hydrocarbon

Coating	Analogous Hydrocarbon	Water solubility at 25°C, mg/mL	Melting Point, °C
C3A	Propane[71]	0.0624	-188
C7A	Heptane[60]	0.0034	-91
C11A	Undecane[62]	0.000044	-26

may differ. This may be indeed the case when the σ value (Table 2) for C11A was an order of magnitude greater than C3A and C7A. In addition, the results suggested that C11A may exist in an extended conformation regime compared to that of the mushroom conformation for the other two coatings. A change in coating conformation due to outside influences such as ice accretion would not be expected since it is driven by packing density of the alkyl chains.

3.5.2 Hydrogen bonding (donor/acceptor) coatings

A single factor ANOVA comparison of the IASS results for the HB (D/Ac) series shown in Fig. 13 determined that the three coatings (C7H, C10H, and C11H) differed statistically at all test temperatures ($p < 0.001$). Since C10H and C11H appeared to be similar, a student t-test comparison of the IASS data of the two coatings determined the two differed with $p \leq 0.020$ at -8 and -12°C. However, at -16°C, $p = 0.479$ suggesting that the performance of these two coatings did not differ statistically. The similarity in behavior for C10H and C11H at -16°C was not surprising given the similar chain lengths, the rapidity of ice formation, and change in surface energy characteristics from impacting SCWD at this temperature. In addition, the silica NP study suggested that C10H and C11H were in the extended conformation regime while C7H existed in a cross-over regime between the mushroom and extended conformation states. Since C11A likewise resides in the cross-over regime based on the NP study, it suggests that this regime is not good for lowering IASS.

The IASS temperature data for each HB (D/Ac) coating was then analyzed using a single factor ANOVA. For C11H, the data at the three test temperatures were determined to differ statistically ($p = 0.001$). However, the data for the three test temperatures for C7H and C10H were found to not differ statistically ($p = 0.645$ and 0.260, respectively). A student t-test was then performed for the various temperature comparisons for the two coatings. The results of these comparisons were found to not differ statistically.

The trend for the HB (D/Ac) series as shown in the ARF vs. temperature graph (Fig. 15) was C11H > C10H > C7H. The slope of the line for each of the coatings in this series was observed to be similar and steeper compared to the non-HB series. This can be related to the surface tension behavior of water and ice at the various temperatures. At higher temperatures (i.e., -8°C), SCWD can remain in a liquid state for a longer period of time after surface impact leading to increased interaction with the more polar surface of this series than that of the hydrophobic non-HB materials as indicated by the θ_R for water. As temperature decreased, the reverse would be true with the HB (D/Ac) series exhibiting better performance due to the increased nonpolar characteristic of ice generated from the rapidly freezing impacting SCWD being repelled from the polar surface of the coating.

Unlike C11A in the non-HB series, the longer n-alkyl chain materials of the HB (D/Ac) series performed better, presumably due to HB interactions between the individual chains of the respective constituents of the coating. This can be likened to individual fence posts (i.e., C11A) that perform independently. When a rail is attached to the top of the individual fence posts (i.e., C11H and C10H via interchain HB) then the assembly performs in concert providing a *pseudo*-surface (i.e., hydrogen-bonded polar head-groups) above the Al surface with the aliphatic chains providing a degree of flexibility (i.e., an elastic interlayer) in between the two. This analogy is based on the fact that alcohols are known to hydrogen bond to one another whereas this is absent in aliphatic compounds of comparable chain length and manifests itself in such properties as boiling point [72]. One reason for the better performance of C11H and C10H compared to C7H may be attributed to the longer n-alkyl chain length providing this underlying flexible surface.

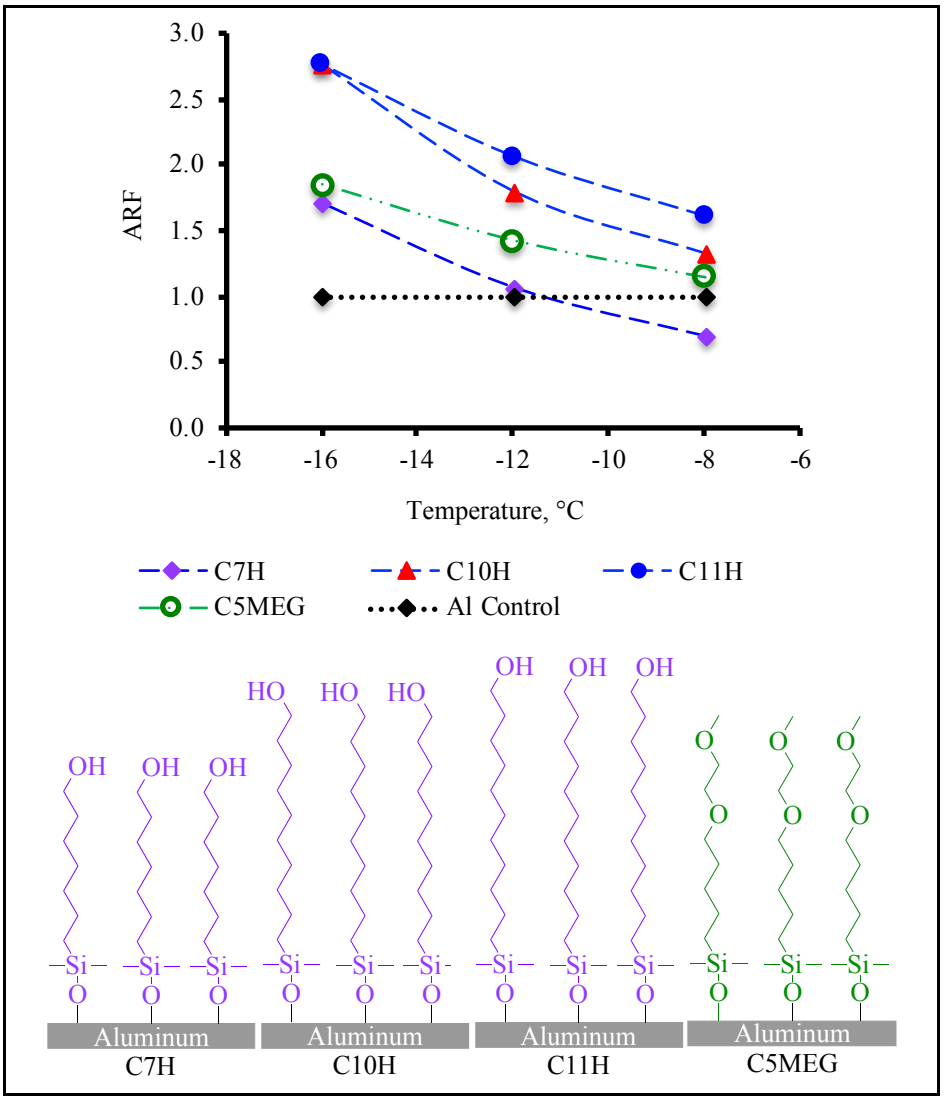

Fig. 15 ARF of neat HB (D/Ac) and HB (Ac) coating compositions compared to uncoated Al.

Flexibility in a coating has been suggested to be beneficial in decreasing ice adhesion (i.e., increasing ARF) as it can encourage crack growth in ice due to stresses being generated [55]. MD simulations evaluating differences in chain length of this series may provide insight to determining if this is the case.

As previously noted, MD simulations of hydroxy-terminated monolayers of uniform length upon ice growth suggested that an odd-numbered alkyl chain would afford a smoother surface and enable better exposure of the hydroxy group to water than an even-numbered alkyl chain [70]. In addition, it is known that IASS increases as surface roughness increases [25]. The similar alkyl chain lengths of C11H and C10H suggested that this odd-even effect may be occurring at the molecular level as well, since the ARF trend of C11H was greater than that for C10H. However, the comparable ARF results for these two coatings at -16°C suggests that this effect is negligible at this temperature. The better performance of C11H compared to C10H may likewise be attributed to differences in the surface roughness of the two coatings (0.320 vs 0.708 μm, respectively) as indicated in Table 3. To determine which effect is the reason for the difference in performance of the C10H and C11H coating, surfaces of comparable roughness would need to be further evaluated.

3.5.2.1 Small hydrogen bonding [HB (D/Ac) and HB (Ac)] compound analogs

Another possible reason for the better performance of the C11H and C10H coatings compared to C7H may be associated with the water solubility of the analogous n-alkyl alcohol as was previously discussed for comparison of n-alkyl compounds to the non-HB series. The water solubility and melting point of the three analogous small compounds are listed in Table 5 [64-66]. The longer chain alcohols (1-decanol and 1-undecanol) have comparable water solubility and are two orders of magnitude less soluble in water than 1-heptanol.

Table 5. HB Coating Comparison to Analogous Hydrocarbon

Coating	Analogous Alcohol	Water solubility at 25°C, mg/mL	Melting Point, °C
C7H	1-Heptanol[64]	1.67	-34
C10H	1-Decanol[65]	0.037	7
C11H	1-Undecanol[66]	0.019	19
C5MEG	1-Methoxybutane[73]	1 to 10	-115
	1,2-Dimethoxyetane[74]	≥100	-58

Here the argument of reduced solubility being beneficial in comparing the results for the different HB (D/Ac) series is in direct opposition with that noted for C11A and the other non-HB coatings (Table 4). Besides hydrogen bonding between the molecules as previously discussed, one needs to look at the melting points of the analogous compounds to gain some insight. To recall, the melting points of the analogous small compounds (Table 4) compared to the non-HB coatings were lower than the test temperatures employed in this study suggesting that the coatings may be in a "fluid-like" state thus allowing for better interaction with impacting SCWD. However, the melting point of the analogous alcohol, 1-heptanol, shown in Table 5 is the only one in the HB (D/Ac) series that is below the test temperatures in this study. The melting points of 1-decanol and 1-undecanol would suggest that the coatings they represent would presumably exhibit a "*pseudo*-solid-like" nature instead of a "fluid-like" behavior. Indeed, this may be the case since the precursor poly(n-alkyldimethylsiloxane)s used in the preparation of the C10H and C11H coatings were semisolids (i.e., waxes) while that for C7H was a liquid. Therefore, considering both water solubility and melting points of the analogous alcohols may afford a better understanding as to the better performance of the longer chain coatings in the HB (D/Ac) series and the differences in performance compared to C11A.

3.5.3 Hydrogen bonding (acceptor) coatings

Modification of the terminal hydroxy functionality of C10H to a methoxy group in C5MEG (Fig. 8) removed the HB donor capabilities of the coating resulting in only HB (Ac) interactions being evaluated. This functionality change was determined to be statistically significant based on a comparison of the IASS results for C10H and C5MEG where $p \leq 0.044$ for all test temperatures. The difference in performance of C5MEG and C10H (Fig. 15) was most pronounced at -16°C, but decreased as temperature increased suggesting that for the neat coating composition the HB donor characteristic was important in reducing the average IASS. A single factor ANOVA comparing the IASS results at the three test temperatures of C5MEG afforded $p = 0.008$ suggesting the data differed statistically. It should be noted the internal ether group [$-Si(CH_3)_2(CH_2)_5\mathbf{O}CH_2CH_2OCH_3$] (oxygen atom in bold) may have contributed to the HB (Ac) effect as well. Comparison of the water solubility of analogous compounds to C5MEG is not available, but is for 1-methoxybutane and 1,2-dimethoxyethane (Table 5). 1-Methoxybutane is slightly soluble in water [73] whereas the water solubility of 1,2-dimethoxyethane is ≥ 100 mg/mL [74]. Slightly soluble is defined as a range of 1 to 10 mg/mL [75]. Based on the water solubility of these two compounds, the IASS data for C5MEG suggests that the internal ether group may have been isolated from interacting with impacting SCWD. It should be noted that the melting point of 1-methoxybutane and 1,2-dimethoxyethane are -115

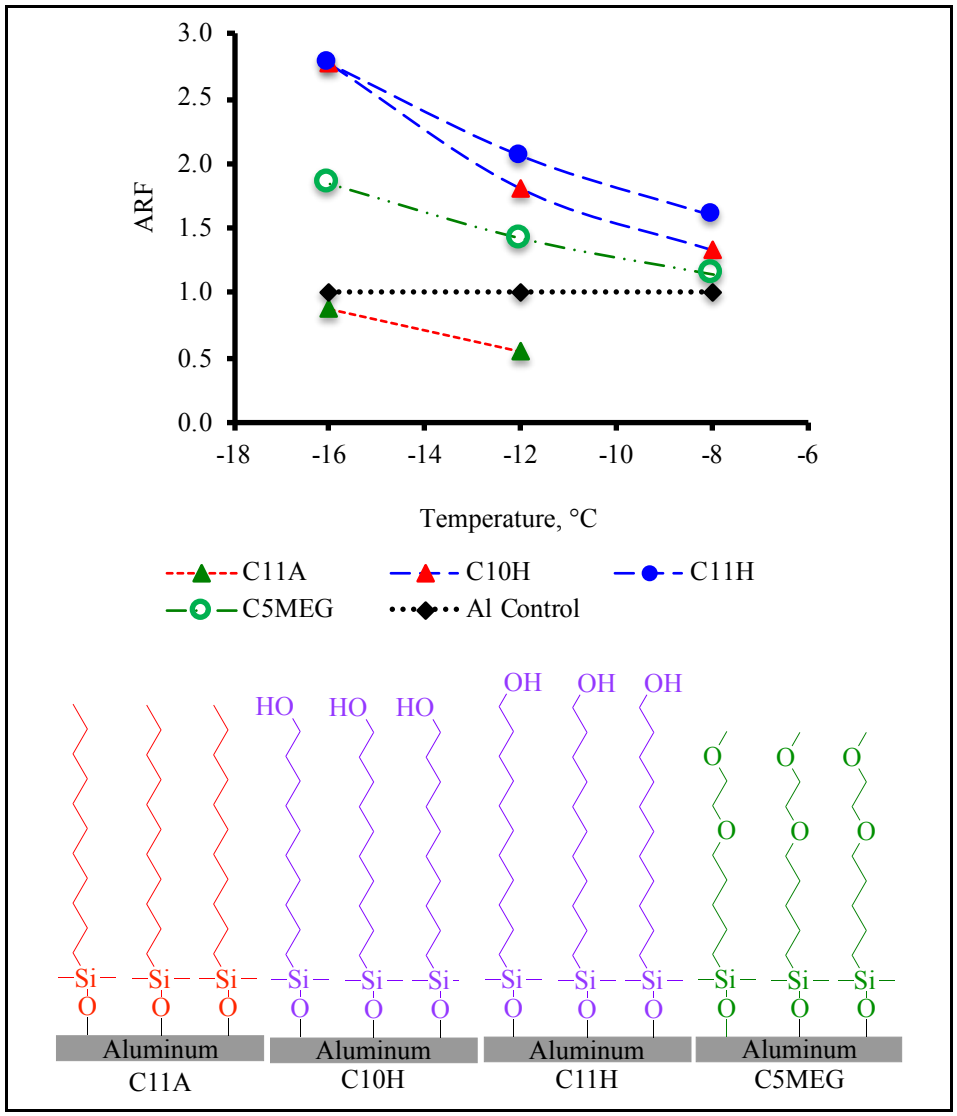

Fig. 16 ARF of C11H, C10H, C5MEG, and C11A compared to uncoated Al.

and -58°C, respectively, [73,74] and are below the test temperatures investigated. This suggests that the C5MEG coating may behave in a "fluid-like" nature similar to that of C7H and the non-HB coatings.

3.5.4 Functional group comparison of comparable n-alkyl chain length

C11H, C10H, C5MEG, and C11A were of similar n-alkyl chain length, thus allowing for comparison of HB characteristics (Figs. 8 and 16). Results of a student t-test were previously discussed for C11H, C10H, and C5MEG. C11A was determined to differ statistically from these three coatings ($p \leq 0.001$). As discussed in Section 3.5.2, C10H and C11H differed statistically at -8 and -12°C and not at -16°C. The IASS data for C5MEG and C10H were also determined to differ statistically at all test temperatures as discussed in Section 3.5.3.

Shown in Fig. 16, the trend with respect to temperature was HB (D/Ac) > HB (Ac) > non-HB. As discussed in Section 3.5.2, the HB (D/Ac) characteristic of the terminal hydroxy group would allow for interchain HB to occur (HB between alcohols is known) thereby presenting a *pseudo*-solid surface to impacting SCWD. The ARF performance difference between HB (D/Ac) and HB (Ac) decreased with increasing temperature and may be related to 1) the rate of ice formation (and associated change in surface energy) from impacting SCWD at the different temperatures and 2) the water solubility and melting points of analogous small compounds (Table 5). The water solubility of the analogous small compounds (Tables 4 and 5) in decreasing order was 1-methoxybutane >> 1-undecanol ≥ 1-decanol > >> undecane

[62,65,66,73]. However, this does not adequately aid in the ARF interpretation. Thus, one must consider the melting points of these analogous compounds as well as previously discussed. The melting point for the two analogous alcohols (1-decanol and 1-undecanol) was greater than the test temperatures used in the AERTS testing suggesting the coatings were presumably "solid-like", while those for the other two analogous compounds (undecane and 1-methoxybutane) were lower thereby suggesting a "fluid-like" behavior [62,65,66,73]. The Σ (Table 2) for C11A suggests that it exists in a cross-over regime between the mushroom and extended conformation regimes while C10H and C11H exist in the extended conformation regimes. The Σ for an analogous C5MEG compound was not determined.

A study conducted by Petrenko and Peng [76] involved the determination of IASS of substituted C11 compounds [i.e., 1-dodecanethiol (C11A) and 11-hydroxyundecane-1-thiol (C11H)] deposited on gold surfaces. The result was that as HB to water increased (i.e., surface became more polar), IASS increased. However, the ice was "freezer ice" since it was generated by the cooling of distilled water on the coated gold surfaces with testing conducted afterwards. This allowed for the intimate interaction of water with the surface; as the test surface became more polar the better the interaction. The work reported herein though found an opposite result with substituted C11 compounds – C11A exhibited higher IASS than C11H at all test temperatures. The reason for this difference may be associated with the difference in how water was applied to the surface to generate ice – in Petrenko's work water was gently placed on the surface and allowed to slowly cool whereas in the current work SCWD impinged the surface at a high velocity.

A similar trend in HB characteristic as the C11 series in the current work was not seen comparing the shorter n-alkyl chain materials C7A and C7H where the ARF performance was non-HB > HB (D/Ac) as shown in Fig. 17. As temperature decreased, the performance of C7H approached that of C7A with

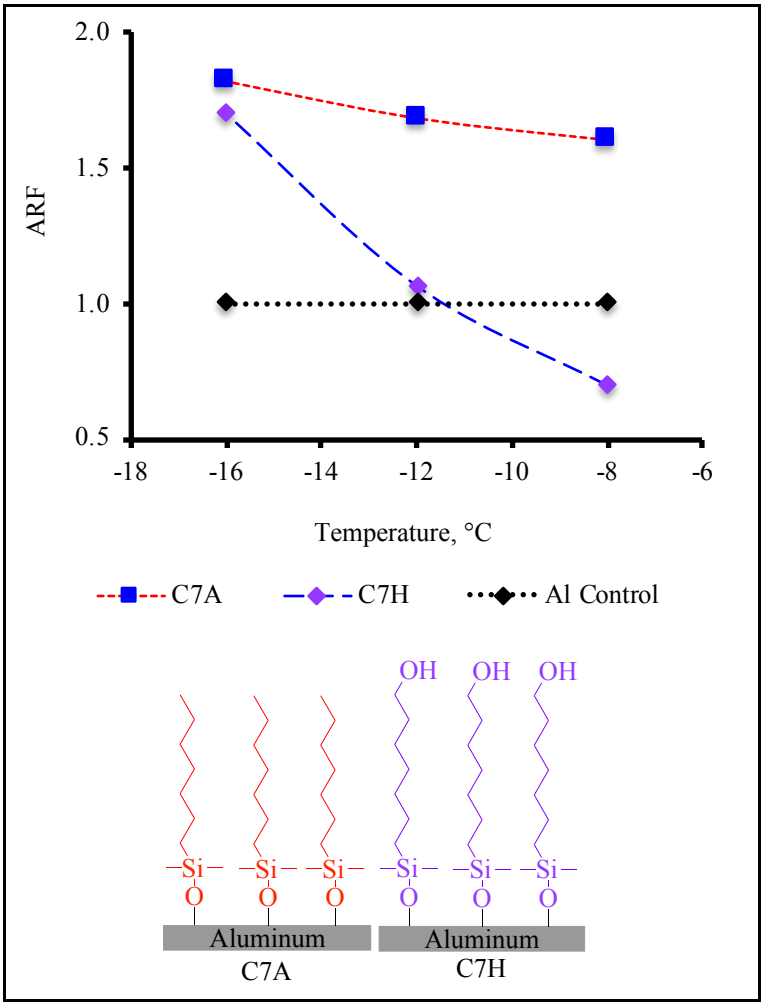

Fig. 17 ARF of C7H and C7A compared to uncoated Al.

apparently similar performance being observed at -16°C. Statistical comparison of the IASS data at all test temperatures determined the two coatings were statistically different at -8 and -12°C ($p \leq 0.002$) but not at -16°C ($p = 0.240$). To aid in explaining these results compared to the longer chain substituted n-alkylsiloxane coatings in Fig. 16, one can refer to the water solubility and melting points of the analogous small compounds (i.e., heptane and 1-heptanol) in Tables 4 and 5. Unlike the longer alkyl chain alcohols and heptane that had low water solubility, 1-heptanol was approximately two to three orders of magnitude more soluble in water [60,64]. This greater water solubility would allow for better interaction with impacting SCWD at -8°C where SCWD would initially persist as water on the surface after impingement, due to thermodynamics, and subsequently freeze upon it. As the temperature decreased, this interaction would decrease due to the rapid phase and surface energy change of impacting SCWD to ice. In addition, the melting points for heptane and 1-heptanol are -91 and -34°C, respectively, and would suggest similar interactions (i.e., fluid-like surface) of the two C7 based coatings with respect to impacting SCWD [60,64]. Based on Σ (Table 2), C7A is suggested to exist in the mushroom regime while C7H would be in the cross-over regime between the mushroom and extended conformation regimes. The results shown in Fig. 17 where C7A exhibited higher ARF (i.e., lower IASS) than C7H at -8 and -12°C agreed well with the conclusion reached by Petrenko and Peng, using substituted C11 thiols [76], that increasing polarity of the surface (i.e., HB) towards water led to higher ice adhesion strength. However, the difference in HB characteristic of the two C7 surfaces towards SCWD and ultimately IASS became negligible at -16°C suggesting that how ice is accreted on the surface is crucial in the interactions observed.

Besides water solubility and melting points of the analogous substituted hydrocarbons for the comparisons shown in Figs. 16 and 17, these results suggest coating performance with regard to IASS due to impacting SCWD was dependent upon the n-alkyl chain length, HB interactions between individual members of the respective coatings, and temperature when impact ice accretes on the surface.

3.5.5 Best neat composition performers

The best performing materials of the non-HB (C7A) and HB (D/Ac) (C11H) series along with the HB (Ac) (C5MEG) material are shown in Fig. 18. It should be noted that C11H and C5MEG were of similar chain length whereas C7A had the shortest n-alkyl chain length. Comparing the ARF values at -8 and -16°C, the trends were HB (D/Ac) ~ non-HB > HB (Ac) and HB (D/Ac) > non-HB ~ HB (Ac), respectively. Statistical comparison (student t-test) of the coatings confirmed this where 1) $p = 0.492$ comparing C7A and C11H at -8°C and 2) $p = 0.434$ comparing C5MEG and C7A at -16°C. These results can be understood by considering the 1) surface energy components of ice and water (Fig. 2) and 2) the θ_R for water for each of the materials (Table 3). As discussed in Section 3.5.2 for the HB (D/Ac) coatings, at -8°C impacting SCWD would persist in the liquid state prior to freezing allowing the liquid to flow across the surface whereas at -16°C the drops would rapidly freeze upon the surface. Given the similar ARF behavior for C7A (non-HB) and C11H [HB (D/Ac)] at -8°C and the dissimilar nature of the two series, the results can be attributed to chain flexibility and HB (D/Ac) interactions between individual substituted n-alkyl chains constituting the C11H coating. For the non-HB C7A surface, the individual C7A chain ends would presumably act independent of one another (e.g., fence posts) whereas the hydroxy groups on the terminus of the C11H chains would be linked together through HB interactions with one another (e.g., rail across the fence post ends), thus generating an elastic underlying surface provided by the long n-alkyl chains. Flexibility has been suggested as being necessary to reduce ice adhesion to a surface [55]. The Σ (Table 2) for C7A suggests it would exist in the mushroom confirmation whereas C11H would be in an extended confirmation implying that molecular confirmation may play a role as well. Further studies are needed to determine if this is indeed the case. The similar ARF values observed for the C7A (non-HB) and C5MEG [HB (Ac)] coatings at -16°C suggests a similar behavior of non-HB and HB (Ac) at this temperature. To recall, the C7A and C5MEG surfaces exhibited comparable Θ_R for water (Table 3), 88° and 79°, respectively. Since the length of the n-alkyl chain differs between these two materials, chain flexibility may

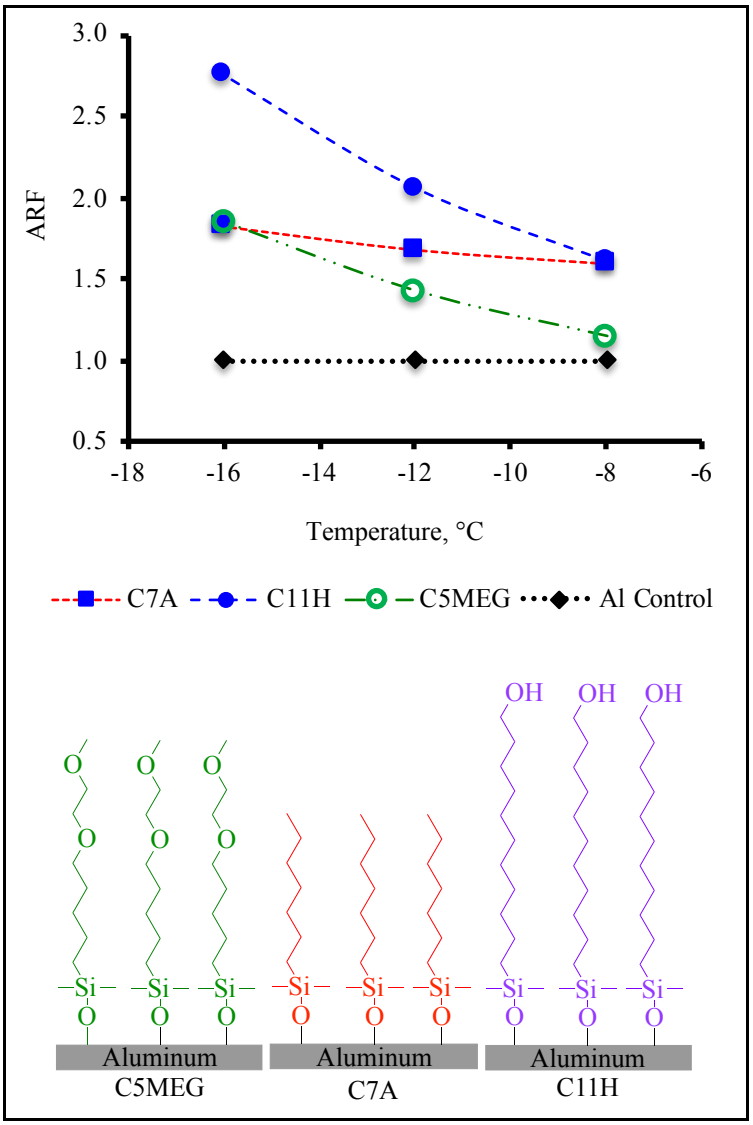

Fig. 18 ARF comparison of best-performing member of the non-HB, HB (D/Ac), and HB (Ac) series to uncoated Al.

also play a role. The trend at -12°C showed the greatest separation between each of the series where HB (D/Ac) > non-HB > HB (Ac).

3.5.6 Conclusions

Based on the results discussed in Sections 3.5.1 - 3.5.3, an interdependency between the HB characteristic of the functionality at the chain terminus and chain length and its effect upon IASS/ARF was observed. First, HB (D/Ac) groups were found to be beneficial in reducing IASS at low temperatures with the effect diminishing as temperature increased due to how impacting SCWD interacted with the surfaces at the respective temperatures. Reductions in IASS of the HB (D/Ac) series were further observed with increasing alkyl chain length between the two functionalities (i.e., silicon and hydroxy). Second, an opposite effect for the non-HB series was observed where an alkyl chain length of seven carbons was found to be best with shorter/longer lengths showing deleterious results, especially longer lengths. Third, the HB (Ac) functionality exhibited a performance that was in between that of non-HB and HB (D/Ac) materials of comparable length. This result suggests that HB donor contributions to reducing IASS are important as shown in Fig. 18. The behaviors of the surfaces evaluated here are based on the limited number of materials examined in this study, but points to complex interactions between SCWD, temperature, HB characteristics,

and molecular flexibility. In addition, the nature of the surface (solid or fluid like) as suggested by the melting point of analogous small compounds (Sections 3.5.1.1 and 3.5.2.1) and water solubility of these may play a role as well.

3.6 50/50 Mixed coating compositions with non-hydrogen bonding C3A and C7A

Usage of a coating on an aircraft requires the material to be durable. Since the compounds evaluated herein would not be expected to be durable, it necessitates that HB functionalities evaluated in this study would be incorporated within a polymer as a pendant group to the backbone, within the polymer backbone, or as a combination of the two. As a pendant group, the concentration of the HB component of interest would be diluted (i.e., ≤ 50%) and spaced across the polymeric surface, thereby exposing the entire substituted n-alkyl chain to the impact icing environment. Thus, it was of interest to investigate the performance of mixed coatings based upon the best-performing materials (i.e., C7A, C11H, C5MEG) discussed in Section 3.5.5, with C3A and C7A in a 50/50 ratio. C3A was selected since it would provide a non-HB organic surface over the bare Al substrate. C7A was chosen so as to limit the length of the n-alkyl chain (i.e., C11H, C5MEG) that could perform as clamping sites when exposed to the icing environment. C10H was used as the HB (D/Ac) component in place of C11H due to a limited amount of the latter available at the time.

The 50/50 mixed compositions were applied to the Al substrate in a similar fashion as that described for the neat coatings. The surfaces were considered to be randomized as attempts to prepare tailored coatings where individual components of the mixture were deposited in such a manner as to impart self-assembly or phase segregation on the Al surface were not performed. It has been reported though that self-assembly by molecules can result into distinct areas on the nanometer scale [77]. The composition, surface roughness, and θ_R of water for the mixed coatings are presented in Table 6. Surface roughness was similar for all of the mixed coatings implying a smooth surface (ASTM A480 Finish #7) [69] and were comparable to those of the neat compositions of Section 3.5 thereby allowing for comparison of the IASS results obtained for the single component coatings. Generally, the trend for the θ_R of water was as expected with non-HB > HB (Ac) > HB (D/Ac). The Θ_R of water for each mixed coating followed a rule of mixtures with calculated values being within ±6% of that measured, with the exception of C5MEG/C7A (50/50), which was approximately 70% of the calculated value. Surprisingly, the θ_R of water for C10H/C7A (50/50) and C5MEG/C7A (50/50) were similar given that the latter has only HB (Ac) interactions with water while the former had both HB (D/Ac) interactions as well. The Θ_R of water for C10H/C3A (50/50) was comparable

Table 6. Surface Characterization of Mixed (50/50) Coatings

Al Surface	Receding Water Contact Angle (θ_r), °		Mean Roughness (Ra), μm		Root Mean Square Roughness (Rq), μm	
	Avg	Stndev	Avg	Stndev	Avg	Stndev
Control (Uncoated)	58	14	0.326	0.048	0.388	0.060
non-HB/non-HB						
C7A/C3A	87	0	0.430	0.087	0.518	0.097
C11A/C3A	97	4	0.650	0.113	0.822	0.149
C11A/C7A	94	4	0.528	0.104	0.656	0.119
HB (D/Ac)/non-HB						
C10H/C3A	93	2	0.271	0.044	0.356	0.084
C10H/C7A	59	5	0.610	0.087	0.766	0.094
HB (Ac)/non-HB						
C5MEG/C3A	81	5	0.264	0.022	0.344	0.038
C5MEG/C7A	59	5	0.382	0.138	0.478	0.121

to that of C11A/C3A (50/50) despite the latter had only non-HB interactions suggesting the isolated C10H chain behaved more like a hydrocarbon.

The average IASS results presented in Fig. 19 followed the expected trend regarding temperature with the exception of C10H/C7A (50/50). The trend reversal seen for this composition may be attributable to mechanical clamping of impact ice with the exposure of the hydroxy terminated n-alkyl chain resulting from reduced interaction of the isolated HB (D/Ac) (i.e., C10H) hydroxy functionality from its nearest C10H neighbor with impacting SCWD. The IASS of the mixed coating compositions differed statistically ($p < 0.002$) from that of the uncoated Al control at the various test temperatures as determined by a student t-test with the exception of 1) C7A/C3A (50/50) at -16°C ($p = 0.171$), 2) C11A/C3A (50/50) at -16°C ($p = 0.325$), and 3) C10H/C3A (50/50) at all test temperatures ($p = 0.152$, 0.107, and 0.060 at -8, -12, and -16°C, respectively). As previously stated, the goal of this work was to elucidate HB and molecular flexibility effects with respect to impact icing. Therefore, ARF values were determined from the average IASS values (Fig. 19) recognizing that some compositions at certain temperatures did not differ statistically from that of the uncoated Al control.

Data for the neat compositions (i.e., C3A, C7A, C10H, and C5MEG) are also included in the following graphs (Figs. 20, 21, 23, 24, 26, 28) for each series along with the corresponding 50/50 mixture.

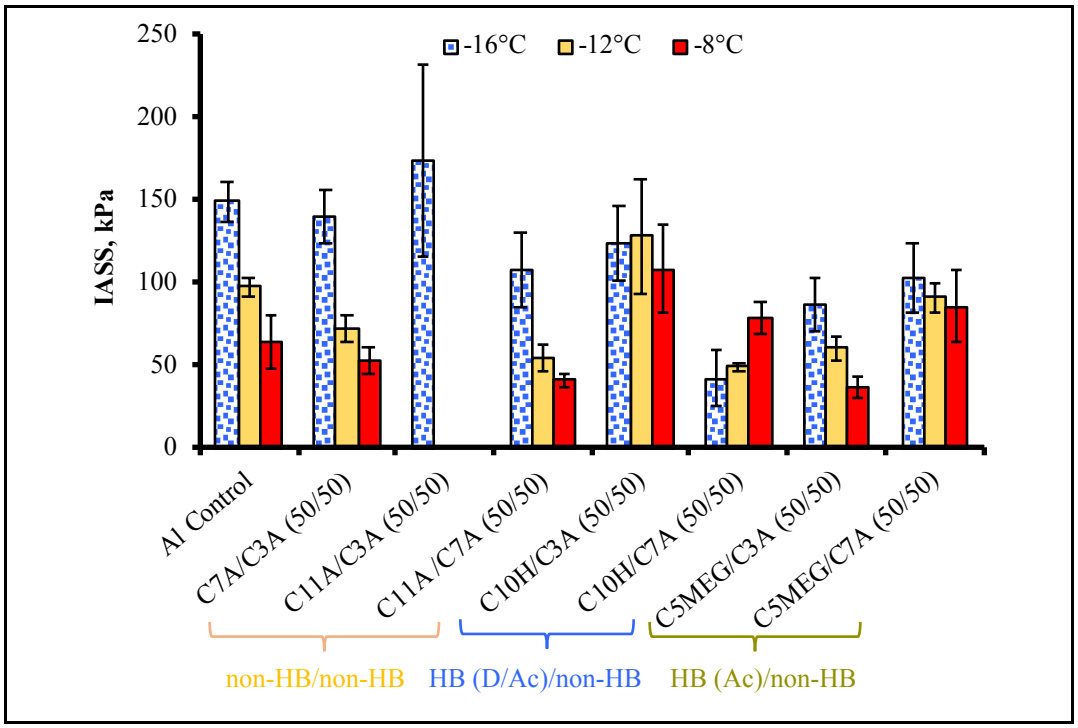

Fig. 19 IASS of mixed coating compositions with Al control.

3.6.1 Non-hydrogen Bonding / non-hydrogen bonding coatings

In this series, C7A and C11A were mixed with C3A in a 50:50 ratio, respectively, and the IASS of each composition compared with that of the pure material. A single factor ANOVA compared the IASS results across the test temperatures for each of the two 50/50 mixed compositions (i.e., C7A/C3A and C11A/C7A). These were determined to differ statistically based on $p < 0.001$. Only one temperature result (-16°C) was obtained for C11A/C3A (50/50) since it appeared to behave similar to the neat C11A coating. To determine if this was the case, it was compared to the neat components (i.e., C3A and C11A) using a student t-test. It was determined to differ statistically from C3A ($p = 0.016$) but not from C11A ($p = 0.454$) suggesting that the long exposed aliphatic chain (eight carbon units) provided an anchor point for ice accretion.

As shown in Fig. 20, the dilution of C7A by C3A in C7A/C3A (50/50) resulted in an antagonistic effect with respect to C7A at all test temperatures. At -8 and -12°C, the ARF values were nearly comparable to that of the shorter chain C3A component. A single factor ANOVA comparing the IASS data of C7A/C3A

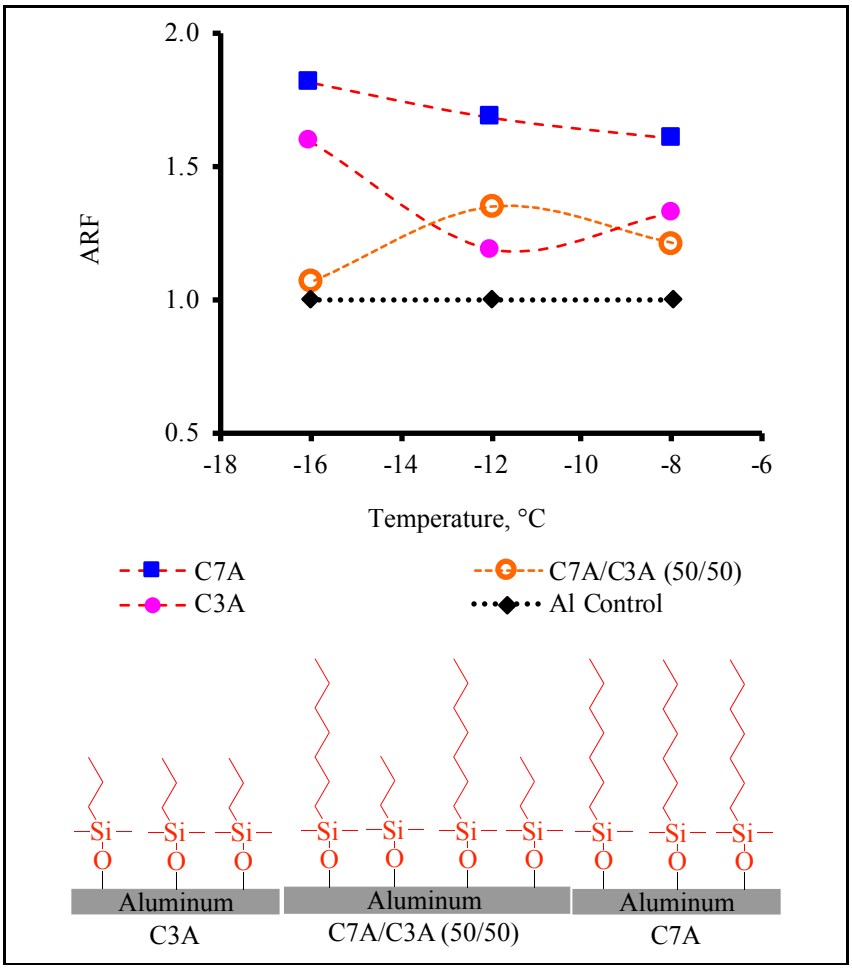

Fig. 20 ARF comparison of C7A, C7A/C3A (50/50), and C3A compared to uncoated Al.

(50/50) to each of the neat components at each test temperature determined that the mixed coating differed statistically from the neat components at -12 and -16°C ($p \leq 0.008$) but not at -8°C ($p = 0.116$). A student t-test comparing the IASS data at -8°C of the neat components to C7A/C3A (50/50) found that the coating differed statistically from C7A ($p = 0.046$) but not C3A ($p = 0.0149$). As discussed in Section 3.5.1, the short n-alkyl chain length of C3A may allow for better interaction of impacting SCWD with the Al surface compared to C7A. To recall, the melting points of both materials were lower than that of the test temperatures used here suggesting that the mixed coating surface may be in a "fluid-like" state. The significant reduction in ARF at -16°C for C7A/C3A (50/50) compared to either pure component can be attributed to the exposed longer chain C7A material (i.e., 4 methylene units longer than C3A) in the mixed composition acting as a nucleation site for rapidly forming ice from impacting SCWD, thereby providing a clamping mechanism. A student t-test comparison of the -16°C IASS data for C7A/C3A (50/50) and C11A/C3A (50/50) found that the coatings did not differ statistically ($p = 0.109$). This suggests that the exposure of a carbon chain of a length ≥ 4 would act as a clamping site for accreting ice in the presence of C3A as the co-component.

Since C11A and C7A differed by four methylene units as C7A and C3A, it was of interest to determine if a mixed coating composition based on these components would exhibit similar behavior as C7A/C3A (50/50). From the ARF vs. temperature graph for the non-HB single neat components (Fig. 14) discussed in Section 3.5.1, C7A performed the best while C11A the worst. Compared to C3A the C7A coating provided better insulation from impacting water as suggested by the data. The state of the C11A/C7A (50/50) surface would be anticipated to be in a fluid-like state similar to the C7A/C3A (50/50) coating given the melting point of the analogous hydrocarbons (Table 4).

The IASS data at the three test temperatures for C11A/C7A (50/50) (Fig. 19) was determined to differ statistically ($p < 0.001$) by a single factor ANOVA. Comparison of the IASS results of C11A/C7A (50/50) in Fig. 19 to that of C11A and C7A (Fig. 13) using a single factor ANOVA found that the mixed coating differed statistically from each of the neat components at -12°C ($p = 0.002$) but not at -16°C ($p = 0.074$). A student t-test comparing C11A/C7A (50/50) to each component at -16°C determined that it differed statistically from C7A ($p = 0.024$) but not C11A ($p = 0.076$). Comparison of the IASS data at -8°C for C7A and C11A/C7A (50/50) using the student t-test found that the two did not differ statistically ($p = 0.440$); similar to what was observed for C7A/C3A (50/50) and C3A. As seen in Fig. 21, the performance of C11A/C7A (50/50) mimicked that of the shorter component (C7A) at -8 and -12°C similar to that observed for C7A/C3A (50/50) in Fig. 20 (C3A). At -16°C, the ARF dropped significantly for C11A/C7A (50/50) (Fig. 21) similar to that seen for C7A/C3A (50/50) (Fig. 20). The C11A/C7A (50/50) results verified MD simulations of a C11A/C6A (50/50) surface, even though C7A was longer than C6A by one methylene unit, that suggested ice formation would be more difficult on this mixed surface compared to the C11A surface due to greater mobility of the C11A chains despite that the former surface was rougher on the molecular level [37]. The decreased ARF at -16°C for C11A/C7A (50/50) compared to the warmer temperatures is presumably due to this rougher surface as suggested by the MD simulations.

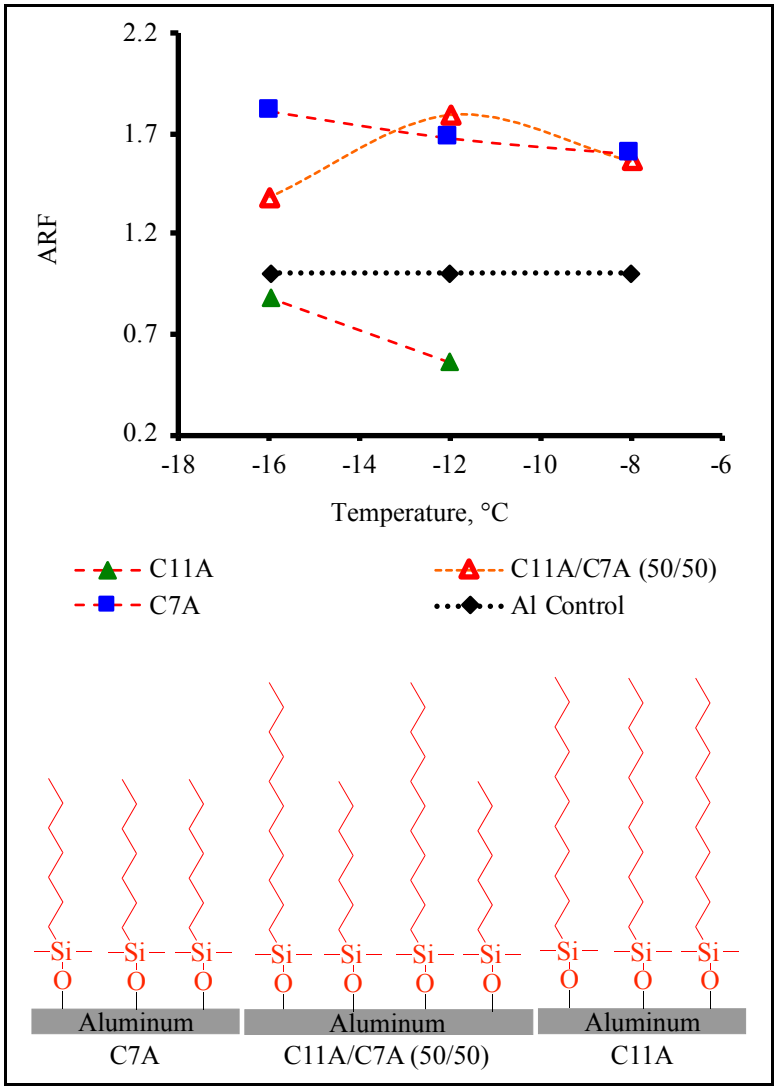

Fig. 21 ARF comparison of C11A, C11A/C7A (50/50), and C7A compared to uncoated Al.

As seen in Fig. 22, the ARF vs. temperature performance trend of the two mixed compositions, C11A/C7A (50/50) and C7A/C3A (50/50), were similar. Statistical comparison of the two coatings at the various test temperatures using a student t-test determined that the two differed statistically ($p \leq 0.009$). The better performance of C11A/C7A (50/50) compared to C7A/C3A (50/50) was due to the longer chain alkyl components of the former as discussed. An additional explanation is that impacting SCWD had a decreased ability to interact with the Al substrate due to the lower water solubility of the analogous longer chain hydrocarbons (Table 4) as discussed in Section 3.5.1.1. The decreased performance at -16°C exhibited by both mixed compositions suggests the exposed four methylene units of the longer hydrocarbon component afforded a nucleating and clamping site due to rapid ice formation from impacting SCWD at this temperature and the associated changes in surface energy components of water and ice. Based on the limited data set, the similar ARF behavior of the two mixed 50/50 compositions compared to the respective neat components (Figs. 20 and 21) suggests dominance of the short chain component (C3A in C7A/C3A and C7A in C11A/C7A) in these mixed compositions.

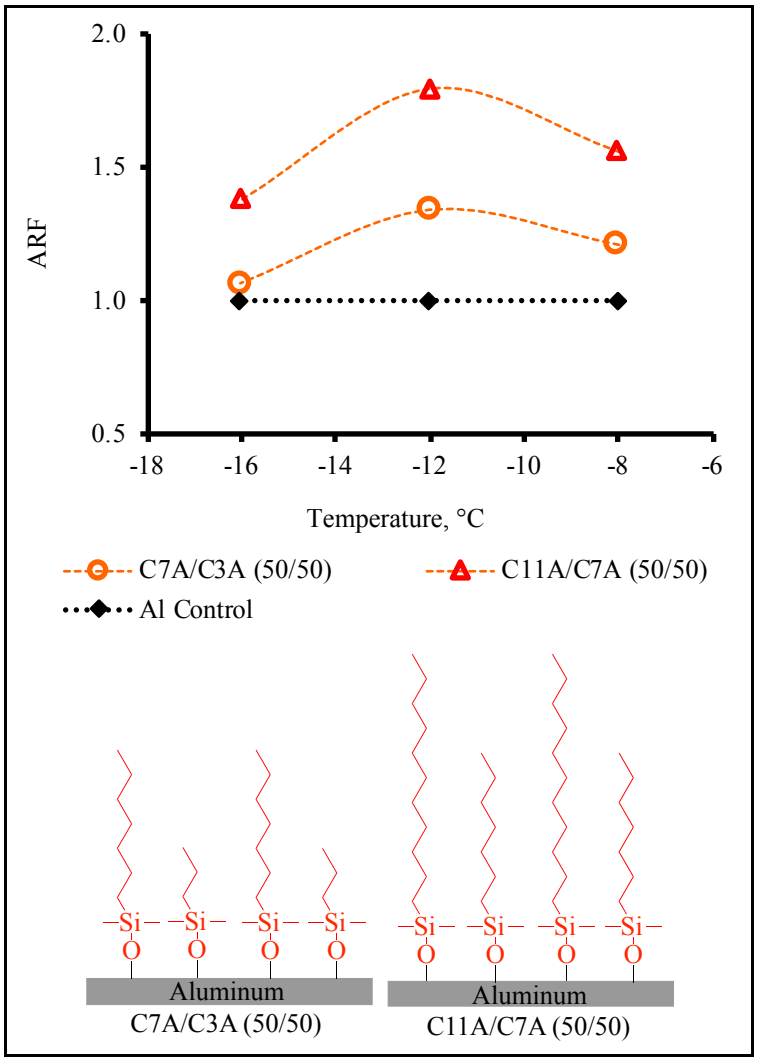

Fig. 22 ARF comparison of C7A/C3A (50/50), C11A/C7A (50/50), and uncoated Al.

3.6.2 Hydrogen bonding (donor/acceptor) / non-hydrogen bonding coatings

From the discussion in Sect. 3.5.2, the hydroxy groups in the neat HB (D/Ac) C10H coating were envisioned to hydrogen bond with a neighboring hydroxy group forming a *pseudo*-surface [72]. Thus, it

was of interest to see the effect that adding 50% non-HB components C3A and C7A would have upon IASS by disrupting this *pseudo*-surface of C10H. These compositions were prepared and exposed to impact ice.

A single factor ANOVA comparing the IASS results of the three test temperatures for C10H/C3A (Fig. 19) determined that the results did not differ statistically ($p = 0.547$). The C10H/C3A (50/50) results were then compared using a student t-test that found the different temperature data did not differ statistically ($p \leq 0.379$). Comparison of the IASS data for the individual components to the C10H/C3A (50/50) composition at the three test temperatures determined that the results differed statistically ($p \leq 0.001$). As seen in Fig. 23, the dilution of C10H with C3A led to a severe performance degradation suggesting that the exposed seven carbon chain of C10H acted as a nucleation and mechanical clamping site for impact ice. Compared to the -16°C IASS for C11A/C3A (50/50) coating (Fig. 19), the terminal hydroxy group in C10H did afford a slight benefit. The two coatings differed statistically ($p = 0.046$) as determined by a student t-test.

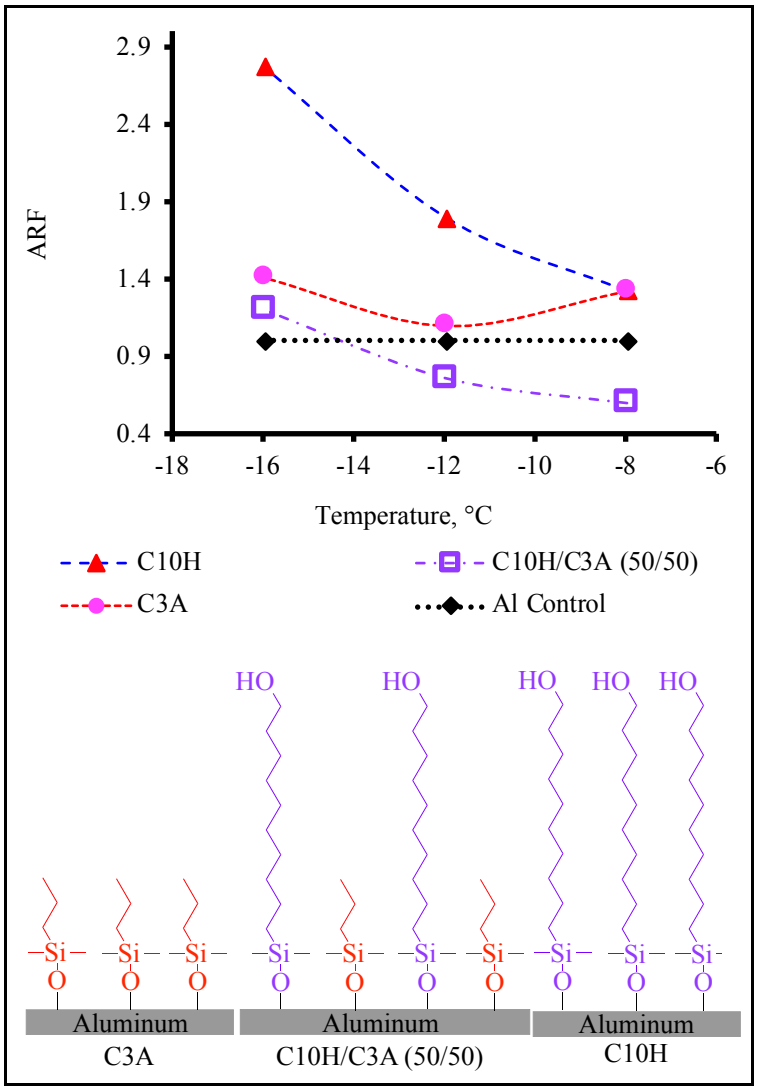

Fig. 23 ARF comparison of C10H, C10H/C3A (50/50), and C3A compared to uncoated Al.

Since it was observed that the incorporation of C7A in C11A/C7A rather than C3A afforded a performance benefit, it was of interest to determine if the same effect would occur with C10H. A single factor ANOVA comparing the IASS results of the three test temperatures for C10H/C7A (50/50) coatings (Fig. 19) determined that the results differed statistically ($p = 0.009$). Even though the ANOVA test determined that the IASS data for the different test temperatures differed for C10H/C7A (50/50) coating,

the results at -12 and -16°C in Fig. 19 appeared to be comparable. The data for these two temperatures were compared using a student t-test which found that the data did not differ statistically ($p = 0.179$). The IASS data for this mixed coating was then compared to that of the individual components (Fig. 13) at each test temperature. It was determined that the three differed statistically at -8 and -16°C ($p \leq 0.003$), but not at -12°C ($p = 0.242$). Further analysis of the data at -12°C for the three coatings by a student t-test determined that the mixed composition differed statistically from C10H ($p = 0.025$) but not C7A ($p = 0.123$). The ARF results for C10H/C7A (50/50) and the neat components in Fig. 24 suggests that at -8°C the exposed and isolated portion of the C10H chain presumably acted as a nucleating/clamping site for the forming ice and degraded performance. To recall, SCWD impacting a surface at -8°C can result in the initial formation of liquid water that can run across the surface and eventually freeze upon it. Comparing the water solubility and melting point of the analogous small compounds for C10H/C7A, heptane and 1-decanol (Tables 4 and 5, respectively), shows the former was an order of magnitude less soluble in water and had a much lower melting point. The exposed three carbon alkyl chain along with the terminal hydroxy group could provide a nucleation and clamping site for impacting SCWD at -8°C. As temperature further decreased, impacting SCWD would persist for a finite period of time in the liquid state prior to freezing upon this mixed surface. Since there was a smaller exposed carbon chain, C10H dominated in this composition at this temperature resulting in an increasing ARF compared to either component. It should be noted that Σ for C7A and C10H

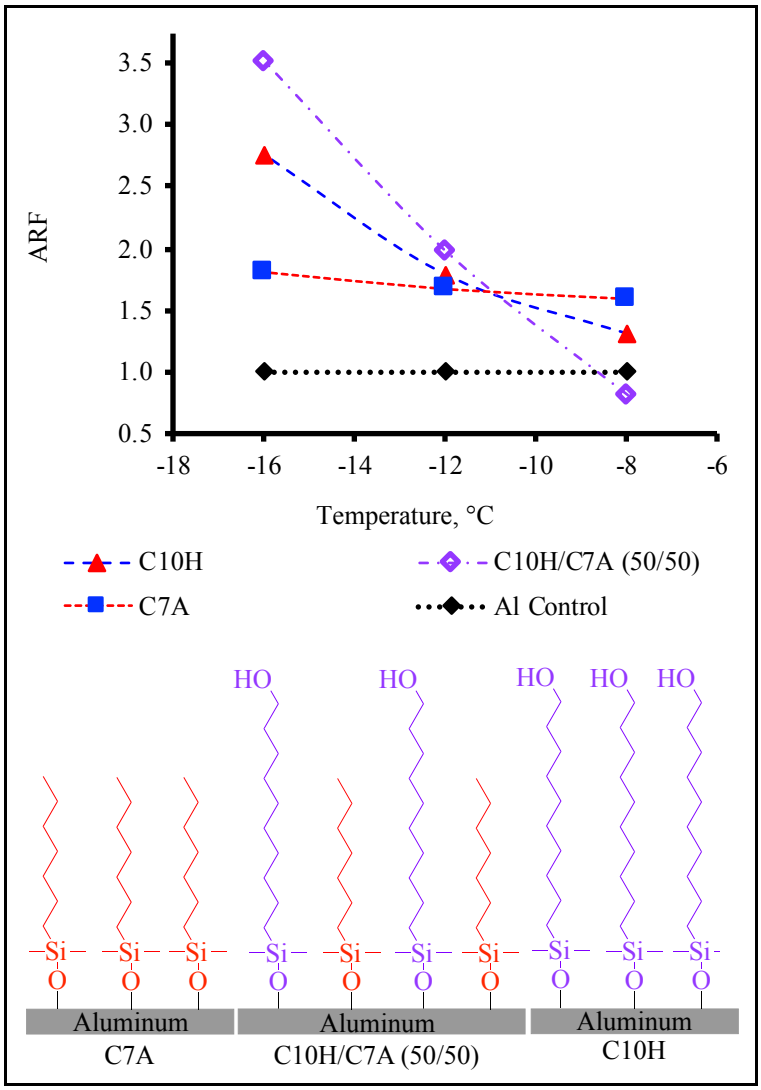

Fig. 24 ARF comparison of C10H, C10H/C7A (50/50), and C7A compared to uncoated Al.

suggests the former exists in a mushroom conformation whereas the latter is in a highly stretched configuration.

Comparing the ARF vs temperature performance for the C10H/C3A and C10H/C7A (50/50) compositions (Fig. 25), one can see the effect of the four-carbon difference in length (C3A vs C7A) of the smaller non-HB component. To note, C10H in the C10H/C3A coating has seven-carbons units exposed to the icing environment while in C10H/C7A there are only three-carbon units exposed. The effect this four-carbon difference of the non-HB component was greatest at -16°C and decreased as temperature increased. At -8°C, the performance difference between the two coatings was nearly comparable. A student t-test comparing these two coatings at -8°C determined that the IASS results differed statistically ($p = 0.005$). The similar behavior at -8°C was not surprising given that impacting SCWD would initially become a liquid, flowing across the surface, and subsequently freezing upon it.

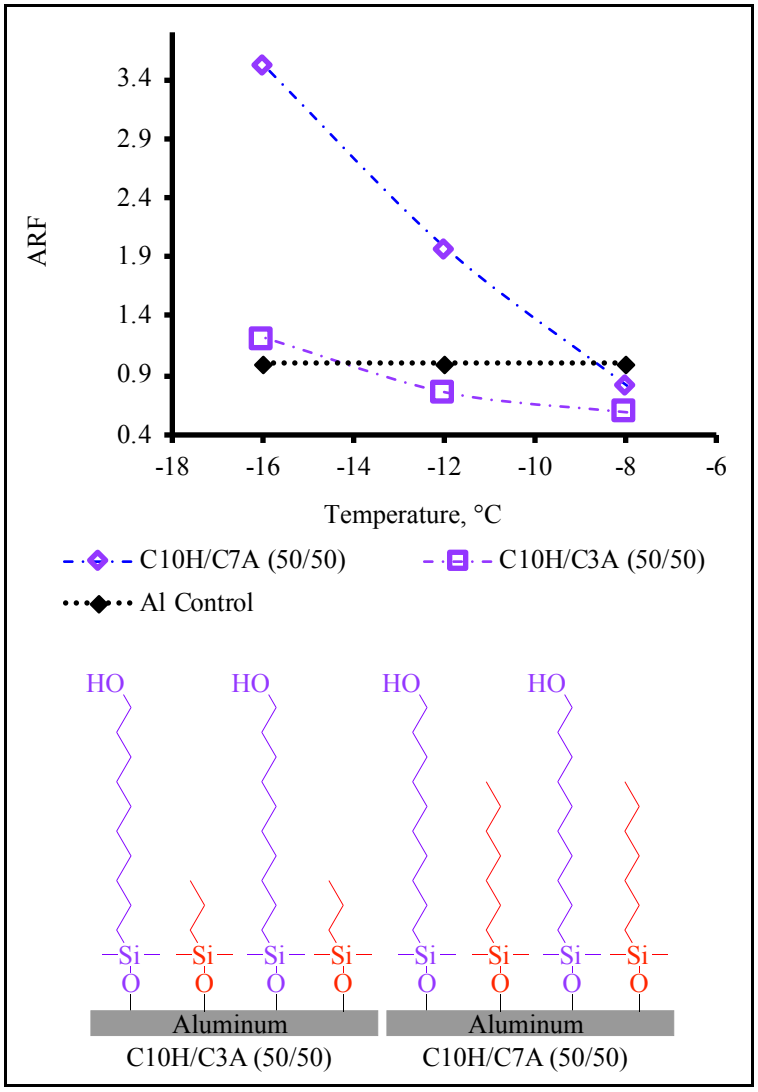

Fig. 25 ARF comparison of C10H/C3A (50/50) and C10H/C7A (50/50) compared to uncoated Al.

3.6.3 Hydrogen bonding (acceptor) / non-hydrogen bonding coatings

The third series investigated were 50/50 mixed compositions of C5MEG with non-HB components C3A and C7A. In these compositions the HB (D) behavior present in the C10H component was removed by changing the hydroxy endgroup of C10H to that of an ethoxymethoxy functionality present in C5MEG. The C5MEG/C7A (50/50) composition exposed only the terminal ether functionality ($-CH_2\mathbf{O}CH_3$) of the

C5MEG chain allowing for the determination of the importance of HB (D) in reducing impact ice adhesion. In contrast, the C5MEG/C3A (50/50) composition exposed both the internal and terminal ether groups of C5MEG (-**O**CH_2CH_2**O**CH_3) to impacting SCWD to determine its effect upon impact ice adhesion.

3.6.3.1 Effect of one hydrogen bonding (acceptor) group in the n-alkyl chain upon IASS

As seen in Fig. 26, the C5MEG/C7A (50/50) composition performed worse than either of the individual components. A single factor ANOVA comparing the IASS results of C5MEG/C7A (50/50) at all three test temperatures (Fig. 19) determined that the values differed statistically ($p = 0.008$). The IASS data for this mixed coating (Fig. 19) was then compared to each of its components (Fig. 13) at all test temperatures using a single factor ANOVA. The result was that the mixed coating differed statistically from each of the components at -8 and -12°C ($p \leq 0.001$), but not at -16°C ($p = 0.102$). Subsequent analysis of the -16°C using a student t-test found that the mixed coating differed statistically from C5MEG ($p = 0.037$) and C7A ($p = 0.049$). Even though C7A differed statistically from C5MEG/C7A (50/50), the value of p was close to 0.05 and suggests that the mixed coating exhibited a performance comparable to the C7A component.

The ARF vs temperature trendline for C5MEG and C5MEG/C7A (50/50) were similar with the latter being lower by 0.4 ARF (i.e., higher IASS). A plausible reason is that the exposed -CH_2OCH_3 portion of the C5MEG chain in the mixed composition was acting as a nucleating site for ice. This is reinforced by

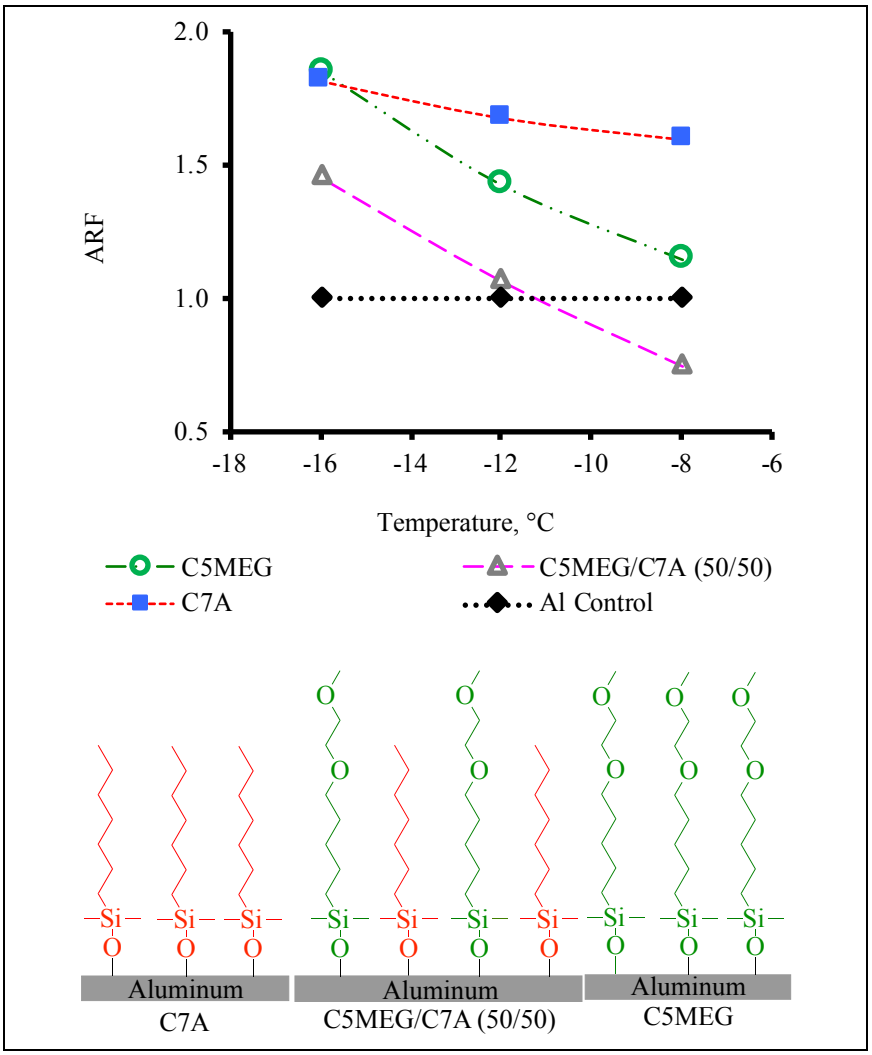

Fig. 26 ARF comparison of C5MEG, C5MEG/C7A (50/50), and C7A compared to uncoated Al.

the IASS data at -16°C for C5MEG and C7A which did not differ statistically ($p = 0.434$) from one another as determined by a student t-test. Similar behavior was observed at -8°C for the C10H and C10H/C7A (50/50) coatings shown in Fig. 24 where the exposed portion was $-CH_2-CH_2-CH_2OH$. However, as temperature decreased the C10H/C7A (50/50) composition exhibited increasingly better performance compared to C10H (Fig. 24) in stark contrast to the C5MEG/C7A (50/50) coating shown in Fig. 26.

C5MEG has two ether functionalities – one internal [$-OSi(CH_3)_2(CH_2)_4CH_2\mathbf{O}CH_2CH_2OCH_3$] and one terminal [$-OSi(CH_2)_4CH_2OCH_2CH_2\mathbf{O}CH_3$]– (oxygen atoms indicated in bold) that could interact with water through HB (Ac) interactions. For the C5MEG/C7A (50/50) composition, it was postulated that the terminal methoxy group would only be available for interaction with the impacting SCWD due to the n-alkyl chain length of the C7A component. With regards to C5MEG, the water solubility of the analogous small compounds for the two cases, 1-methoxybutane and 1,2-dimethoxyethane, in Table 5 ranged from slightly to highly soluble, respectively [73,74]. The water solubility of the analogous hydrocarbon for C7A, heptane, in Table 4 was significantly lower than either of those cited for C5MEG. All of the analogous compounds had melting points (Tables 4 and 5) that were lower than the test temperatures in this study suggesting that the surfaces were in a similar state (i.e., "fluid-like"). Based on these analogous small compound characteristics water would be anticipated to interact with the exposed $-CH_2OCH_3$ functionality of C5MEG. The Θ_R for water for C5MEG/C7A (50/50) (59°, Table 6) vs.C5MEG (79°, Table 3) supports water interaction with this exposed group. Given that C10H/C7A (50/50) had a comparable Θ_R for water (59°, Table 6) suggests that the HB (D) interaction, with respect to the terminal functionality, is important in reducing ice adhesion.

3.6.3.2 Effect of hydrogen bonding characteristic of similar chain length components in mixed C7A (50/50) coatings

As seen in Fig. 27 the HB characteristic of the long n-alkyl chain component of the mixed C7A compositions upon ARF were temperature dependent. The C11A/C7A (50/50) and C5MEG/C7A (50/50) surfaces would be presumably in a "fluid-like" state based on the melting point of the analogous compounds (Tables 4 and 5). The 1-decanol (i.e., alcohol analog of C10H, Table 5) component of C10H/C7A (50/50) coating has a melting point greater than the test temperatures in this study that may have afforded a mixed nature to the surface. However, this may not be the case as the C5MEG/C7A (50/50) and C10H/C7A (50/50) compositions had similar θ_R of water (59°, Table 6). C11A/C7A (50/50) had a Θ_R of water of 89° and was expected given the non-HB behavior of the components. At -8°C, impacting SCWD can initially flow as a liquid over the surface with subsequent freezing with the trend being non-HB >> HB (D/Ac) >HB (Ac). This trend is what one would expect regarding HB effects towards ice. The ARF at -8°C for both HB coatings appeared to be comparable. A single factor ANOVA however suggested that the coatings differed statistically from one another at all test temperatures ($p \leq 0.001$). However, a student t-test performed on the IASS for C10H/C7A (50/50) and C5MEG/C7A (50/50) at -8°C (Fig. 19) determined that the two coatings did not differ statistically ($p = 0.265$). The trend at -12°C was HB (D/Ac) > non-HB >> HB (Ac). The IASS data for the HB (D/Ac) and non-HB based mixed surfaces, C10H/C7A and C11A/C7A (50/50) respectively, though was determined not to differ statistically according to a student t-test ($p = 0.103$). The HB (Ac) surface had performance similar to that of the uncoated Al control at -12°C implying that the HB (D) characteristic of the coating towards impacting SCWD and subsequent ice formation was important to reducing IASS (i.e., increasing ARF). The C5MEG/C7A coating though differed statistically from the uncoated Al surface ($p = 0.012$) according to a student t-test. The trend at -12°C suggests that the effect of the change in surface energy components of water occurring during the phase change of SCWD to ice becomes increasingly important as temperature decreases. The importance of the HB (D) capacity is further seen at -16°C where the trend was HB (D/Ac) >> HB (Ac) ~ non-HB. The IASS data of C5MEG/C7A (50/50) and C11A/C7A (50/50) did not differ statistically ($p = 0.334$) as determined from a student t-test. To summarize the results in Fig. 27, a mixed non-HB surface appeared to provide the most benefit at -8°C whereas the mixed surface with a HB (D/Ac) as the co-component afforded the best performance at -16°C. At -12°, a mixed non-HB or a HB (D/Ac)/non-HB surface would equally perform. These conclusions appear to be reasonable based on how SCWD interact with these surfaces at the various test temperatures.

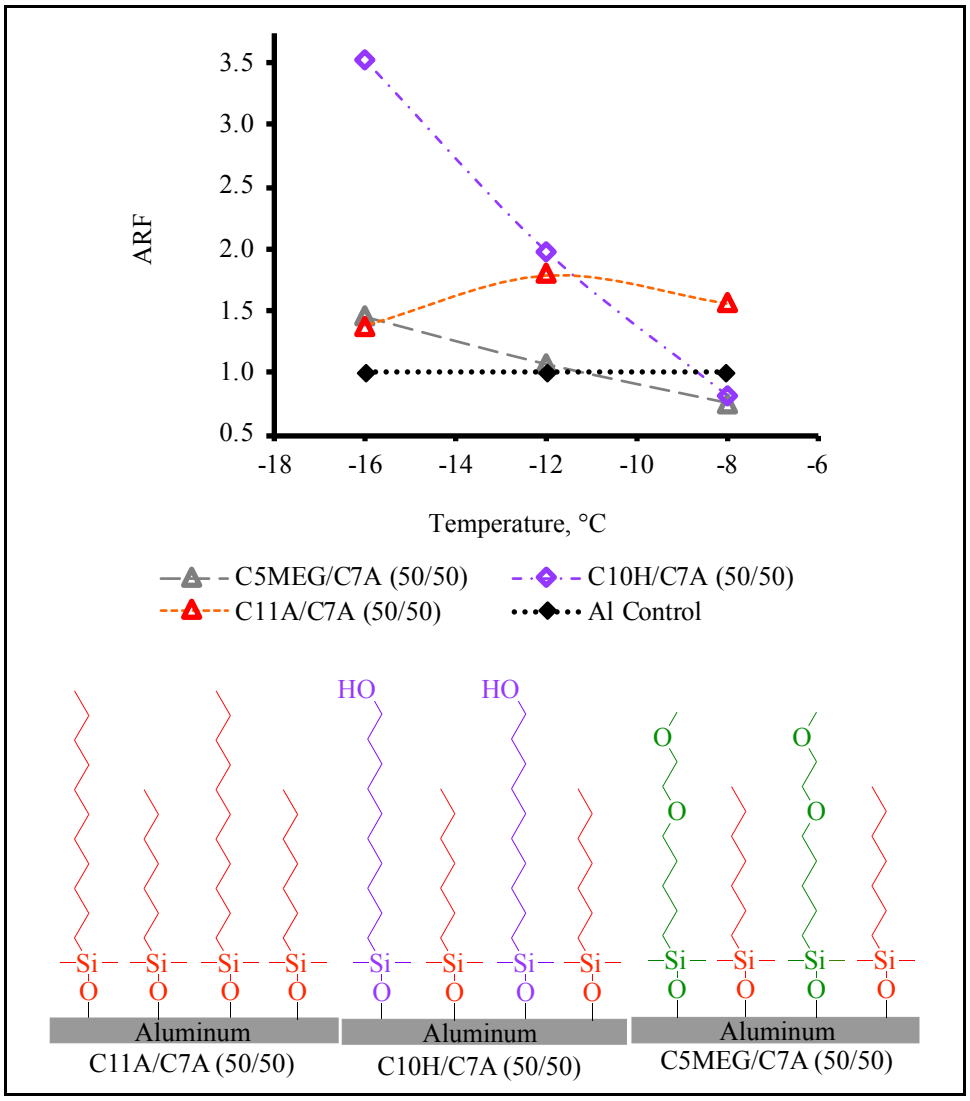

Fig. 27 ARF comparison of C11A/C7A (50/50), C10H/C7A (50/50), and C5MEG/C7A (50/50) compared to uncoated Al.

As previously reported, MD simulations of a C11H/C6A (50/50) surface suggested that it was rougher on the molecular level than C11A/C6A (50/50) and that C11H was not as mobile compared to C11A [39]. The overall effect would imply that forming ice would adhere more to C11H/C6A (50/50) than to C11A/C6A (50/50) based on the accepted observations that as surface roughness increased so does ice adhesion. The ARF results at -8°C for C10H/C7A (50/50) compared to C11A/C7A (50/50) in Fig. 27 support the results from the MD simulations. However, as temperature decreased a reversal in performance was observed. The increasingly better performance of C10H/C7A (50/50) as temperature decreased may be attributed to 1) the terminal group characteristic of the long n-alkyl chain component [HB (D/Ac) of C10H], 2) the dramatic changes in the surface energy components of impacting SCWD (Fig. 2) as ice is formed and 3) the speed of ice formation at -16°C after SCWD impact on the surface as previously discussed.

3.6.3.3 Effect of two hydrogen bonding (acceptor) groups in the same n-alkyl chain upon IASS

In Section 3.6.3.1 the terminal ether group (i.e., $-CH_2OCH_3$) was determined to be the dominant factor regarding interaction with impacting SCWD in the C5MEG/C7A (50/50) coating (Fig. 26). Therefore, it was of interest to evaluate the combined HB(Ac) characteristics of both the internal and terminal ether

groups of C5MEG [-OSi$(CH_3)_2(CH_2)_4CH_2$**$OCH_2CH_2OCH_3$**] had upon ARF, since this group combination is a methoxy-terminated glycol. Glycols are known to be effective at preventing ice formation through bonding with water and are effectively used as deicing fluids. Atomistic force field simulations have shown that the binding of water to 1,2-dimethoxyethane is similar to the bonding between two water molecules, suggesting strong HB interactions despite the fact that the former can only bond to water through HB (Ac) interactions [78]. This combination of two HB (Ac) groups within the same chain manifests itself in the greater water solubility of 1,2-dimethoxyethane compared to 1-methoxybutane (Table 5) as discussed.

To evaluate the effect this combined HB (Ac) characteristic afforded by the two ether groups in C5MEG had upon IASS, a mixed 50/50 coating with C3A was prepared and tested with the results presented in Fig. 19. A single factor ANOVA of the IASS data at the three test temperatures for the C5MEG/C3A (50/50) composition determined that the values differed statistically ($p \leq 0.008$). Comparing the IASS data at each temperature for this mixed coating to each of the components using a single factor ANOVA found that the mixed coating differed statistically at -8 and -12 °C ($p \leq 0.003$) but not at -16°C ($p = 0.067$). A student t-test comparing the data at -16°C for the mixed composition to each component determined did not differ statistically from either C5MEG or C3A ($p = 0.254$ and 0.052, respectively). However, the larger value of p for C5MEG compared to C3A suggests the mixed coating performed similar to the former at -16°C. The mixed coating was likewise determined to not differ statistically from C5MEG ($p = 0.075$) at -12°C. The comparable behavior of C5MEG/C3A (50/50) and C5MEG at the test temperatures of ≤ -12°C suggests that the exposed methoxy glycol functionality did not provide a benefit or a detriment with respect to impact

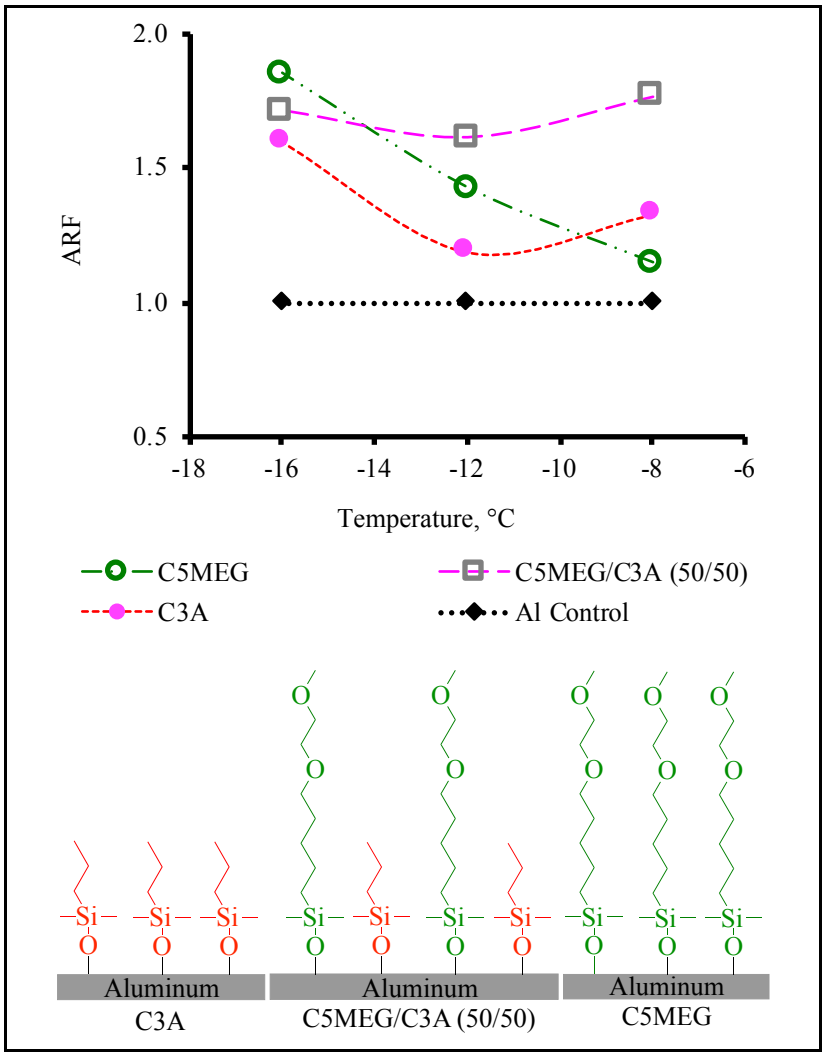

Fig. 28 ARF comparison of C5MEG, C5MEG/C3A (50/50), and C3A compared to uncoated Al.

icing. A substantial performance increase though was observed (Fig. 28) for this mixed coating at -8°C with respect to either of the pure components. Since impacting SCWD at -8°C remains fluid after impact prior to freezing, this exposed methoxy-terminated glycol group has time to effectively interact with the cold water resulting in an improvement in ARF compared to C5MEG.

The impact the internal ether group had upon ARF is further seen by comparing the results for both C5MEG/non-HB (i.e., C3A and C7A) coatings in Fig. 29. The greatest effect upon ARF was observed at -8°C where impacting SCWD can remain fluid for some time prior to freezing thus being able to spread across the surface and interact with the combined HB (Ac) characteristic of the internal and terminal ether groups (i.e., methoxy terminated glycol functionality). The greater water solubility of 1,2-dimethoxyethane compared to 1-methoxybutane (Table 5) may provide an explanation. As temperature decreased, the performance benefit of the combined internal and terminal ether groups of C5MEG that was exposed to impacting SCWD in the C5MEG/C3A (50/50) coating was observed to diminish, approaching that of C5MEG/C7A (50/50) where the terminal methoxy group of C5MEG was only exposed to the environment. This decrease in performance as temperature decreased may be associated with the increased speed of ice formation after SCWD impacts the coating surface and change in surface energy components as the phase change to ice occurred.

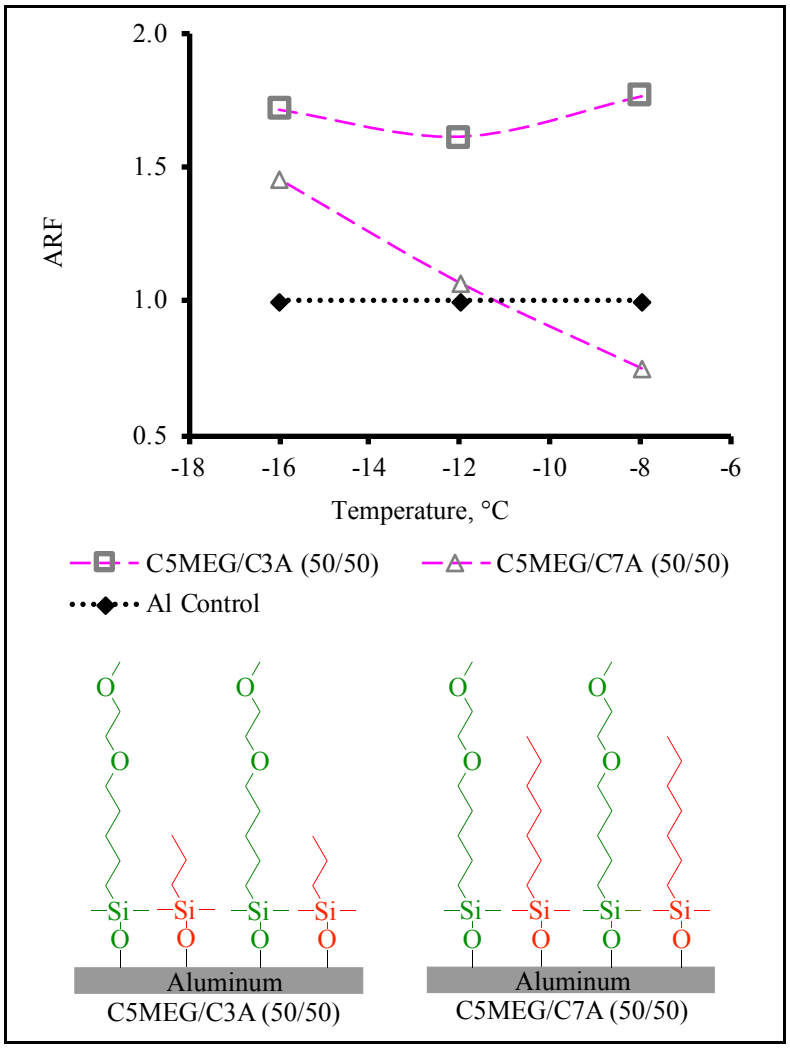

Fig. 29 ARF comparison of C5MEG/C3A (50/50) and C5MEG/C7A (50/50) compared to uncoated Al.

3.6.3.4 Effect of hydrogen bonding characteristic of similar chain length components in mixed C3A (50/50) coatings

Unlike the mixed C7A series discussed in Section 3.6.3.2, the best performing composition was C5MEG/C3A (50/50) with C10H/C3A (50/50) the worst (Fig. 30). Previously it had been seen that exposure of greater than four carbon units of the longer component in the mixed coatings to the icing environment resulted in high IASS values (low ARF). However, this did not hold true for the C5MEG/C3A (50/50) composition for reasons discussed in Section 3.6.3.3. The exposure of the methoxy terminated glycol to impacting SCWD provided an enhanced performance at all test temperatures illustrating the benefit of the second ether functionality (i.e., methoxy terminated glycol) in negating the exposure of the long alkyl chain to the icing environment.

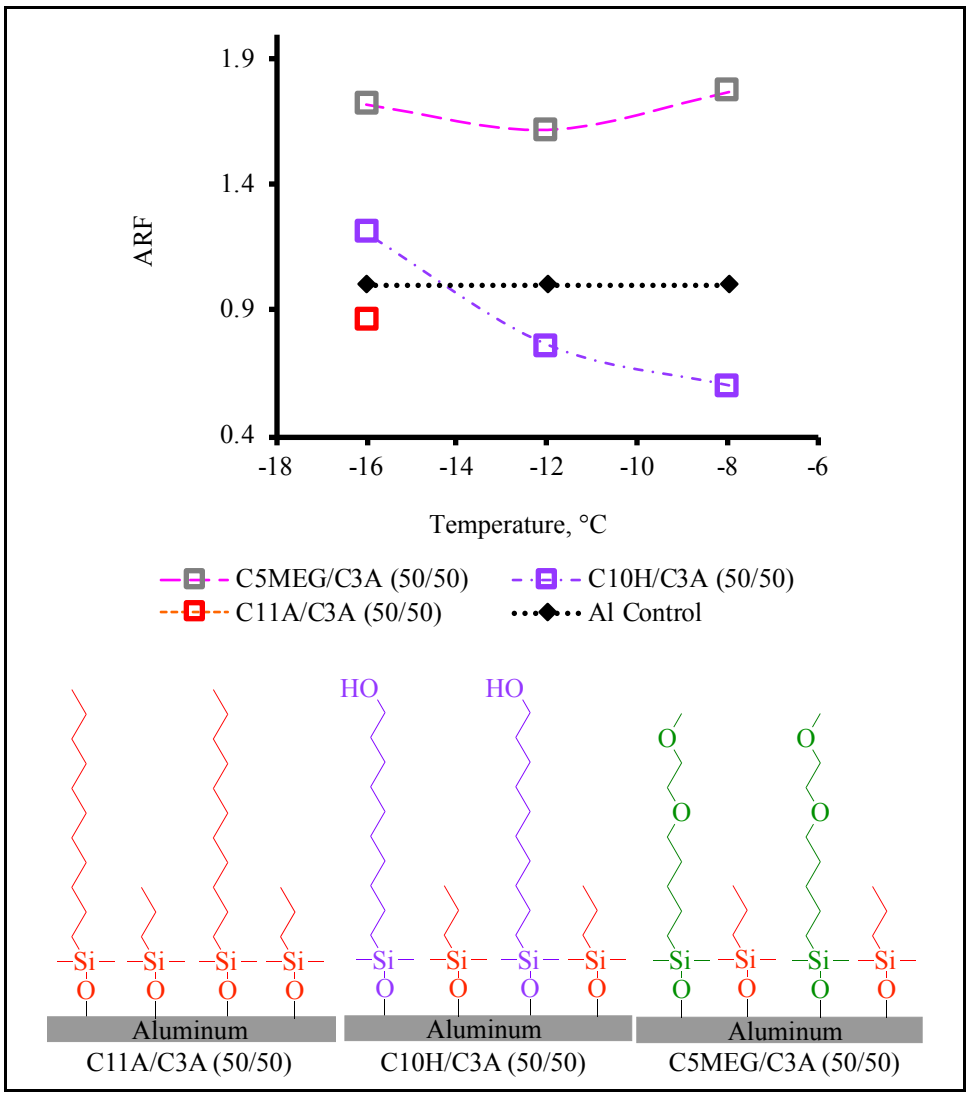

Fig. 30 ARF comparison of C11A/C3A (50/50), C10H/C3A (50/50), and C5MEG/C3A (50/50) compared to uncoated Al.

3.6.4 Best mixed composition performers

The best performance balance over the temperature range investigated was provided by the C11A/C7A (50/50) and C5MEG/C3A (50/50) compositions shown in Fig. 31. A student t-test comparing the IASS data for two coatings at each temperature (Fig. 19) determined that the two did not differ statistically at -8 and -12°C ($p = 0.0080$ and 0.109, respectively) but did differ statistically at -16°C ($p = 0.046$). This was surprising given that glycols are known to be effective as deicing fluids by preventing ice formation through

bonding with water. The IASS data suggests that 1) the exposed four carbon unit chain of C11A in C11A/C7A (50/50) may be as effective as the exposed methoxy glycol functionality ($-OCH_2CH_2OCH_3$) and 2) the exposed $-CH_2CH_2OCH_2CH_2OCH_3$ may negate some of the beneficial properties of glycols due to mechanical clamping of the ice.

The ARF data for the two coatings in Fig. 31 uses the average IASS data and thus does not reflect the similarities reflected by the statistical treatment of the data. Based on the ARF data C5MEG/C3A would exhibit better performance at the two temperature extremes (-8 and -16°C) while the mixed non-HB coating performed better at -12°C. To determine if C5MEG/C3A (50/50) is the better composition, more tests would need to be conducted.

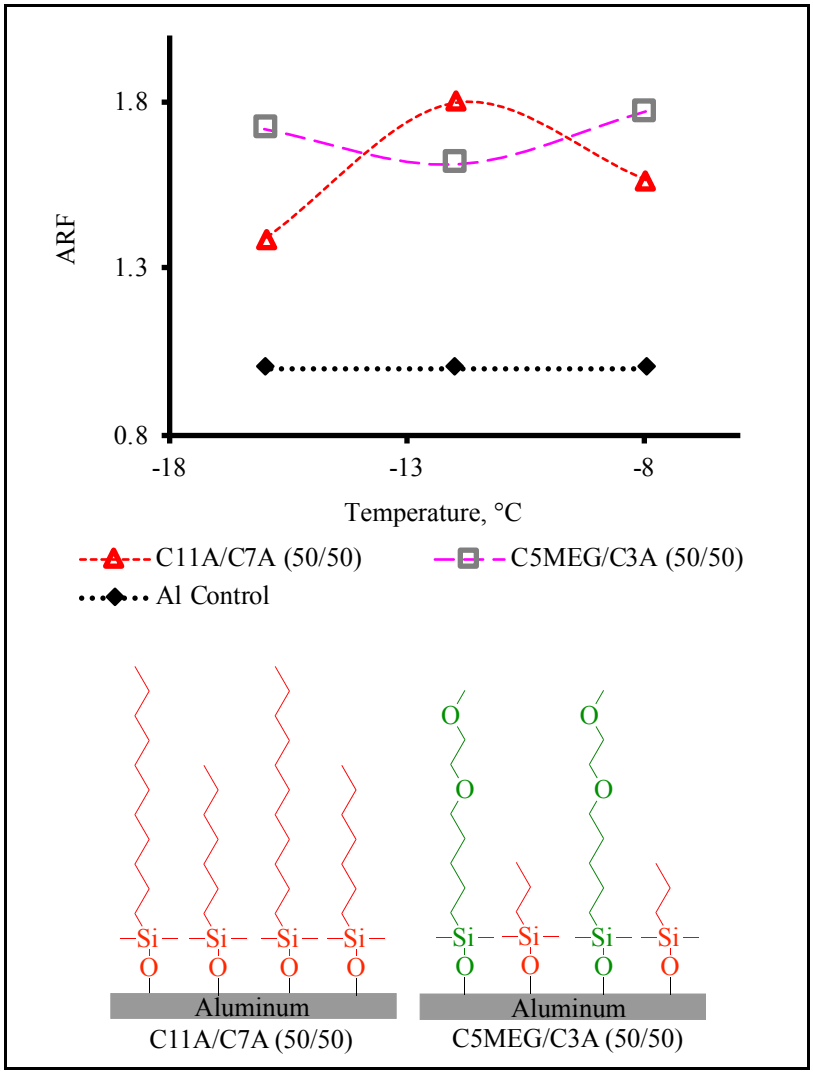

Fig. 31 ARF comparison of C11A/C7A (50/50) and C5MEG/C3A (50/50) compared to uncoated Al.

3.6.5 Conclusions

Based on the results discussed in Sections 3.6.1 - 3.6.3, the shorter n-alkyl chain length in the 50/50 compositions was found to have a profound influence upon the longer n-alkyl chain component. If the difference between the short and long chain components exceeded four methylene units, a significant deterioration in performance compared to the pure materials was observed. An exception to this was C5MEG where the exposure of the second HB (Ac) group forming a methoxy terminated glycol functionality resulted in a performance increase over the temperature range investigated despite the exposure of the long C5MEG chain to the icing environment. Would the same response as C5MEG/C3A

(50/50) hold true for a methoxy terminated species not containing this glycol unit in the chain? Perhaps not given the results for the C10H series with C3A and C7A.

For the C7A mixed coating series as shown in Fig. 27, the HB (D/Ac) functionality of C10H afforded the best performance at low temperatures (i.e., -16°C) whereas the non-HB group of C11A performed better at warmer temperatures (i.e., -8°C). This observation is similar to the neat component study discussed in Section 3.5. The 50/50 compositions with C3A did not exhibit the same result as the C7A 50/50 series. When combined with C3A, the HB (Ac) group of C5MEG was the best performer at all temperatures due to the exposure of the methoxy terminated glycol to the icing environment. Would a glycol terminated species combined with C3A in the same ratio exhibit better or worse performance given that it would possess both HB (D/Ac) and HB (Ac) characteristics? This would be subject of further investigation.

For the intended application a performance balance across the temperature range is required. The results suggest that HB (Ac) characteristics provided by exposure of a methoxy terminated glycol to impact icing conditions may satisfy this requirement. Applying the knowledge gained in this study to polymeric materials will determine if this is the case. The behaviors observed here are based on the limited number of materials examined and suggests complex interactions between SCWD, temperature, and HB characteristics.

4. Summary

Substituted n-alkyldimethylalkoxysilanes coated on Al substrates were used to study the effects of HB [i.e., non-HB, HB (D/Ac), and HB (Ac)] and molecular flexibility (provided by the n-alkyl chain length) upon impact icing to provide guidance for the development of low ice adhesion coatings. IASS results obtained from testing in the AERTS facility at PSU under a simulated environment that was within the FAR Part 25/29 Appendix C icing envelope revealed a complex behavior that was interdependent upon ice accretion temperature, HB characteristics of the substituent evaluated, and the length of the n-alkyl chain. To aid in explaining the results, the changes in the surface energy component values (i.e., non-polar and polar as shown in Fig. 2) that water undergoes during its' phase change from liquid to solid that arise from the freezing of impacting SCWD on the surface depended upon the temperature during accretion. Due to the accretion environment, at -8°C impacting SCWD is initially in a liquid phase that initially flows along the surface and then freezes upon it whereas at -16°C impacting SCWD freezes instantly. Comparison of the substituted n-alkyldimethylalkoxysilanes used in this study to the physical properties (i.e., water solubility and melting point) of analogous small compounds aided in explaining the results.

ARF values calculated for each coating at each temperature allowed for IASS data comparison. In general, the non-HB and non-HB/non-HB series had similar ARF values across the temperature regime examined whereas the HB (D/Ac), HB (Ac), and mixed HB (D/Ac)/non-HB series displayed increasing ARF as temperature decreased. The slope of the ARF vs. temperature graph for the HB (Ac)/non-HB series was dependent upon the chain length of the non-HB component evaluated. A majority of the coatings exhibited ARFs that ranged from nominally better than uncoated Al (i.e., > 1) up to >2. At -16°C, two HB (D/Ac) coatings had ARF values as high as 2.75 and one HB (D/Ac)/non-HB coating had a value of 3.5. A few samples of each HB series investigated had ARF less than uncoated Al and were deemed poor performers. Given that it would be desirable to have a coating that exhibited comparable and durable performance across the entire temperature regime, the non-HB materials appear to be candidates with the caveat that the exposed chain be approximately four carbon units in length when incorporated as a pendant group in a polymer. A chain length of three as provided by C3A provided some improvement with respect to uncoated Al. How an isolated C3A would perform in a polymer was not investigated here. Long alkyl lengths may be beneficial when incorporated in the polymer backbone thus providing a flexible component as has been suggested [50]. While the hydroxy functionality [HB (D/Ac)] afforded the best properties at -16°C, the performance at -8°C diminished its attractiveness as result of how it interacts with impacting SCWD. A pendant glycol or methoxyglycol [mixed HB (D/Ac)] and HB (Ac) or entirely HB (Ac)] may likewise provide a balanced temperature performance based on the results of C5MEG/C3A (50/50).

How do the results obtained herein compare with what IASS values are needed? An ice adhesion strength of ~20 kPa has been suggested as a benchmark for passive ice removal by wind or vibration [21];

however, the temperature for this benchmark was not provided. Using 20 kPa as the value to meet at the three test temperatures, the ARF for this "suggested" coating was calculated and compared to the best coatings in this study (Fig. 32). The results show that the coatings in this study had lower performance than the "suggested" benchmark which became exacerbated as temperature decreased. This is not surprising given the goal of this study was to determine the effect HB functionality and molecular flexibility had upon IASS so as to guide future research. Unexpectedly, the slope for this notional coating is similar to that observed for the neat HB (D/Ac) coatings (Fig. 16). C11H was approximately 45% of the values indicated for this notional coating across the temperature regime examined.

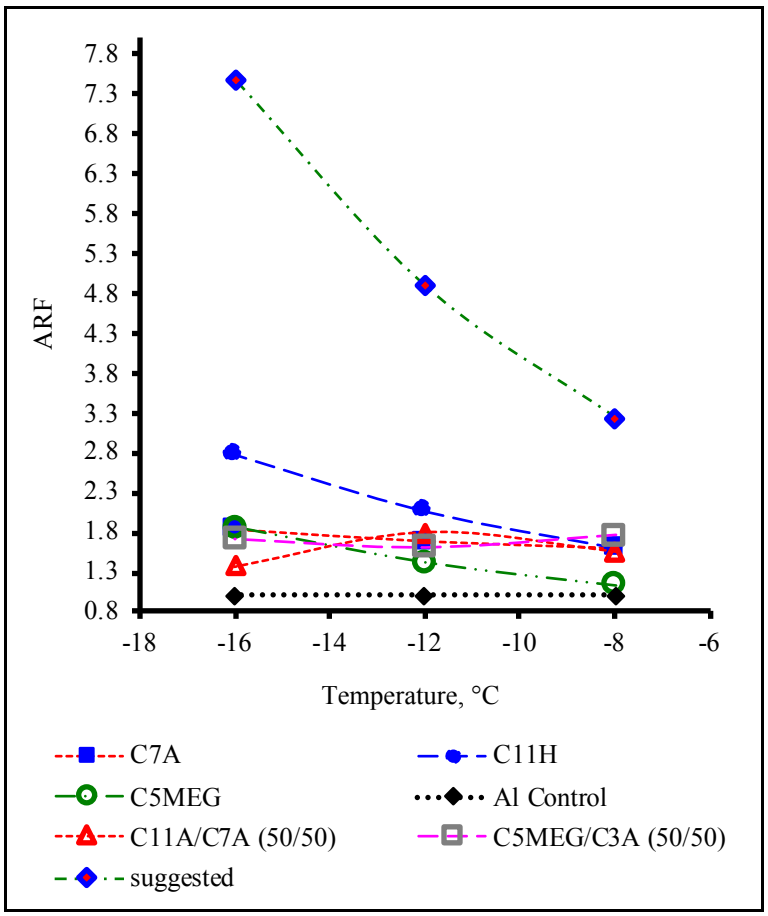

Fig. 32 Comparison of the best performing coatings in this study to the ARF generated for the 20 kPa benchmark (suggested) with respect to uncoated Al in this study.

Based on the study results, a long aliphatic chain in a polymer backbone (with or without internal ether linkages) could be advantageous as suggested by C11A/C7A (50/50) data. Some flexibility in combination with material rigidity was noted to reduce ice adhesion by aiding crack growth through local stress generation and subsequent propagation [55]. As isolated pendant groups along the polymer backbone, non-HB groups of approximately four carbon units may be useful.

The reader should be aware that the results of this study were determined under a specific set of conditions and may or may not hold true under other ice accretion conditions. This is especially true given the effect of ice accretion temperature and test methodology. The calculation of an ARF from IASS allows for comparing results from different facilities (AMIL vs. AERTS) using similar methods (i.e., centrifugal in the case of this study). Since ARF is calculated from average IASS values, the difference in coating performance between uncoated surfaces, other coatings, and with itself at different temperatures may be masked due to the standard deviations typically observed in these tests (acceptable range is 20%). Statistical

treatment of the data therefore is imperative. Therefore, it necessitates the need for a standardized test method as put forth by Kreder et al. [21].

References

1. DeMott, P.J.; Rogers, D.C. Freezing Nucleation Rates of Dilute Solution Droplets Measured between -30°C and -40°C in Laboratory Simulations of Natural Clouds. *J. Atmos. Sci.* 1990, 47,1056-1064.
2. Thomas, S.K.; Cassoni, R.P.; MacArthur, C.D. Aircraft Anti-Icing and De-Icing Techniques and Modeling. *J. Aircraft.* 1996, 5,841-854.
3. Ballough, J.J. Advisory Circular -Pilot Guide: Flight in Icing Conditions. FAA AC No. 91-74A, 2007.
4. SKYbrary Aviation Safety. Supercooled Water Droplets. 2015. http://www.skybrary.aero/index.php/Supercooled_Water_Droplets (accessed Dec. 13, 2019).
5. National Transportation Safety Board, http://www.ntsb.gov/Pages/default.aspx (accessed Dec. 13, 2019).
6. Anonymous. Aviation Weather for Pilots and Flight Operations Personnel. FAA AC 00-6A, 1975.
7. Potapczuk, M.G. Aircraft Icing Research at NASA Glenn Research Center. *J. Aerosp. Eng.* 2013, 26, 260-276.
8. Cabler, S.J.M. Aircraft Ice Protection. FAA AC-No. 20-73A, 2006.
9. SKYbrary Aviation Safety. Ice-Protection Systems. 2016. http://www.skybrary.aero/index.php/Ice_Protection_Systems (accessed Dec. 13, 2019).
10. Alizadeh, A.; Yamada, M.; Li, R.; Shang, W.; Otta, S.; Zhong, S.; Ge, L.; Dhinojwala, A.; Conway, K.R.; Bahadur, V.; Vinciquerra, A.J.; Stephens, B.; Blohn, M.L. Dynamics of Ice Nucleation on Water Repellent Surfaces. *Langmuir* 2012, 28, 3180-3186.
11. Sojoudi, H.; Wang, M.; Boscher, N.D.; McKinley, G.H.; Gleason, K.K. Similarities and Distinctions from Superhydrophobic Surfaces. *Soft Matter* 2016, 12, 1938-1963.
12. Hacker, P.T. Experimental Values of the Surface Tension of Supercooled Water Technical Note 2510, 1951. http://naca.central.cranfield.ac.uk/reports/1951/naca-tn-2510.pdf (accessed Dec. 13, 2019).
13. Kloubek, J. Calculation of Surface Free Energy Components of Ice According to Its Wettability by Water, Chlorobenzene, and Carbon Disulfide. *J. Colloids Interf. Sci.* 1974, 46, 185-190.
14. Messinger, B.L. Equilibrium Temperature of an Unheated Icing Surface as a Function of Airspeed. *J. Aeron. Sci.* 1953, 20, 29-42.
15. SKYbrary Aviation Safety In-Flight Icing. 2016. http://www.skybrary.aero/index.php/In-Flight_Icing (accessed Dec. 13, 2019).
16. Addy Jr., H.E.; Potapczuk, M.G.; Sheldon, D.W. Modern Airfoil Ice Accretions. NASA TM 107423, 1997.
17. Scavuzzo, R.J.; Chu, M.L. Structural Properties of Impact Ices Accreted on Aircraft Structures. NASA CR 179580, 1987.
18. Hempe, D.W. Turbojet, Turboprop, and Turbofan Engine Induction System Icing and Ice Ingestion. FAA AC No. 20-147, 2004.
19. Lv, J.; Song, Y.; Jiang, L.; Wang, J. Bio-Inspired Strategies for Anti-Icing. *ACS Nano* 2014, 4, 3152-3169.
20. Schutzius, T.M.; Jung, S.; Maitra, T.; Eberle, P.; Antonini, C.; Stamatopoulos, C.; Poulikakos, D. Physics of Icing and Rotational Design of Surfaces with Extraordinary Icephobicity. *Langmuir* 2015, 31, 4807-4821.
21. Kreder, M.J.; Alvarenga, J.; Kim, P.; Aizenberg, J. Design of anti-icing surfaces: smooth, textured or slippery? *Nat. Rev. Matls.* 2016, 1, 1-15.
22. Kulinich, S.A.; Farhadi, S.; Nose, K.; Du, X.W. Superhydrophobic Surfaces: Are They Really Ice-Repellent? *Langmuir* 2011, 27, 25-29.
23. Farhadi, S.; Farzanehl, M.; Kulinich, S.A. Anti-icing Performance of Superhydrophobic Surfaces. *App. Surf. Sci.* 2011, 257, 6264–6269.
24. Soltis, J.; Palacios, J.; Eden, T.; Wolfe, D. Ice Adhesion Mechanisms of Erosion-Resistant Coatings. *AIAA Journal* 2015, 53(3), 654-662.

25. Soltis, J.; Palacios, J.; Eden, T.; Wolfe, D. Evaluation of Ice Adhesion Strength on Erosion Resistant Materials, 54th AIAA/ASME/ASCE/AHS/ASC Structures, Structural Dynamics, and Materials Conference, Boston, MA, April 8-11, 2013, AIAA 2013-1509; Evaluation of Ice Adhesion Strength on Erosion Resistant Materials. *AIAA Journal* 2015, 53(7), 1825-1835.
26. Mishchenko, L.; Hatton, B.; Bahadur, V.; Taylor, J.A.; Krupenkin, T.; Aizenberg, J. Design of Ice-free Nanostructured Surfaces Based on Repulsion of Impacting Water Droplets. *ACS Nano* 2010, 4, 7699-7707.
27. Smith, J.D.; Dhiman, R.; Anand, S.; Reza-Garduno, E.; Cohen, R.E.; McKinley, G.H.; Varanasi, K.K. Droplet Mobility on Lubricant-Impregnated Surfaces. *Soft Matter* 2013, 9, 1772–1780.
28. Subramanyam, S.B.; Rykaczewski, K.; Varanasi, K.K. (2013) Ice Adhesion on Lubricant-Impregnated Textured Surfaces. *Langmuir* 2013, 29, 13414–13418.
29. Vogel, N.; Belisle, R.A.; Hatton, B.; Wong, T.-S.; Aizenberg, J. Transparency and Damage Tolerance of Patternable Omniphobic Lubricated Surfaces Based on Inverse Colloidal Monolayers. Nat Commun [online journal] 2013, 4, 2176. http://www.nature.com/ncomms/2013/130731/ncomms3176/pdf/ncomms3176.pdf (accessed Dec. 13, 2019).
30. Anitei, S. Fish 'Antifreeze' Against Icy Aeroplanes. 2007. http://news.softpedia.com/news/Fish-Antifreeze-Against-Icy-Aeroplanes-62189.shtml (accessed Dec. 13, 2019).
31. Grunwald, I.; Rischka, K.; Kast, S.M.; Scheibel, T.; Bargel, H. Mimicking Biopolymers on a Molecular Scale: Nano(bio)technology Based on Engineered Proteins. *Phil. Trans. R. Soc. A* 2009, 367, 1727-1747.
32. Inada, T.; Lu, S.S. Inhibition of Recrystallization of Ice Grains by Adsorption of Poly(Vinyl Alcohol) onto Ice Surfaces. *Crys. Growth. Des.* 2003, 3, 747-752.
33. Inada, T.; Lu, S.S. Thermal Hysteresis Caused by Non-Equilibrium Antifreeze Activity of Poly(Vinyl Alcohol). *Chem. Phys. Lett.* 2004, 394, 361-365.
34. Inada, T.; Modak, P.R. Growth Control of Ice Crystals by Poly(Vinyl Alcohol) and Antifreeze Protein in Ice Slurries. *Chem. Eng. Sci.* 2006, 61, 3149-3158.
35. Wang, H.Y.; Inada, T.; Funakoshi, K.; Lu, S.S. Inhibition of Nucleation and Growth of Ice by Poly(Vinyl Alcohol) in Vitrification Solution. *Cryobio*. 2009, 59, 83-89.
36. Inada, T.; Koyama, T.; Goto, F.; Seto, T. Ice Nucleation in Emulsified Aqueous Solutions of Antifreeze Protein Type III and Poly(Vinyl Alcohol). *J. Phys. Chem. B* 2011, 115, 7914-7922.
37. Smith Jr., J.G.; Wohl, C.J.; Kreeger, R.E.; Hadley, K.R.; McDougall, N. Hydrogen-Bonding Surfaces for Ice Mitigation. NASA TM 2014-218291, 2014.
38. Smith Jr., J.G.; Wohl, C.J.; Kreeger, R.E.; Palacios, J.; Knuth, T. Surface Chemical Functionality Effect Upon Ice Adhesion Shear Strength., 8th AIAA Atmospheric and Space Environments Conference, AIAA Aviation 2016, Washington, D.C. June 13-17, 2016, AIAA 2016-3444, 2016.
39. Federal Aviation Regulation Part 25 Airworthiness Standards: Transport Category Airplanes and Part 29 Airworthiness Standards: Transport Category Rotorcraft. http://www.faa.gov/ (accessed Dec. 13, 2019).
40. Jeck, R.K. Icing Design Envelopes (14 CFR Parts 25 and 29, Appendix C) Converted to a Distance-Based Format. DOT/FAA/AR-00/30, 2002.
41. Susoff, M.; Siegmann, K.; Pfaffenroth, C.; Hirayama, M. Evaluation of Icephobic Coatings—Screening of Different Coatings and Influence of Roughness. *Applied Surf. Sci.* 2013, 282, 870– 879.
42. Brassard, J.D.; Sarkar, D.K.; Perron, J.; Audibert-Hayet, A.; Melot, D. Nano-Micro Structured Superhydrophobic Zinc Coating on Steel for Prevention of Corrosion and Ice Adhesion. *J. Coll. Interface Sci.* 2015, 447, 240–247.
43. Laforte, C.; Blackburn, C.; Perron, J. A Review of Icephobic Coating Performances over the Last Decade. SAE Technical Paper 2015-01-2149, 2015.
44. Light, J.; Breslow, R. A Water-Soluble Tin Hydride: Tris[3-(2-Methoxyethoxy)propyl]stanne. *Org. Synth.* 1995, 72, 199-208.
45. Badia, A.; Cuccia, L.; Demers, L.; Morin, F.; Lennox, R. B. Structure and Dynamics in Alkanethiolate Monolayers Self-Assembled on Gold Nanoparticles: A DSC, FT-IR, and deuterium NMR study. *J. Am. Chem. Soc.* 1997, 119, 2682–2692

46. Yaws, C. L. Thermophysical Properties of Chemicals and Hydrocarbons. 2nd ed. Elsevier Inc, New York, 2014. https://books.google.com/books?id=WJdjAwAAQBAJ&pgis=1 (accessed Dec. 13, 2019).
47. Chinthamanipeta, P. S.; Kobukata, S.; Nakata, H.; Shipp, D. Synthesis of Poly(methyl methacrylate)–Silica Nanocomposites using Methacrylate-Functionalized Silica Nanoparticles and RAFT Polymerization. *Polymer* 2008, 49, 5636–5642.
48. Brouwers, E.; Peterson, A.; Palacios, J.; Centolanza, L. Ice Adhesion Strength Measurements for Rotor Blade Leading Edge Materials. 67th American Helicopter Society Forum, 67-2011-000272, 2011.
49. Arkles, B. Silane Coupling Agents: Connecting Across Boundaries, v2.0. Gelest Inc, 2006.
50. Arkles, B. Hydrophobicity, Hydrophilicity, and Silane Surface Modification. Gelest Inc, 2006.
51. Arkles, B. Tailoring Surfaces with Silanes . *Chemtech* 1977, 7, 766-778
52. Plueddemann, E.P. Silane Coupling Agents, 2nd ed. Plenum Press, New York and London, 1991.
53. Stevens, M.P. Polymer Chemistry - An Introduction 2nd ed. Oxford University Press, New York, 1990.
54. Tamao, K.; Nakagawa, Y.; Ito, Y. Regio- and Stereoselective Intramolecular Hydrosilylation of α-Hydroxy Enol Ethers: 2,3-syn-2-MethoxyMethoxy-1,3-Nonanediol. *Org. Synth.* 1996, 73, 94-109.
55. Sayward, J.M. Seeking Low Ice Adhesion. Special Report 79-11, 1979.
56. Linford, M.R.; Renter, P.; Eisenberger, P.M.; Chidsey, C.E.D. Alkyl Monolayers on Silicon Prepared from 1-Alkenes and Hydrogen-Terminated Silicon. *J. Am. Chem. Soc.* 1995, 117, 3145-3155.
57. Mittal, K. L.; Bothorel, P. Surfactants in Solution Vo. 4. Plenum Press, New York and London, 1986.
58. Alessandrini, A.; Facci, P. Phase transitions in supported lipid bilayers studied by AFM. *Soft Matter* 2014, 10, 7145-7164.
59. Wen, K.; Maoz, R.; Cohen, H.; Sagiv, J.; Gibaud, A.; Desert, A.; Ocko, B.M. Post Assembly Chemical Modification of a Highly Ordered Organosilane Multilayer: New Insights into the Structure, Bonding, and Dynamics of Self-Assembling Silane Monolayers. *ACS Nano* 2008, 2, 579-599.
60. National Center for Biotechnology Information. PubChem Compound Database; CID=8900, Heptane. https://pubchem.ncbi.nlm.nih.gov/compound/8900 (accessed Dec. 13, 2019).
61. National Center for Biotechnology Information. PubChem Compound Database; CID=15600, Decane. https://pubchem.ncbi.nlm.nih.gov/compound/decane (accessed Dec. 13, 2019).
62. National Center for Biotechnology Information. PubChem Compound Database; CID=14257, Undecane. https://pubchem.ncbi.nlm.nih.gov/compound/14257 (accessed Dec. 13, 2019).
63. National Center for Biotechnology Information. PubChem Compound Database; CID=8182, Dodecane. https://pubchem.ncbi.nlm.nih.gov/compound/8182 (accessed Dec. 13, 2019).
64. National Center for Biotechnology Information. PubChem Compound Database; CID=8129, 1-Heptanol. https://pubchem.ncbi.nlm.nih.gov/compound/8129 (accessed Dec. 13, 2019).
65. National Center for Biotechnology Information. PubChem Compound Database; CID=8174, 1-Decanol. https://pubchem.ncbi.nlm.nih.gov/compound/8174 (accessed Dec. 13, 2019).
66. National Center for Biotechnology Information. PubChem Compound Database; CID=8184, 1-Undecanol. https://pubchem.ncbi.nlm.nih.gov/compound/8184 (accessed Dec. 13, 2019).
67. National Center for Biotechnology Information. PubChem Compound Database; CID=8193, 1-Dodecanol. https://pubchem.ncbi.nlm.nih.gov/compound/1-dodecanol (accessed Dec. 13, 2019).
68. HyperChem Lite. http://www.hyper.com/Products/HyperChemLite/tabid/369/Default.aspx (accessed Dec. 13, 2019).
69. ASTM International. Standard Specification for General Requirements for Flat-Rolled Stainless and Heat-Resisting Steel Plate, Sheet, and Strip. ASTM A480-15, 2015.
70. Dai, Y.; Evans, J.S. Molecular Dynamics Simulations of Template-Assisted Nucleation: Alcohol Monolayers at the Air-Water Interface and Ice Formation. *J. Phys. Chem. B* 2001, 105, 10831-10837.
71. National Center for Biotechnology Information. PubChem Compound Database; CID=6334, Propane. https://pubchem.ncbi.nlm.nih.gov/compound/6334 (accessed Dec. 13, 2019).
72. Robert, J.D.; Caserio, M.C. Basic Principles of Organic Chemistry, 2nd ed. Chapter 15 Alcohols and Ethers W. A. Benjamin, Inc., Menlo Park, CA, 1977.
73. National Center for Biotechnology Information. PubChem Compound Database; CID=12338, 1-Methoxybutane. https://pubchem.ncbi.nlm.nih.gov/compound/12338 (accessed Dec. 13, 2019).

74. National Center for Biotechnology Information. PubChem Compound Database; CID=8071, 1,2-Dimethoxyethane. https://pubchem.ncbi.nlm.nih.gov/compound/8071 (accessed Dec. 13, 2019).
75. Sigma-Aldrich Solubility Information. http://www.sigmaaldrich.com/united-kingdom/technical-services/solubility.html (accessed Dec. 13, 2019).
76. Petrenko, V.F.; Peng, S. Reduction of Ice Adhesion to Metal using Self-Assembling Monolayers. *Can. J. Phys.* 2003, 81, 387-393.
77. Stranick, S.J.; Parikh, A.N.; Tao, Y.-T.; Allara, D.L.; Weiss, P.S. Phase Separation of Mixed-Composition Self-Assembled Monolayers into Nanometer Scale Molecular Domains. *J. Phys. Chem.* 1994, 98, 7636-7646.
78. Bedrov, D.; Pekny, M.; Smith, G.D. Quantum-Chemistry-Based Force Field for 1,2-Dimethoxyethane and Poly(ethylene oxide) in Aqueous Solution. *J. Phys. Chem. B* 1998, 102, 996-1001.

Appendix

$$Mass\ of\ Material\ at\ 150°C = M_{150°C}$$

$$Mass\ Loss\ at\ 500°C\ (M^-) = SiO_2\ mass\ loss\ \left(M^-_{particle}\right) + Silane\ mass\ loss\ (M^-_{silane})$$

$$Mass\ total\ (M_{Total}) = M^- + Remaining\ mass\ at\ 500°C\ (M_R)$$

$$M_{Total} = M_R + M^-_{Particle} + M^-_{silane}$$

$$M^-_{silane} = \frac{\#\ moles\ silane}{molecular\ weight\ of\ silane} = \frac{mol_{silane}}{\frac{\mu g}{mol}}$$

$$Mass\ of\ SiO_2\ Particle = M_{SiO_2} = volume * density$$

$$volume\ of\ SiO_2\ Particle = V_{SiO_2} = \frac{4\pi r^3}{3} = \frac{4\pi(50\ nm)^3}{3} = 5.24x10^5 nm^3$$

$$density\ of\ SiO_2\ Particle = \rho_{SiO_2} = \frac{1x10^{-16}\mu g}{nm^3}$$

$$\#\ particles = \frac{M_R}{M_{SiO_2}}$$

$$Surface\ area\ of\ particles = SA_{SiO_2} = 4\pi r^2 = 4\pi(50\ nm)^2 = 31{,}415.93\ nm^2$$

$$Total\ surface\ area = SA_{SiO_2} x\ (\#\ particles)$$

$$graft\ density = \sigma = \frac{(mol_{silane})(\frac{6.023x10^{23} molecules}{mol})}{Total\ SA_{SiO_2}} = \frac{molecules\ of\ silane}{nm^2}$$

$$Total\ SA\ nm^2\ x\ \frac{5\ hydroxy\ sites}{nm^2} = potential\ functionalization\ sites$$

$$Total\ SA\ nm^2\ x\ \frac{molecules}{nm^2} = sites\ functionalized$$

$$\%\ functionalization = \left(\frac{sites\ functionalized}{potential\ functionalization\ sites}\right) x100$$

REPORT DOCUMENTATION PAGE

Form Approved
OMB No. 0704-0188

1. REPORT DATE *(DD-MM-YYYY)*
1-02-2020

2. REPORT TYPE
Technical Memorandum

3. DATES COVERED *(From - To)*

4. TITLE AND SUBTITLE

Effects of Hydrogen Bonding and Molecular Chain Flexibility of Substituted n-Alkyldimethylsilanes On Impact Ice Adhesion Shear Strength

5a. CONTRACT NUMBER

5b. GRANT NUMBER

5c. PROGRAM ELEMENT NUMBER

6. AUTHOR(S)

Smith, Joseph G.; Wohl, Christopher J.; Kreeger, Richard E.;
Palacios, Jose; Hernandez, Maricely

5d. PROJECT NUMBER

5e. TASK NUMBER

5f. WORK UNIT NUMBER
081876.02.07.50.08.03

7. PERFORMING ORGANIZATION NAME(S) AND ADDRESS(ES)

NASA Langley Research Center
Hampton, VA 23681-2199

8. PERFORMING ORGANIZATION REPORT NUMBER

L-21121

9. SPONSORING/MONITORING AGENCY NAME(S) AND ADDRESS(ES)

National Aeronautics and Space Administration
Washington, DC 20546-0001

10. SPONSOR/MONITOR'S ACRONYM(S)

NASA

11. SPONSOR/MONITOR'S REPORT NUMBER(S)
NASA-TM-2020-220567

12. DISTRIBUTION/AVAILABILITY STATEMENT

Unclassified-
Subject Category 23
Availability: NASA STI Program (757) 864-9658

13. SUPPLEMENTARY NOTES

14. ABSTRACT

The effects of hydrogen bonding and molecular flexibility upon ice adhesion shear strength were investigated using aluminum substrates coated with substituted n-alkyldimethylalkoxysilanes. The location of the chemical group substitution was on the opposing end of the linear n-alkyl chain with respect to silicon. Three hydrogen-bonding characteristics were evaluated: 1) non-hydrogen bonding, 2) donor/acceptor, and 3) acceptor. Varying the length of the n-alkyl chain provided an assessment of molecular chain flexibility. Coated and uncoated aluminum surfaces were characterized by receding water contact angle and surface roughness. Ice adhesion shear strength was determined in the Adverse Environment Rotor Test Stand facility from -16 to -8°C that simulated aircraft in-flight icing conditions within the FAR Part 25/29 Appendix C icing envelope. Surface roughness of the coatings was similar allowing for comparison of the test results. An adhesion reduction factor, based on the ice adhesion shear strength data with respect to uncoated aluminum obtained at the same temperature, was calculated to compare the data. The results revealed complex interactions with impacting supercooled water droplets that was interdependent upon ice accretion temperature, surface energy characteristics of water and ice, hydrogen bonding characteristic of the substituent, and length of the n-alkyl chain.

15. SUBJECT TERMS

Coating; ice adhesion; molecular flexibility; supercooled water; surface energy

16. SECURITY CLASSIFICATION OF:			17. LIMITATION OF ABSTRACT	18. NUMBER OF PAGES	19a. NAME OF RESPONSIBLE PERSON
a. REPORT	b. ABSTRACT	c. THIS PAGE			STI Help Desk (email: help@sti.nasa.gov)
U	U	U	UU	56	19b. TELEPHONE NUMBER *(Include area code)* (757) 864-9658